CARBON BIOGEOCHEMISTRY IN THE POLAR OCEANS

A DISSERTATION

SUBMITTED TO THE PROGRAM IN

EARTH, ENERGY AND ENVIRONMENTAL SCIENCES

AND THE COMMITTEE ON GRADUATE STUDIES

OF STANFORD UNIVERSITY

IN PARTIAL FULFILLMENT OF THE REQUIREMENTS FOR THE

DEGREE OF

DOCTOR OF PHILOSOPHY

SUDESHNA PABI

JULY 2008

INFORMATION TO USERS

The quality of this reproduction is dependent upon the quality of the copy submitted. Broken or indistinct print, colored or poor quality illustrations and photographs, print bleed-through, substandard margins, and improper alignment can adversely affect reproduction.

In the unlikely event that the author did not send a complete manuscript and there are missing pages, these will be noted. Also, if unauthorized copyright material had to be removed, a note will indicate the deletion.

ProQuest LLC
789 E. Eisenhower Parkway
PO Box 1346
Ann Arbor, MI 48106-1346

I certify that I have read this dissertation and that, in my opinion, it is fully adequate in scope and quality as a dissertation for the degree of Doctor of Philosophy.

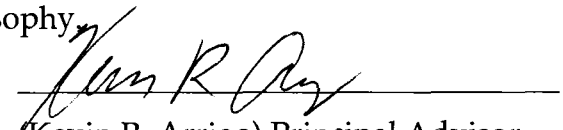

(Kevin R. Arrigo) Principal Advisor

I certify that I have read this dissertation and that, in my opinion, it is fully adequate in scope and quality as a dissertation for the degree of Doctor of Philosophy.

(Leif N. Thomas)

I certify that I have read this dissertation and that, in my opinion, it is fully adequate in scope and quality as a dissertation for the degree of Doctor of Philosophy.

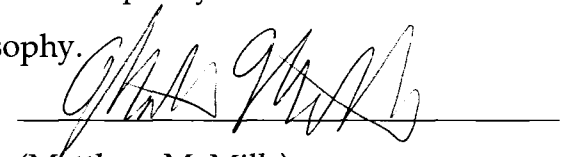

(Matthew M. Mills)

I certify that I have read this dissertation and that, in my opinion, it is fully adequate in scope and quality as a dissertation for the degree of Doctor of Philosophy.

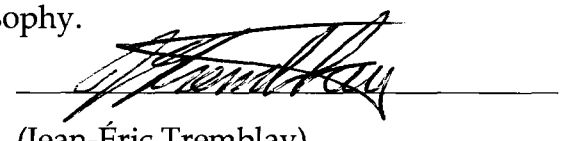

(Jean-Éric Tremblay)

Approved for the University Committee on Graduate Studies

ABSTRACT

Polar regions have been disproportionately affected by recent changes in climate, including the dramatic reduction in sea ice thickness and extent, increased air temperature, and an increase in river discharge. In light of these recent environmental changes, three key aspects of the carbon biogeochemistry in both polar oceans have been assessed as part of this dissertation.

First, a new satellite remote sensing algorithm was developed to measure particulate organic carbon in the surface ocean directly from space. This approach was a departure from the conventional method of converting satellite-baased estimates of chlorophyll (Chl) to carbon (C) using an empirically-derived C to Chl ratio. Application of this algorithm to the Ross Sea, Antarctica helped to quantify concentrations of particulate organic carbon in waters dominated by two dominant bloom-forming phytoplankton taxa that differ markedly in their ability to draw down carbon dioxide (CO_2).

Second, changes in sea ice and primary production in the Arctic Ocean were quantified for the period 1998-2006. For this purpose, multi-platform

satellite data were used to derive best estimates of open water (ice free water) area, sea surface temperature (SST) and Chl in conjunction with a primary production algorithm. Interannual variability in primary production over the entire Arctic Ocean, as well as in the various geographical and ecological sectors, was assessed. Results show that, since 1998, open water area in the Arctic has increased at a rate of 0.07×10^6 km^2 yr^{-1}, with the greatest increases in the Barents, Kara, and Siberian sectors, particularly over the continental shelf. Between 1998 and 2006, mean annual open water area in the Arctic Ocean increased by 19%. The pan-Arctic primary production averaged 419±33 Tg C yr^{-1} during 1998-2006 reaching a nine-year peak in 2006.

Finally, air-sea flux of CO_2 (FCO_2) was quantified in the Arctic Ocean for the period 1998-2003. For this purpose, dissolved inorganic carbon and total alkalinity were estimated from in-situ measurements of salinity, sea surface temperature (SST), and Chl. This allowed computation of the partial pressure of CO_2 and the quantification of air-sea flux of CO_2 using salinity, SST and, wind speed. Pan-Arctic application of this algorithm was accomplished using a combination of remotely sensed chlorophyll and modeled derived SST and salinity. The results show that Arctic Ocean is a net sink of atmospheric CO_2, with an annual flux of 169±9 Tg C yr^{-1} from the air to the ocean. This is about

8% of the world's uptake of CO_2. Increasing annual FCO_2 with time was observed only in Siberian sector which was due to a significant increase in open water area.

Thus, this study contributes towards better understanding of the carbon biogeochemistry in the polar oceans and facilitates future assessment of the same in these regions.

ACKNOWLEDGMENTS

First and foremost I would like to thank my PhD advisor, Kevin R. Arrigo, for his constant support and advice. I would also like to thank him for the invaluable opportunity to work in exciting projects related to the Arctic Ocean. His immense knowledge and intensity of thought have always been a constant source of motivation. Also, anything readable in this thesis is because of him.

Thanks to Jean-Éric Tremblay, Matt Mills, Leif Thomas and Gary Mavko for serving on my orals committee. Jean-Éric Tremblay also provided a great opportunity to work in the Arctic Ocean as part of the scientific crew on board of CCGS Amundsen.

I would also like to thank members of the Arrigo research group. I would especially like to thank Gert van Dijken from whom I have learnt much about remote sensing, data analysis and attention to details. I would also like to thank each and every member of this group (Al, Anna, Ben, Gemma, Lindsey, Mine, Molly, Rochelle, Tasha, Viola) for making this journey so memorable

with their insights, help, and thoughtfulness. Special thanks to Mine and Lindsey for their help with the manuscript.

Thanks to Graduate life office (especially, Chris Griffith and Ken Hsu) and Bechtel International Center whose help and service makes significant difference to the life of many international students like me. I would like to acknowledge support from the School of Earth Sciences (Edmund Wattis Littlefield Fellowship, McGee Fellowship) and the NASA Earth Systems Science Fellowship. I would also like to thank Dennis Michael for access to the CEES cluster and related computational support.

Thanks to my friends at Stanford for the wonderful time I have had with them and for their constant encouragement. Thanks to Jamie, Arpi, Sam, Arthi, Raghav, Dinesh, Dos, Jayanth, Mukul, Nikhil, Sahoo, Madhup, Navneet, Garima, Ashmi, and Bipin for being more like an extended family. Thanks to Divya Manjari for being a constant source of encouragement and inspiration right from my undergraduate days.

I would like to thank my late grandparents for instilling in me a thirst for knowledge and for all their love and warmth. I fondly remember the letters from Dada filled with encouragement to strive for more. His struggles to attain education in spite of adverse conditions were a source of inspiration.

Thanks to Dadu and Dida for all their wisdom, encouragement and love. Thanks to Amma for all her help, encouragement and prayers.

Special thanks are due to my dearest husband Dileep, for his love, understanding, amazing sense of humor and constant encouragement and support throughout the PhD period. I really doubt that my PhD would have been possible without him.

Finally, none of this would have been possible without the long term support and encouragement of my parents whom I call Mani and Bapi. I learnt from Bapi about hard work, sincerity and to approach everything with an open mind. And Mani to me is an epitome of compassion, sacrifice, love and wisdom. This dissertation is dedicated to them.

TABLE OF CONTENTS

List of Tables

Chapter 3

Chapter 4

List of Figures

Chapter 2

Chapter 3

Chapter 1

Introduction

The objective of this work has been to study the marine biogeochemistry of the high latitude oceans using satellite remote sensing as a unifying tool. While previous studies have shown that the biogeochemistry of these regions is unique in many respects, the study of polar oceans has been adversely affected by the inaccessibility and harsh environmental conditions that have limited ship-based measurements. However, the advent of satellite remote sensing has revolutionized the field of oceanography in terms of temporal and spatial coverage of the ocean. This is true especially for the relatively inaccessible polar oceans. In this work I have used remote sensing to measure new variables in the Southern Ocean (e.g., particulate organic carbon) and have used conventionally measured variables (e.g., chlorophyll *a* and sea surface temperature) to do the first ever quantification of interannual changes in primary production and air-sea CO_2 exchange throughout the entire Arctic Ocean.

1. Importance of high latitudes:

The high latitude oceans are of paramount importance in controlling global biogeochemical cycling. Cooling and salinization of surface waters in both the

Antarctic and the Arctic results in the formation of dense, deep water that ultimately makes its way into the Atlantic, Indian and Pacific Oceans within a timeframe of about 1600 years as part of the global thermohaline circulation [*Rahmstorf*, 2003; *Primeau*, 2005]. As they travel throughout the globe, these waters regenerate nutrients in intermediate and bottom waters, upwelling of which provides vital nutrients for the phytoplankton growing in surface waters that drive the biological pump. The formation of deep waters also affects the solubility pump which carries dissolved carbon dioxide (CO_2) from the surface towards the bottom of the ocean where it remains for hundreds to thousands of years. As a result of the solubility and biological pumps, the ocean is the world's largest reservoir of CO_2, containing 40-50 times more CO_2 than the atmosphere. Changes in the physical conditions of the high latitudes, such as intensified stratification due to increased warming and freshening caused by accelerated sea ice melting and higher riverine influx, could impede the formation of deep water [*Swift and Aagaard*, 1981; *Aagaard and Carmack*, 1989].

A signature feature of the high latitude oceans is the presence of sea-ice that greatly influences the physics, biology, and biogeochemistry of these regions. Sea ice strongly attenuates the light received by surface waters that is crucial for phytoplankton growth. Sea ice also limits the exchange of heat and gases between the atmosphere and the ocean. The melting and freezing of ice

alters the salinity that controls surface water stratification. The albedo of the ice modulates the amount of global warming resulting from an increase in the atmospheric greenhouse gas inventory. Lastly, the sea ice acts as a habitat and foraging ground for numerous marine and land-based organisms ranging from microscopic ice-algae to large penguins in the southern hemisphere and polar bears in the north.

Although the environment of the north and south polar oceans share many similarities, these two regions also differ significantly in many respects. For example, the Arctic Ocean is almost completely landlocked by the continents of North America, Europe, and Asia, causing it occasionally to be referred to as the 'Arctic Mediterranean'. This geographic configuration allows only limited entry of waters from the surrounding Atlantic and Pacific oceans. The Arctic Ocean also has a very broad continental shelf, onto which flow numerous rivers that affect both its salinity and its alkalinity. In contrast, the Antarctic landmass is comparatively surrounded by a large expanse of ocean, dominated by the Antarctic Circumpolar Current, the strongest ocean current on the planet. In addition, the Antarctic continent has a relatively narrow continental shelf and no river runoff.

Recent changes in climate have affected sea ice cover in the two polar regions very differently. While sea ice extent in the Antarctic has not experienced any anomalous changes in the last two decades [*Arrigo et al.*, 2008;

Overland et al., 2008], the loss of sea ice in the Arctic has been so dramatic that it may have crossed a tipping point beyond which summer sea ice can no longer exist [*Lindsay and Zhang*, 2005]. The summer sea ice extent in the Arctic in 2007 was 40% below the mean minimum sea ice extent of the 1980s and was 23% below that of the previously low sea ice year (2005) [*Comiso et al.*, 2008; *Overland et al.*, 2008]. Apart from a reduction in extent, Arctic sea ice has also experienced a 12% reduction in thickness since 1960 [*Holloway and Sou*, 2001]. This dramatic decrease in sea ice mass has been attributed to multiple environment factors that includes increased advection of sea ice out of the Arctic basin due to changes in wind stress [*Zhang et al.*, 2000; *Holloway and Sou*, 2002] and increased melting resulting in a positive feedback on sea ice loss [*Smith*, 1998; *Laxon et al.*, 2003]. The increase in melting is attributed to an increase in temperature [*Stewart*, 1998], longer ice-free summers [*Smith*, 1998], influx of warmer Pacific waters entering through the Bering Strait [*Fukasawa et. al.*, 2004; *Shimada et al.*, 2006], and a rise in downward longwave radiation due to changing cloud properties [*Francis and Hunter*, 2006].

2. Overview of remote sensing of the polar oceans

The one tool that has been used consistently throughout my work is satellite remote sensing. One of the most important parameters measured by remote sensing in the field of ocean biogeochemistry is chlorophyll *a* (Chl *a*), an index of phytoplankton abundance that allows us to estimate rates of

marine primary productivity. Empirical algorithms are used to convert the radiance upwelling from the ocean surface measured by all ocean color sensors into an estimate of Chl *a* concentration. Although analytical algorithms for the same purpose exist, most of the empirical algorithms outperform the analytical algorithms not only with respect to their ease of application but also in their accuracy. All ocean color sensors are 'passive' in that they measure the amount of solar energy scattered back from the ocean surface. This is in contrast to active sensors that operate by actively sending out energy to the surface and measuring the backscattered signal.

Another important remotely sensed quantity used extensively in my work is sea surface temperature (SST). The role of SST cannot be understated because of its importance in understanding of variability in the global climate. The SST used in this study was obtained from the Advanced Very High Resolution Radiometer (AVHRR) carried by a series of polar orbiting spacecraft operated by NOAA. However, SST also is available from the MODerate resolution Imaging Spectroradiometer (MODIS) operated by NASA. The AVHRR channels are located in the thermal infrared portion of the electromagnetic spectrum between 3.5-3.9 μm and 10-12.5 μm.

The final remotely sensed data set used in this study is of sea ice distributions. Sea ice concentration in a given location is determined by measurement of the passive microwave signal emitted from the surface using

the Special Sensor Microwave Imager (SSM/I). This sensor is of relatively low resolution (~25 km) but has the advantage of being able to provide data in cloudy conditions.

3. Structure of this dissertation:

This dissertation consists of three primary chapters. Chapter two focuses on the formulation and application of algorithms for satellite remote sensing of particulate organic carbon in waters dominated by two different groups of phytoplankton. Chapter three focuses on quantification of primary production in the Arctic Ocean and its interannual variations as a result of changes in sea ice. Finally, Chapter four focuses on quantification of the interannual changes in the air-sea flux of CO_2 in the Arctic Ocean.

The primary rationale behind Chapter 2 was the observation that CO_2 drawdown by phytoplankton in the Southern Ocean appears to be taxon-specific, with the haptophyte *Phaeocystic antarctica* taking up twice as much CO_2 per mole of phosphate as the diatoms [*Arrigo et al.*, 1999]. Furthermore, it has been shown that diatoms outcompete *P. antarctica* when surface waters are more stratified [*Arrigo et al.*, 1999], a condition expected to intensify as a result of continued climate change [*Sarmiento et al.*, 1998]. Alternatively, deeper mixing due to intensified westerlies in a warmer climate [*Russel et al.*, 2006] may favor the growth of *P. antarctica* over diatoms [*Arrigo et al.*, 1999]. Changes in community composition could have dramatic impacts on carbon

export to the deeper ocean if diatoms, with their lower CO_2 uptake ability, were to be favored over *P. antarctica*. Therefore, understanding the distributions of these two phytoplankton taxa is of critical importance.

Taking the cue from this difference in taxon-specific CO_2 drawdown, I investigated whether differences in the distribution of diatoms and *P. antarctica* could be quantified using a remote sensing approach. For this purpose, I developed statistical relationships between remote sensing reflectance and particulate organic carbon (POC) measured *in-situ* in waters dominated by each of these two phytoplankton taxa. I then used this information to develop an algorithm that allows us to quantify POC concentrations in waters dominated by diatoms and *P. antarctica* from space-based measurements of remote sensing reflectance. The Ross Sea sector of the Southern Ocean was a perfect natural laboratory for this purpose because the phytoplankton taxonomic distributions are so well demarcated, with the diatoms primarily dominating the western continental shelf and Terra Nova Bay while *P. antarctica* dominated the deeper mixed layers of the rest of southwestern Ross Sea. The algorithm described in Chapter 2 is one of the very few available that allows quantification of ocean carbon directly from space. Results of this work have been published in the Journal of Geophysical Research (Pabi, S. and K. R. Arrigo. 2006. Satellite estimation of marine particulate organic carbon in waters dominated by different phytoplankton

taxa, Journal of Geophysical Research, 111, C09003, doi:10.1029/2005JC003137).

In Chapter 3, the focus is shifted to the Arctic Ocean. Although the Arctic Ocean has not been historically considered a significant CO_2 sink, the biogeochemical importance of this region is being reconsidered in recent years, given the dramatic reduction in sea ice cover. If the current rate of reduction in sea ice continues, then most conservative estimates predict that the Arctic Ocean to become ice-free during the summer by 2040 [*Holland et. al.*, 2006]. However, more recent evidence suggests that summer ice-free conditions could be reached as early as 2013 [*W. Maslowski, pers. comm.*].

The first step in estimating the ecological and biogeochemical impact of these sea ice losses is to quantify annual primary production in these regions and then relate annual variations to observed changes in sea ice cover. This was done using a primary productivity algorithm that was forced by remotely sensed observations of Chl *a*, SST, and sea ice cover. A 9-year time series was constructed, which outlined regional and temporal changes in primary production in relation to changes in climate (e.g. the AO) and related changes in sea ice cover. Results of this work also have been published recently (Pabi, S., G. L. van Dijken, and K. R. Arrigo. 2008. Primary production in the Arctic Ocean, 1998-2006. Journal of Geophysical Research 113. doi:10.1029/2007JC004578.).

In Chapter 4, the Arctic work on phytoplankton productivity was expanded to include estimates of the spatial variability and interannual changes in air-sea CO_2 fluxes. While regional studies have attempted to quantify air-sea CO_2 flux in the Arctic [*Anderson and Katlin*, 2001; *Fransson et al.*, 2001; *Kaltin et al.*, 2002; *Bates et al.*, 2006; *Nitishinsky et al.*, 2007], all current basin-scale estimates were calculated from regional extrapolation [*Bates et al.*, 2006] or mass-balance calculations [*Anderson and Katlin*, 2001], with large uncertainties. Hence, a basin-scale estimate of the air-sea CO_2 flux in all north polar seas will provide a better understanding of Arctic Ocean's role as a sink for atmospheric CO_2. For this purpose, *in-situ* data from shipboard measurements of salinity, SST, and Chl *a* were used to derive an algorithm to calculate alkalinity and dissolved inorganic carbon (DIC). The partial pressure of CO_2 (pCO_2) in surface waters over the entire Arctic Ocean was calculated from spatial and temporal variations in salinity, temperature, and total alkalinity. Finally, the air-sea CO_2 flux was quantified for the Arctic Ocean from CO_2 solubility, the air-sea pCO2 gradient and wind speed.

This work provides some important insight necessary to evaluate the repercussions of global climate change on carbon biogeochemistry in the polar oceans. While some of the effects of the global climate change in these regions are already evident (e.g. reduction in sea ice), it is still unclear how other aspects will be affected (e.g. community structure, more stratification vs.

increased wind mixing). Regardless of these changes, this work leads the way in the quantification of large-scale changes in the carbon uptake capability of the polar oceans (especially the Arctic) using satellite-derived data. Using the most current remotely sensed data instead of historical data allows us to make current basin-scale estimates (nowcast), and also allows us to discern temporal trends for the prediction of near-future changes.

References:

Aagaard, K., and E. C. Carmack (1989), The role of sea ice and other fresh water in the Arctic circulation. Journal of Geophysical Research, 94, 14,485-14,498.

Anderson, L. G., and S. Kaltin (2001), Carbon fluxes in the Arctic Ocean - potential impact by climate change, Polar Research, 20(2), 225-32.

Arrigo, K. R., D. H. Robinson, D. L. Worthen, R. B. Dunbar, G. R. DiTullio, M. VanWoert, and M. P. Lizotte (1999), Phytoplankton community structure and the drawdown of nutrients and CO2 in the southern Ocean, Science (Washington D C), 283(5400), 365-367.

Arrigo, K. R., G. V. Dijken, and S. Bushinsky (2008), Primary production in the Southern Ocean, 1997-2006, J. Geophys. Res., doi:10.1029/2007JC004551, in press.

Bates, N. R. (2006), Air-sea CO2 fluxes and the continental shelf pump of carbon in the Chukchi Sea adjacent to the Arctic Ocean, Journal of Geophsical Research-Part C-Oceans, 111, 21.

Comiso, J. C., C. L. Parkinson, R. Gersten, and L. Stock (2008), Accelerated decline in the Arctic sea ice cover, Geophysical Research Letters, 35(1).

Francis, J. A. and E. Hunter (2006), New insight into the disappearing Arctic sea ice, Eos Trans. AGU, 87(46), 509.

Fransson, A., M. Chierici, L. C. Anderson, I. Bussmann, G. Kattner, E. P. Jones, and J. H. Swift (2001), The importance of shelf processes for the modification of chemical constituents in the waters of the Eurasian Arctic Ocean: implication for carbon fluxes, Continental Shelf Research, 21(3), 225-242.

Fukasawa, M., H. Freeland, R. Perkin, T. Watanabe, H. Uchida, and A. Nishina (2004), Bottom water warming in the North Pacific Ocean, Nature, 427(6977), 825-7.

Holland, M. M., C. M. Bitz, and B. Tremblay (2006), Future abrupt reductions in the summer Arctic sea ice, Geophysical Research Letters, 33(23).

Holloway, G., and T. Sou (2002), Has Arctic sea ice rapidly thinned? Journal of Climate, 15(13), 1691-701.

Kaltin, S., L. G. Anderson, K. Olsson, A. Fransson, and M. Chierici (2002), Uptake of atmospheric carbon dioxide in the Barents Sea, Journal of Marine Systems, 38(1-2), 31-45.

Laxon, S., N. Peacock, and D. Smith (2003), High interannual variability of sea ice thickness in the Arctic region, Nature, 425(6961), 947-50.

Lindsay, R. W., and J. Zhang (2005), The thinning of Arctic sea ice, 1988-2003: have we passed a tipping point? Journal of Climate, 18(22), 4879-94.

Nitishinsky, M., L. G. Anderson, and J. A. Holemann (2007), Inorganic carbon and nutrient fluxes on the Arctic Shelf, Continental Shelf Research, 27(10-11), 1584-1599.

Overland J., J. Turner, J. Francis, N. Gillett, G. Marshall, and M. Tjernström (2008), The Arctic and Antarctic: Two Faces of Climate Change, Eos Trans. AGU, 89(19), 177.

Francis, J. A. and E. Hunter (2006), New insight into the disappearing Arctic sea ice, Eos Trans. AGU, 87(46), 509.

Primeau, F. (2005), Characterizing transport between the surface mixed layer and the ocean interior with a forward and adjoint global ocean transport model, Journal of Physical Oceanography, 35(4), 545-64.

Rahmstorf, S., 2003, The concept of the thermohaline circulation. Nature, 421, 699, doi:10.1038/421699a.

Russell, J. L., K. W. Dixon, A. Gnanadesikan, R. J. Stouffer, and J. R. Toggweiler (2006), The Southern Hemisphere westerlies in a warming world: propping open the door to the deep ocean, Journal of Climate, 19(24), 6382-90.

Sarmiento, J. L., T. M. C. Hughes, R. J. Stouffer, and S. Manabe (1998), Simulated response of the ocean carbon cycle to anthropogenic climate warming, Nature, 393(6682), 245-9.

Shimada, K., T. Kamoshida, M. Itoh, S. Nishino, E. Carmack, F. McLaughlin, S. Zimmermann, and A. Proshutinsky (2006), Pacific Ocean inflow: influence on catastrophic reduction of sea ice cover in the Arctic Ocean, Geophysical Research Letters, 33(8), 4.

Smith, D. M. (1998), Recent increase in the length of the melt season of perennial Arctic sea ice, Geophysical Research Letters, 25(5), 655-8.

Stewart, R.E., H.G. Leighton, P. Marsh, G.W.K. Moore, H. Ritchie, W.R. Rouse, E.D. Soulis, G.S. Strong, R.W. Crawford,and B.Kochtubajda. (1998), The Mackenzie GEWEX study: The water and energy cycles of a major North American River Basin, Bulletin of the American Meteorological Society, (79), 2665-2683.

Swift, J. H., and K. Aagaard (1981), Seasonal transitions and water mass formation in the Iceland and Greenland seas, Deep-Sea Research, Part A (Oceanographic Research Papers), 28(10), 1107-29.

Zhang, J. L., D. Rothrock, and M. Steele (2000), Recent changes in Arctic sea ice: the interplay between ice dynamics and thermodynamics, Journal of Climate, 13(17), 3099-3114.

Chapter 2

Satellite estimation of marine particulate organic carbon in waters dominated by different phytoplankton taxa

Abstract

We present a new bio-optical algorithm for estimation of surface particulate organic carbon (POC) concentration from satellite ocean color imagery in the Ross Sea, Antarctica. This algorithm is phytoplankton taxon-specific and is based on the significant differences in the relationship between *in situ* remote sensing reflectance (*Rrs*) and POC observed for waters dominated by either *Phaeocystis antarctica* or diatoms. Differences in the size and cell composition, as well as detrital degradation products, of these two phytoplankton taxa are likely responsible for the distinct relationships between POC and *Rrs*. The algorithm requires estimates of the relative abundance of these two taxa and satellite measurements of *Rrs* to calculate surface POC concentrations. Applying this algorithm to satellite-derived *Rrs* from the Ross Sea, where distributions of *P. antarctica* and diatoms are reasonably well known, yields distributions of POC and POC:chlorophyll ratios that are in good agreement with field measurements. Performance of the algorithm can be improved by characterization of the detrital contribution

to total particle backscatter, and ultimately, remote detection of phytoplankton taxonomic composition.[1]

[1] Elements of this chapter appeared in: Pabi, S. and K. R. Arrigo. 2006. Satellite estimation of marine particulate organic carbon in waters dominated by different phytoplankton taxa, Journal of Geophysical Research, 111, C09003, doi:10.1029/2005JC003137

1. Introduction

The ocean plays an important role in the carbon cycle of our planet. Recent studies have found that oceanic sinks account for about half of the anthropogenic carbon production [*Sabine et al.*, 2004]. The biological pump is one of the vital mechanisms for sequestration of this carbon to the deep ocean. Fueled by sunlight, phytoplankton in surface waters utilize new and recycled nutrients to convert dissolved inorganic carbon to particulate organic carbon (POC) [*Eppley and Peterson*, 1979; *Longhurst and Harrison*, 1989]. A fraction of this POC is then exported to depth by various mechanisms such as consumption by zooplankton and fish and excretion of fecal pellets, as well as by particle aggregation and sinking. The export potential of POC is determined by various food web characteristics such as phytoplankton cell size, the relative abundance of large and small grazers, and bacterial remineralization [*Boyd and Newton*, 1995].

Traditionally, chlorophyll *a* (Chl) has served as a convenient proxy for phytoplankton biomass in models of carbon fixation and primary production because it is easy to measure and is specific to this group of organisms [*Behrenfeld and Falkowski*, 1997; *Taylor et al.*, 1992]. Moreover, the ability to measure Chl non-invasively from space, beginning with the Coastal Zone

Color Scanner and now using the Sea-viewing Wide Field-of-view Sensor (SeaWiFS) and the Moderate Resolution Imaging Spectroradiometer (MODIS), has allowed characterization of phytoplankton Chl variability over large temporal and spatial scales. To convert these Chl measurements to the units of C used in most productivity algorithms, a Chl:C ratio is used. This ratio may be either an explicit variable within the algorithm or an implicit component of a transfer function such as P^B_{opt} that calculates the Chl-specific production of C based on temperature and light availability.

Unfortunately, the Chl content of phytoplankton cells, and hence their Chl:C ratio, can vary widely depending on nutrient and light conditions [*Falkowski et al.*, 1985; *Geider*, 1987] making it difficult to apply a suitable Chl:C ratio to large-scale measurements of surface Chl. A better approach would be to measure phytoplankton C directly, which is not possible using currently remote sensing technology, or derive phytoplankton C from remote estimates of bulk POC, assuming that the two quantities covary [*Behrenfeld et al.*, 2005]. Although phytoplankton generally dominate the POC pool, sub-μm sized particles, including detritus, colloids, heterotrophic bacteria, and viruses, are also important [*Koike et al.*, 1990; *Longhurst et al.*, 1992]. Furthermore, these small particles are major contributors to the backscattering of light [*Morel and Ahn*, 1991; *Stramski and Kiefer*, 1991]. Nevertheless, the reduced variability of algal backscattering coefficients that have been observed when normalized to

POC instead of Chl, suggests that estimates of POC concentration can be derived from remote observations [*Vaillancourt et al.*, 2004].

Recently, surface water POC was estimated from satellite imagery using algorithms based on relationships between POC concentration and optical backscattering, beam attenuation, and normalized water leaving radiance [*Behrenfeld et al.*, 2005; *Mishonov et al.*, 2003; *Stramski et al.*, 1999]. However, the relationship between POC and the particulate backscattering coefficient appears to vary spatially. For example, the particulate backscattering coefficient measured at 510 nm was over an order of magnitude greater in the Ross Sea than in the Antarctic Polar Frontal Zone of the Southern Ocean in waters with similar levels of POC [*Stramski, et al.*, 1999]. This variability may be due to high particulate backscattering associated with differing amounts of detritus, minerals, and bacterial abundance in the two regions [*Stramski et al.*, 2001]. However, some of this variability also may be due to spatial differences in the taxonomic composition of the phytoplankton and their associated microbial communities. An ideal area in which to assess the importance of phytoplankton taxonomic composition on the relationship between POC and bio-optical properties is the southwestern Ross Sea, Antarctica.

The Ross Sea is the most biologically productive region of the Southern Ocean [*Arrigo et al.*, 1998c] and supports two major phytoplankton communities. Diatoms, primarily pennate forms such as *Fragilariopsis curta, F.*

cylindrus, and *F. kerguelensis*, as well as centric forms such as *Thalassiosira gracilis* and *T. antarctica* [*Leventer and Dunbar*, 1996], dominate in the strongly stratified waters of the western continental shelf, including Terra Nova Bay, while the haptophyte *Phaeocystis antarctica* dominates in the more weakly stratified waters of the Ross Sea polynya [*Arrigo et al.*, 1998b]. These two taxa exhibit different carbon to phosphorus uptake ratios and POC:Chl ratios [*Arrigo et al.*, 1999], cell sizes (diatoms ~6-20 μm in length, *P. antarctica* 2-5 μm in diameter), life-history strategies (*P. antarctica* can form spherical colonies of 2 mm in diameter, [*Hamm*, 2000]), and support different microbial communities. The region of the Ross Sea dominated by *P. antarctica* generally contains the highest algal biomass, with Chl concentrations reaching as high as 11 mg m^{-3} in late spring [*Arrigo et al.*, 2000a; *Arrigo et al.*, 2000b; *Smith and Gordon*, 1997], dropping to ca. 1 mg m^{-3} or lower by late January or February [*El-Sayed et al.*, 1983; *Smith and Nelson*, 1986]. Diatoms near Terra Nova Bay generally bloom about a month later than *P. antarctica* and attain maximum Chl concentrations of <10 mg m^{-3}. Surface POC concentrations associated with both of these blooms exceed 200 mg m^{-3} over most of southwestern Ross Sea and reach as high as 1400 mg m^{-3} (*Arrigo et al.*, 2000). It should be noted that because the POC:Chl ratio is spatially variable, the region of highest Chl concentration in the Ross Sea does not necessarily correspond to the region of highest surface POC concentration.

The objective of the present study is to use *in situ* data to develop an optical algorithm for the retrieval of surface ocean POC concentrations using satellite-derived estimates of remote sensing reflectance (*Rrs*) from the southwestern Ross Sea. One important goal is to quantify the extent to which the relationship between surface POC concentration and *Rrs* observed in these waters varies as a function of phytoplankton taxa. It is anticipated that accounting for bio-optical differences between phytoplankton taxa should markedly improve satellite retrievals of POC in waters where this information is reasonably well known.

2. POC Algorithm

Over 100 hydrographic stations within the southwestern Ross Sea (from 163°E to 170°W and from 74°S to 78°S, Fig. 1) were sampled during two field seasons aboard the *R/V Nathaniel B. Palmer* as part of the Research on Ocean Atmosphere Variability and Ecosystem Response in the Ross Sea (ROAVERRS) program. The first field season took place between 16 December 1996 and 8 January 1997 and the second developed in the former year, as indicated by the generally higher algal biomass. Measurements of

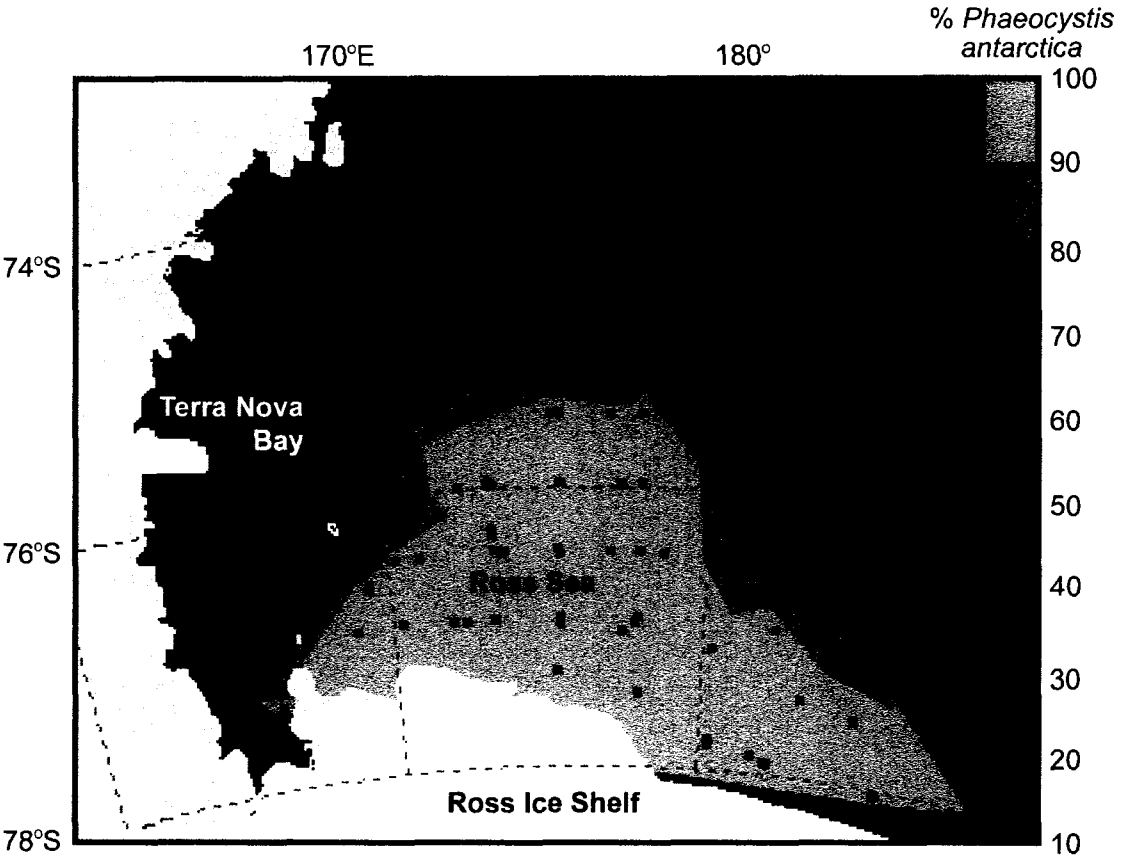

Figure 1. Map of the southwestern Ross Sea showing phytoplankton taxonomic distributions from ROAVERRS. Red dots and black dots denote locations of stations sampled during ROAVERRS 96-97 and ROAVERRS 98, respectively.

in situ POC, Chl, and bio-optical properties were obtained as described in *Arrigo et al.* [1998a].

Our approach was to calculate *Rrs* from *in situ* optical measurements and evaluate surface POC abundance as a function of phytoplankton taxonomic composition. *Rrs* just above the water surface was calculated as the ratio of water leaving radiance (L_w) to downwelling irradiance (E_d) at each station. To compute taxon-specific POC in the Ross Sea, *P. antarctica*-dominated stations and diatom-dominated stations were identified [*Arrigo et al.*, 1998a]. A separate relationship between the calculated *Rrs* and *in situ* POC was then derived for both *P. antarctica*-dominated and diatom-dominated stations. We evaluated *Rrs* at 555 nm because the low absorption by Chl in this region of the spectrum will minimally interfere with backscattering, and hence the reflectance will be maximized due to relatively higher backscatter at this wavelength [*Morel and Prieur*, 1977]. For brevity, *Rrs*(555) will be denoted *Rrs* henceforth in this study.

POC concentrations at stations dominated by either diatoms or *P. antarctica* demonstrated marked taxon-specific differences. During ROAVERRS, the average POC concentration of 915 ± 277 mg m^{-3} (n = 22) in the *P. antarctica*-dominated region was significantly higher than in the diatom-dominated region, where the bloom had not yet reached its peak and POC concentrations averaged 490 ± 205 mg m^{-3} (n=15) (ANOVA, $p < 0.005$). More importantly, the

relationship between POC abundance and *Rrs* was markedly different in waters dominated by these two taxa. In both cases, *Rrs* exhibited a statistically significant ($p < 0.05$) positive linear correlation with POC concentration, although the slope of the regression was over two-fold higher in waters dominated by *P. antarctica* (Fig 2a). The regression equation for *P. antarctica*-dominated waters is:

$$POC = 268619 * Rrs + 66.82, \; R = 0.70 \qquad (1)$$

and for diatom-dominated waters is:

$$POC = 57326 * Rrs + 153.96, \; R = 0.81 \qquad (2)$$

While Eqs. 1 and 2 represent the extreme conditions of 100% P. antarctica and 100% diatoms, respectively, the following expression allows computation of POC from Rrs for any combination of these two taxa:

$$POC = \frac{(M_1 * P + M_2 * D) * Rrs + K_1 P + K_2 D}{100} \qquad (3)$$

where P and D are the percent *P. antarctica* and percent diatoms, respectively ($P + D = 100\,\%$), M_1 = 268,619, and M_2 = 57,326 and K_1= 66.82 and

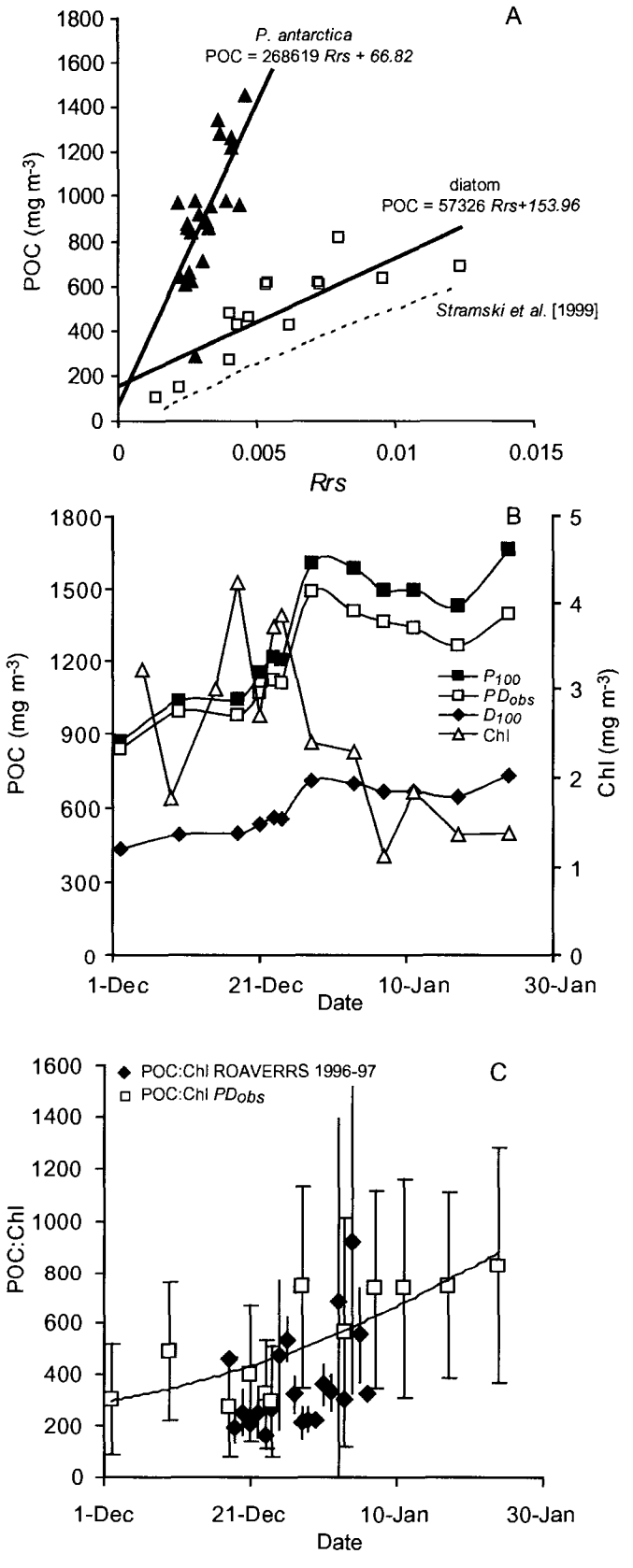

Figure 2. A) The relationship between POC and Rrs for waters dominated by either P. antarctica (solid triangles) or diatoms (open squares). The solid lines represent fit of these data by least-squares linear regression. The dashed line shows the relationship between POC and Rrs given in Stramski et al. [1999] for diatom-dominated waters. B) Temporal variation in spatial mean surface POC concentration during 1998-99 for the P100, PDobs and D100 scenarios derived from SeaWiFS data. Also shown is the spatial mean Chl concentration during this time period. C) The POC:Chl ratio computed from the satellite-based estimates of Chl and POC (PDobs scenario) shown in Fig. 2b and the surface POC:Chl measured during ROAVERRS 1996-97. Vertical bars denote one standard deviation from the mean.

K_2=153.96. When the population is either 100% *P. antarctica* or 100% diatoms, Eq. 3 simplifies to Eq. 1 or Eq. 2, respectively. For all other conditions, by substituting $D = 100\% - P$, inserting M_1, M_2, K_1 and K_2 and rearranging, we obtain:

$$POC = \frac{(211293 * P + 5732600)Rrs - 87.14 * P + 15396}{100} \qquad (4)$$

Although the expression only requires specification of the percent abundance of *P. antarctica*, diatoms are implicitly represented because $P = 100\% - D$.

3. Application of POC algorithm to SeaWiFS Images

The algorithm relating *in situ Rrs* to POC in diatom and *P. antarctica*-dominated waters (Eq. 4) was applied to individual satellite images of *Rrs*. Daily SeaWiFS Level 1A GAC (4 km resolution) data consisting of raw radiances for calculating *Rrs* were obtained from the Goddard Earth Sciences Data and Information Services Center. These images were then processed to retrieve *Rrs* using the NASA SeaWiFS Data Analysis System (SeaDAS) image processing software. Chlorophyll images were obtained from Level 2 GAC data processed using the OC4V4 algorithm [*O'Reilly et al., 1998*].

Mapping of *Rrs* and POC distributions and implementation of our POC algorithm was performed using Interactive Data Language (IDL, Research Systems, Inc.) scripts for SeaDAS. Multi-day (1-7 d) composites from December 1998 through January 1999, coinciding with the 1998 ROAVERRS cruise (no SeaWiFS data are available for the 1996-97 ROAVERRS cruise), were constructed to compensate for spatial coverage losses due to cloud cover. Unfortunately, SeaWiFS imagery from November 1998 was of limited use because of excessive cloud contamination, and has been excluded from this analysis. Temporal variation of POC from December through January were quantified by spatial averaging over the southwestern Ross Sea (colored areas in Fig. 1).

Because phytoplankton taxonomic information, which is not yet available from satellite data, is required for the application of our algorithms, distributions of *P. antarctica* and diatoms were defined in one of three different ways. First, we assumed that the southwestern Ross Sea phytoplankton blooms consisted of 100% *P. antarctica* during December and January (scenario P_{100}). Second, we assumed 100% diatom dominance over the same region and time period (scenario D_{100}). These two scenarios provide both upper and lower bounds for estimates of POC that can be obtained from measurements of *Rrs* in the southwestern Ross Sea when no taxonomic information is available. Finally, an overlay mask was created using the mean

phytoplankton taxonomic distributions measured between December and January during ROAVERRS (scenario PD_{obs}). This mask was created by triangular interpolation between stations (Interactive Data Language, IDL) and then contouring at intervals of 10% dominance (Fig. 1).

4. Temporal and spatial variation of POC under different scenarios

The mean surface POC concentration from December through January in the southwestern Ross Sea is highest for scenario P_{100}, averaging 1284±251 mg m^{-3}, followed closely by PD_{obs} (1179±208 mg m^{-3}). The lowest average POC during this time period was obtained for scenario D_{100}, which yielded values that were approximately half that of either the P_{100} or PD_{obs} scenarios (588±93 mg m^{-3}).

In all three scenarios, the surface POC concentration increases during the month of December (Fig. 2b and Fig. 3). This increase in POC concentration roughly coincides with elevated Chl (~4 mg m^{-3}) associated with the *P. antarctica* bloom in the Ross Sea polynya observed by SeaWiFS (Fig. 2b) and shown as the region of highest POC in Fig 3. Following this maximum in December, surface POC concentrations decreased moderately and then remained relatively constant throughout January (Fig. 2b). After mid-January, there is an increase in *Rrs* and POC concentration (Fig. 2b) due to a late bloom

of diatoms in Terra Nova Bay (Fig 3).

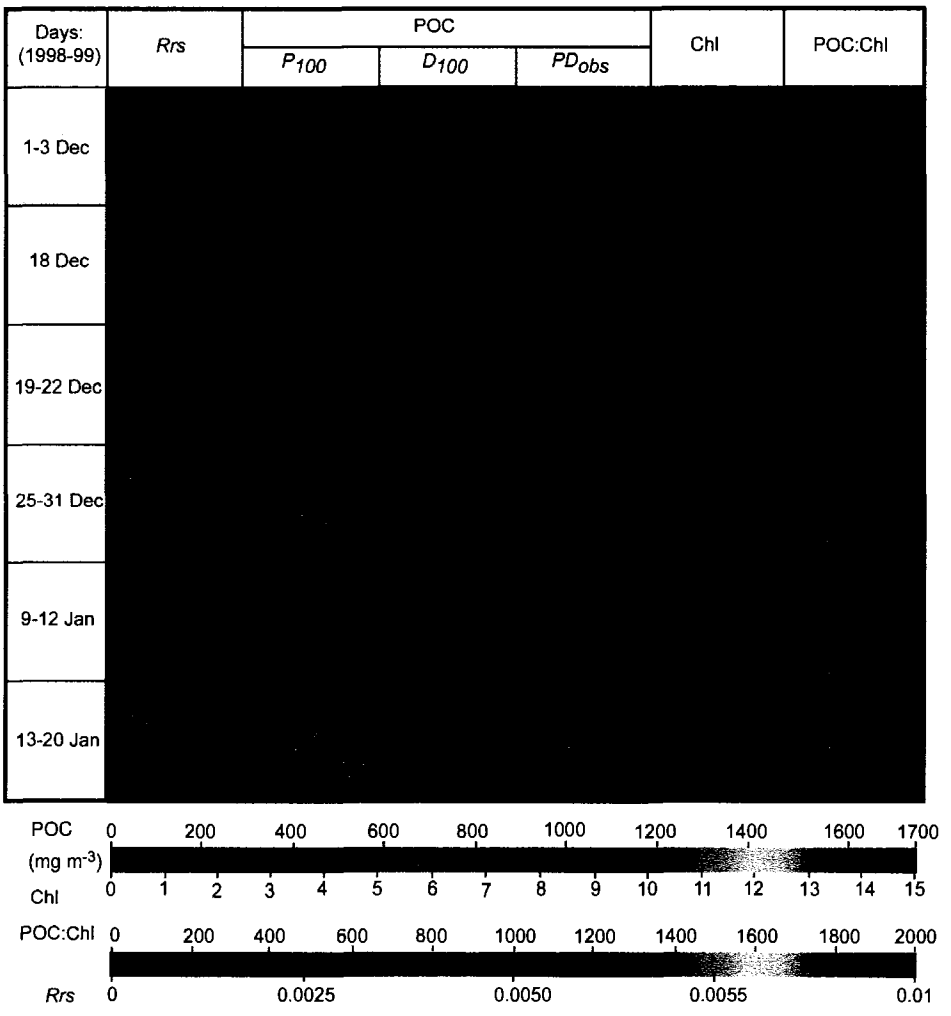

Figure 3. Temporal changes in surface water distributions of Rrs, satellite-derived POC calculated for the P100, D100 and PDobs scenarios, Chl, and POC:Chl.

It is evident that for the southwestern Ross Sea during December-January, the average POC concentration in the hypothetical *scenario* P_{100} closely matches the average POC concentration of scenario PD_{obs}, which utilizes the observed phytoplankton taxonomic distribution of the Ross Sea. The similarity between scenarios P_{100} and PD_{Obs} (Fig. 2b and Fig. 3) is due to the fact that the southwestern Ross Sea is dominated by the extensive *P. antarctica* bloom, which covers ~85% of the area, particularly in December. The POC curves for the P_{100} and PD_{Obs} scenarios start to diverge in late December and this divergence continues through January as the diatom bloom develops in Terra Nova Bay (Fig. 3) and the proportion of total POC associated with *P. antarctica* begins to decline. The POC concentration are well within the range of POC measured during the ROAVERRS cruises and also conforms well with the range of POC reported by *Gardner et al.* [2000] for the Ross Sea during 1997.

Estimates of POC from Eq. 4 using PD_{Obs} scenario and SeaWiFS-derived Chl concentrations were used to calculate a satellite-based POC:Chl ratio. When applied to the 1998 SeaWiFS data, the average POC:Chl ratio over the whole of Ross Sea increased from 273 on in early December to 825 in late 24 January. These values agree well, in both magnitude and their temporal trend, with surface water POC:Chl ratios measured during ROAVERRS,

which increased from an average of 297±145 in December to as high as 919±596 in late January (Fig. 2c).

5. Spatial variation in *Rrs*

Rrs can be expressed in terms of the inherent optical properties [*Morel and Prieur*, 1977] absorption (*a*) and backscattering (*bb*) [*Gordon et al.*, 1988],

$$Rrs(\lambda) = 0.33\frac{b_b(\lambda)}{a(\lambda)} \qquad (5)$$

where λ is wavelength. At the chosen wavelength of 555 nm, *Rrs* is primarily influenced by backscattering rather than absorption. Therefore, any observed difference in the *Rrs* in *P. antarctica*- and diatom-dominated waters is likely to be due to regional differences in the backscattering coefficient at 555 nm. Eqs. 1 and 2 demonstrate that *Rrs* can differ substantially in waters dominated by different phytoplankton taxa, even when the POC concentrations are the same. On the other hand, observed temporal changes in POC (Fig. 2b) resulted solely from changes in *Rrs* in each of the scenarios (taxonomic composition was held constant through time). Thus, it is of interest to investigate the possible causes of this difference in *Rrs* and hence backscattering properties between *P. antarctica*- and diatom-dominated regions.

Total backscattering is the sum of particulate backscattering (*bbp*) and backscattering by water molecules, the latter of which is constant and so can

be ignored in this analysis. Particles such as viruses, bacteria, suspended minerals, detritus, and phytoplankton all contribute to *bbp* (and thus to *Rrs*), but to different degrees. Backscattering is a function of size and refractivity and the dominant contribution to *Rrs* is from particles in the sub-μm size range [*Morel and Ahn*, 1991; *Stramski and Kiefer*, 1991]. Of these, viruses do not contribute appreciably to the total backscattering coefficient at 555 nm [*Stramski, et al.*, 2001]. Although viruses are the most abundant organism in the ocean [*Proctor et al.*, 1988], attaining concentrations of 10^{10} cells L^{-1} [*Bergh et al.*, 1989], their effect on *bbp* is insignificant due to their small scattering coefficient [*Balch et al.*, 2000; *Stramski and Kiefer*, 1991].

Bacterial contribution to *bbp* is often high, typically several orders of magnitude greater than that of viruses [*Stramski and Kiefer*, 1991]. Their importance was demonstrated by *Balch et al.* [2000], who showed that viral lysis of bacteria markedly reduced *bbp* within several hours of viral infection. However, bacterial abundance throughout the southwestern Ross Sea is generally low compared to other eutrophic regions [*Ducklow et al.*, 2000]. Furthermore, bacterial concentrations in the *P. antarctica*-dominated waters of the Ross Sea polynya are similar in magnitude to those measured in the diatom-dominated Terra Nova Bay [*Umani et al.*, 2002]. Hence, it is unlikely that the higher *Rrs* per unit POC observed in Terra Nova Bay is due to higher bacterial concentrations.

The effect of minerals on optical backscattering also must be considered when investigating spatial differences in surface water optical properties. Theoretical calculations for oligotrophic waters indicate that mineral particles are the most important backscattering component, comprising up to 85% of total *bbp* [*Stramski et al.*, 2001]. However, the small intercepts in Fig. 2a imply that there is little contribution to *Rrs* by constituents, such as minerals, that do not also covary with POC. It is also notable that glacial meltwater, which can have important contribution to mineral inputs are present are insignificant in the Ross Sea. Thus, although mineral content was not measured directly, it is unlikely that there was a substantial contribution of inorganic minerals to *Rrs* during our study.

Given that the higher POC-specific *Rrs* in diatom-dominated waters is not likely attributable to backscattering by viruses, bacteria, or suspended minerals, phytoplankton and any co-varying particles must play an important role. The chief covarying substance known to have a significant effect on *bbp* is sub-μm sized detrital particles [*Morel and Ahn*, 1991; *Stramski and Kiefer*, 1991]. *Reynolds et al.* [2001] attributed the higher magnitude of *bbp* in the Antarctic Polar Front Zone (APFZ), compared to the *P. antarctica*-dominated Ross Sea, to the large numbers of small non-chlorophyllous detrital particles found there. Both the elevated POC:Chl ratios (Fig. 2c) and the high detrital absorption coefficients measured during ROAVERRS [*Arrigo et al.*, 1998a] imply that

detrital or nonchlorophyllous organic content was abundant. However, detrital absorption did not differ significantly ($p<0.05$) between diatom- and *P. antarctica*-dominated stations, implying that detrital abundance did not vary markedly between these two regions. While zooplankton concentrations in the Ross Sea are reported to be somewhat higher in the diatom-dominated Terra Nova Bay than in the *P. antarctica*-dominated Ross Sea [*Tagliabue and Arrigo*, 2003], fecal-pellets of the appropriate size to impact *bbp* account for much less than 1% of the total mass flux [*Dunbar et al.*, 1998], not high enough to substantially affect *bbp* in either region.

Even though the abundance of detrital particles may be comparable in both regions, their optical characteristics can differ substantially due to structural differences between the dominant phytoplankton of the region, whose remains often compose the bulk of the detrital pool. Earlier investigations have shown that coccolithophores and diatoms scatter more light than algae without a refractive outer covering [*Morel and Bricaud*, 1986]. Furthermore, *P. antarctica*-dominated regions are often characterized by an abundance of large aggregates [*Asper and Smith*, 1999]. It is likely that the smaller sized siliceous detritus associated with diatom blooms may contribute to a higher *bbp* per unit POC than the larger, primarily organic aggregates associated with *P. antarctica*-dominated waters.

Finally, morphological differences between the two phytoplankton taxa, as opposed to their detrital byproducts, may contribute directly to the difference in *Rrs* observed in the diatom- and *P. antarctica*-dominated regions. The lower *bbp* per unit POC concentration in *P. antarctica*-dominated waters may be due to the fact that POC is contained within much larger (>1 mm) mucilaginous colonies (which possibly contribute less to *bbp*) than the POC associated with much smaller (6-20 μm) diatoms. This is consistent with the speculation by *Reynolds et al.* [2001] that the reduced Chl-specific *bbp* in the *P. antarctica*-dominated Ross Sea is due to the fact that Chl is contained in larger particles which contribute comparatively less to backscattering. Furthermore, *Stramski et al.* [1999] observed that *bbp* associated with the *P. antarctica*-dominated Ross Sea was lower than that in APFZ at moderate to high POC concentrations. They postulated that phytoplankton cells with a smaller contribution to *bbp* also contribute comparatively more to POC in the Ross Sea than in the APFZ.

6. Application of the POC algorithm

An important aspect of our POC algorithm is that its proper application requires knowledge of phytoplankton taxonomic distributions. The simplest approach would be to apply prior knowledge of taxonomic distributions in cases where these distributions are predictable in a given region. This may

work well in regions like the Ross Sea, for example, where *P. antarctica* blooms consistently form in waters north of the Ross Ice Shelf. Application of Eq. 1 (for *P. antarctica*) to satellite-derived *Rrs* from these waters results in estimates of POC that differ by <10% from those made using observed distributions of diatoms and *P. antarctica* (e.g. *PDobs*). In contrast, erroneously applying Eq. 2 to these waters (by mistakenly assuming that the southwestern Ross Sea was dominated by diatoms) would have resulted in POC estimates that were a factor of two too low. Hence, prior knowledge of taxonomic distribution may be sufficient in many cases for the application of our algorithm.

An even more desirable approach would be to acquire phytoplankton taxonomic information from satellite imagery. This has proven difficult, however, primarily due to the lack of spectral resolution of current satellite ocean color sensors. Detailed analysis of absorption spectra from a variety of phytoplankton taxa [*Garver and Siegel*, 1997] indicates that their high degree of similarity would render extraction of species composition information from satellite measurements of *Rrs* difficult, if not impossible. For example, the accessory pigments that are often used to distinguish between *P. antarctica* and diatoms (fucoxanthin for diatoms and 19'hexanoyloxyfucoxanthin for *P. antarctica*) have absorption maxima at 449 nm and 446 nm, respectively [*Zapata et al.*, 2000]. Resolving these wavelengths is beyond the ability of current

multi-spectral sensors such as SeaWiFS and MODIS, although future hyperspectral sensors may be more successful.

The use of bio-optical parameters other than absorption may have greater potential for determining phytoplankton taxa from space. For example, the different backscattering signatures of coccolithophorids [*Balch et al.*, 1991] and *Trichodesmium* [*Subramaniam et al.*, 1999], as well as phycoerythrin fluorescence by cyanobacteria [*Campbell and Iturriaga*, 1988; *Hoge et al.*, 1998], can all be used to characterize these algal groups from airborne sensors. Further work needs to be done to develop the ability to extract more phytoplankton taxonomic information from satellite data, including that of *P. antarctica* and diatoms.

However, phytoplankton taxonomic information alone may not be sufficient for appropriate application of POC algorithms based on satellite measurements of *Rrs*. The POC algorithm of *Stramski et al.* [1999] (Fig. 2a) was developed using POC and *Rrs* data collected from the APFZ, which, like Terra Nova Bay, was dominated by diatoms [*Landry et al.*, 2001]. Nevertheless, the *Stramski, et al.* [1999] algorithm yields estimates of POC for Terra Nova Bay that are only 50% of those calculated using our diatom algorithm. This suggests that spatial differences in the relationship between POC and *Rrs* may be important, even when waters are dominated by similar taxa. The difference in the POC-*Rrs* relationship between the Ross Sea and the APFZ may be due to differences in the amount of non-chlorophyllous detrital particles in the two

regions [*Reynolds et al.*, 2001]. It is hoped that in the future, even this component of POC will be resolvable by a more advanced suite of satellite sensors, furthering our ability to distinguish phytoplankton taxa and estimating total POC.

Improved quantification of POC from satellite imagery would improve our ability to study ocean biogeochemical cycling. It would provide direct information about the total oceanic POC pool without having to estimate it from observations of Chl, as is commonly done today. Bypassing Chl is particularly desirable because POC:Chl ratios vary dramatically both spatially and temporally, and therefore are difficult to apply. Accurate estimates of POC will require additional knowledge of regional variability in the relationship between Rrs (or some other bio-optical measurement) and POC. This underscores the need for future studies that investigate the underlying physical and biological reasons for the disparate optical signatures emanating from different oceanic regions.

References

Arrigo, K. R., D. H. Robinson, D. L. Worthen, B. Schieber, and M. P. Lizotte (1998a), Bio-optical properties of the southwestern Ross Sea., J. Geophys. Res., 103, 21683-21695.

Arrigo, K. R., A. M. Weiss, and W. O. Smith, Jr. (1998b), Physical forcing of phytoplankton dynamics in the southwestern Ross Sea, J. Geophys. Res., 103, 1007-1021.

Arrigo, K. R., D. L. Worthen, A. Schnell, and M. P. Lizotte (1998c), Primary production in Southern Ocean waters, J. Geophys. Res., 103, 15587-15600.

Arrigo, K. R., D. H. Robinson, D. L. Worthen, R. B. Dunbar, G. R. DiTullio, M. Van Woert, and M. P. Lizotte (1999), Phytoplankton community structure and the drawdown of nutrients and CO2 in the Southern Ocean, Science, 203, 365-367.

Arrigo, K. R., G. R. DiTullio, R. B. Dunbar, D. H. Robinson, M. Van Woert, D. L. Worthen, and M. P. Lizotte (2000a), Phytoplankton taxonomic variability and nutrient utilization and primary production in the Ross Sea, J. Geophys. Res., 105, 8827-8846.

Asper, V., and W. Smith (1999), Particle fluxes during austral spring and summer in the southern Ross Sea, Antarctica., J. Geophys. Res., 104, 5345-5359.

Balch, W. M., P. M. Holligan, S. G. Ackleson, and K. J. Voss (1991), Biological and optical properties of mesoscale coccolithophore blooms in the Gulf of Maine North Atlantic Ocean, Limnol. Oceanogr, 36, 629-643.

Balch, W. M., J. Vaughn, J. Navotny, D. T. Drapeau, V. R., J. Lapierre, and A. Ashe (2000), Light scattering by viral suspensions, Limnol. Oceanogr, 45, 492-498.

Behrenfeld, M., and P. Falkowski (1997), Photosynthetic rates derived from satellite-based chlorophyll concentration, Limnol. Oceanogr, 42, 1-20.

Behrenfeld, M. J., E. Boss, D. A. Siegel, and D. M. Shea (2005), Carbon-based ocean productivity and phytoplankton physiology from space, Global Biogeochem. Cycles, 19, GB1006.

Bergh, O., K. Y. Borsheim, G. Bratbak, and M. Heldal (1989), High abundance of viruses found in aquatic environments, Nature, 340, 467-468.

Boyd, P., and P. Newton (1995), Evidence of the potential influence of planktonic community structure on the interannual variability of particulate organic carbon flux, Deep-Sea Res., Part I, 42, 619-639.

Campbell, L., and R. Iturriaga (1988), Identification of Synechococcus spp in the Sargasso Sea by immunofluorescence and fluorescence excitation spectroscopy performed on individual cells, Limnol. Oceanogr, 33, 1196-1201.

Ducklow, H., M. Dickson, D. Kirchman, G. Steward, J. Orchardo, J. Marra, and F. Azam (2000), Constraining bacterial production, conversion efficiency and respiration in the Ross Sea, Antarctica, January-February, 1997, Deep-Sea Res., Part II, 47, 3227-3247.

Dunbar, R., A. Leventer, and D. Mucciarone (1998), Water column sediment fluxes in the Ross Sea, Antarctica: atmospheric and sea ice forcing., J. Geophys. Res., 103, 30741-30759.

El-Sayed, S., D. Biggs, and O. Holm-Hansen (1983), Phytoplankton standing crop primary productivity and near surface nitrogenous nutrient fields in the Ross Sea Antarctica, Deep-Sea Res., Part A, 30, 871-886.

Eppley, R. W., and B. J. Peterson (1979), Particulate organic matter flux and planktonic new production in the deep ocean, Nature, 282, 677-680.

Falkowski, P., Z. Dubinsky, and K. Wyman (1985), Growth-irradiance relationships in phytoplankton., Limnol. Oceanogr, 30, 311-321.

Garver, S. A., and D. A. Siegel (1997), Inherent optical property inversion of ocean color spectra and its biogeochemical interpretation. 1. Time series from the Sargasso Sea, J. Geophys. Res., 102, 18607-18625.

Gardner, W. D., M. J. Richardson, W. O. Smith (2001), Seasonal patterns of water column particulate organic carbon and fluxes in the Ross Sea, Antarctica, Deep-Sea Res., Part II, 47, 3423-3449

Geider, R. (1987), Light and temperature dependence of the carbon to chlorophyll a ratio in microalgae and cyanobacteria implications for physiology and growth of phytoplankton, New Phytologist, 106, 1-34.

Gordon, H. R., O. B. Brown, R. H. Evans, J. W. Brown, R. C. Smith, K. S. Baker, and D. K. Clark (1988), A semianalytic radiance model of ocean color, J. Geophys. Res., 93, 10909-10924.

Hamm, C. E. (2000), Architecture, ecology and biogeochemistry of Phaeocystis colonies, J. Sea Res., 43, 307-315.

Hoge, F. E., C. W. Wright, T. M. Kana, R. N. Swift, and J. K. Yungel (1998), Spatial variability of oceanic phycoerythrin spectral types derived from airborne laser-induced fluorescence emissions, Appl. Opt., 37, 4744-4749.

Koike, I., S. Hara, K. Terauchi, and K. Kogure (1990), Role of sub-micrometre particles in the ocean., Nature, 345, 242-244.

Landry, M. R., S. L. Brown, K. E. Selph, M. R. Abbott, R. M. Letelier, S. Christensen, R. R. Bidigare, and K. Casciotti (2001), Initiation of the spring phytoplankton increase in the Antarctic Polar Front Zone at 170 degrees W, J. Geophys. Res., 106, 13903-13915.

Leventer, A., and R. B. Dunbar (1996), Factors influencing the distribution of diatoms and other algae in the Ross Sea, J. Geophys. Res, 101, 18489-18500.

Longhurst, A. R., and W. G. Harrison (1989), The biological pump profiles of plankton production and consumption in the upper ocean, Prog. Oceanogr, 22, 47-123.

Longhurst, A. R., I. Koike, W. Li, J. Rodriguez, P. Dickie, P. Kepay, F. Partensky, B. Bautista, J. Ruiz, and M. Wells (1992), Submicron particles in northwest Atlantic shelf water, Deep-Sea Res., Part A, 39, 1-7.

Mishonov, A. V., W. D. Gardner, and M. J. Richardson (2003), Remote sensing and surface POC concentration in the South Atlantic, Deep-Sea Res., Part II, 50, 2997-3015.

Morel, A., and Y.-H. Ahn (1991), Optics of heterotrophic nanoflagellates and ciliates. a tentative assessment of their scattering role in oceanic waters compared to those of bacterial and algal cells, J. Mar. Res, 49, 177-202.

Morel, A., and A. Bricaud (1986), Inherent optical properties of algal cells including picoplankton theoretical and experimental results, Can. Bull. Fish Aquat. Sci, 214, 521-560.

Morel, A., and L. Prieur (1977), Analysis of variations in ocean color, Limnol. Oceanogr, 22, 709-722.

Proctor, L. M., J. A. Fuhrman, and M. C. Ledbetter (1988), Marine bacteriophages and bacterial mortality, Eos Trans. Am. Geophys. Union, 69, 1111-1112.

Reynolds, R. A., D. Stramski, and B. G. Mitchell (2001), A chlorophyll-dependent semianalytical reflectance model derived from field measurements of absorption and backscattering coefficients within the southern ocean., J. Geophys. Res, 106, 7125-7138.

Sabine et. al. (2004), The oceanic sink for anthropogenic CO2, Science, 305, 367-371.

Smith, W. O., and L. I. Gordon (1997), Hyperproductivity of the Ross Sea (Antarctica) polynya during austral spring, Geophys. Res. Lett., 24, 233-236.

Smith, W. O., and D. M. Nelson (1986), Importance of Ice Edge Phytoplankton Production in the Southern-Ocean, Bioscience, 36, 251-257.

Stramski, D., A. Bricaud, and A. Morel (2001), Modeling the inherent optical properties of the ocean based on the detailed composition of the planktonic community, Appl. Opt., 40, 2929-2945.

Stramski, D., and D. A. Kiefer (1991), Light scattering by microorganisms in the open ocean, Prog. Oceanogr, 28, 343-383.

Stramski, D., R. A. Reynolds, M. Kahru, and B. G. Mitchell (1999), Estimation of particulate organic carbon in the ocean from satellite remote sensing, Science, 285, 239-242.

Subramaniam, A., E. J. Carpenter, D. Karentz, and P. G. Falkowski (1999), Bio-optical properties of the marine diazotrophic cyanobacteria Trichodesmium spp. I. Absorption and photosynthetic action spectra, Limnol. Oceanogr, 44, 608-617.

Tagliabue, A., and K. R. Arrigo (2003), Anomalously low zooplankton abundance in the Ross Sea: An alternative explanation, Limnol. Oceanogr, 48, 686-699.

Taylor, A., A. Watson, and J. Robertson (1992), The influence of the spring phytoplankton bloom on carbon dioxide and oxygen concentrations in the surface waters of the northeast Atlantic during 1989., Deep-Sea Res., Part A, 39, 137-152.

Umani, S. F., A. Accornero, G. Budillon, M. Capello, S. Tucci, M. Cabrini, P. Del Negro, M. Monti, and C. De Vittor (2002), Particulate matter and plankton dynamics in the Ross Sea Polynya of Terra Nova Bay during the Austral Summer 1997/98, J. Mar. Sys., 36, 29-49.

Vaillancourt, R. D., C. W. Brown, R. R. L. Guillard, and W. M. Balch (2004), Light backscattering properties of marine phytoplankton: Relationships to cell size, chemical composition and taxonomy, J. Plankt. Res., 26, 191-212.

Zapata, M., F. Rodriguez, and J. L. Garrido (2000), Separation of chlorophylls and carotenoids from marine phytoplankton: a new HPLC method using a reversed phase C-8 column and pyridine-containing mobile phases, Mar. Ecol. Prog. Ser., 195, 29-45.

Chapter 3

Primary Production in the Arctic Ocean, 1998-2006

Abstract

Sea ice in the Arctic Ocean has undergone an unprecedented reduction in area and thickness in the last decade, exposing an ever-increasing fraction of the sea surface to solar radiation and increasing the habitat suitable for phytoplankton growth. Here we use a primary production algorithm that utilizes remotely sensed chlorophyll *a*, sea surface temperature, and sea ice extent data to quantify interannual changes in phytoplankton production in the Arctic Ocean between 1998 and 2006. Our results show that since 1998, open water area in the Arctic has increased at the rate of 0.07×10^6 km^2 yr^{-1}, with the greatest increases in the Barents, Kara and Siberian sectors, particularly over the continental shelf. Although pan-Arctic primary production averaged 419±33 Tg C yr^{-1} during 1998-2006, recent increases in open water area have lead to higher rates of annual production, which reached a nine-year peak in 2006. Annual production was roughly equally distributed between pelagic waters (less productive but greater area) and waters located over the continental shelf (more productive but smaller area).

Interannual differences are most tightly linked to changes in sea ice extent, with changes in sea surface temperature (related to the Arctic Oscillation) and incident irradiance playing minor roles. Estimation of primary production in the Arctic will aid the assessment of air-sea CO_2 fluxes and improve our understanding of the ecological and biogeochemical changes that could take place if ice cover continues to decrease. [1]

[1] Elements of this chapter appeared in: Pabi, S., G. L. van Dijken, and K. R. Arrigo. 2008. Primary production in the Arctic Ocean, 1998-2006. Journal of Geophysical Research 113. doi:10.1029/2007JC004578.

1. Introduction

The Arctic Ocean is currently in the forefront of climate change caused by both natural and anthropogenic factors. Since 1950, the mean annual air temperature has increased by 2-3°C and by 4°C in winter [Chapman and Walsh, 2003], resulting in markedly longer summers [*Smith*, 1998]. Temperature is projected to increase by an additional 4-5°C by the end of the 21st century [ACIA, 2005]. In conjunction with these higher temperatures, sea ice cover in the Arctic Ocean has been contracting over the past three decades, with dramatic reductions in recent years [Levi, 2000; Parkinson, 2000]. Changes in sea ice cover also include an increase in the length of the ice melt season [Smith, 1998; Rigor et al., 2002; Serreze et al., 2007; Comiso et al., 2008] and a decrease in ice thickness over the central Arctic Ocean [Rothrock et al., 1999]. The result is greater open water area and enhanced shelf break upwelling, the latter of which is expected to increase the input of nutrients from offshore waters to shallower shelves [ACIA, 2005]. While a reduction in sea ice should favor the growth of phytoplankton and increase the net air-to-sea flux of CO2 [Anderson and Kaltin; 2001; Bates et al., 2006], it also will reduce the amount of production contributed by algae growing within the sea ice [Subba Rao and Platt, 1984; Legendre et al., 1992; Gosselin et al., 1997],

although sea ice communities generally account for a relatively small fraction of total primary production in Arctic waters.

One step towards a better understanding of the effects of these environmental changes on the marine ecosystem and carbon biogeochemistry in the Arctic is to quantify current rates of basin-scale phytoplankton primary production. While a number of primary production estimates are already available for the Arctic [e.g., Platt et al., 1982; Wassman and Slagstad, 1993; Vedernikov et al., 1994; Gosselin et al., 1997; Boetius and Damm, 1998; Tremblay et al., 2002], these cover relatively small temporal and spatial scales. This is primarily due to the difficulty of sampling such a harsh and often inaccessible environment. The data that are available suggest that rates of primary production in this region are governed by its unique physical environment. For example, the shallow bathymetry of much of the Arctic Ocean greatly influences the light and nutrient inventories that are required for primary production. Discharge from rivers both enhances primary production by supplying additional nutrients and inhibits it by limiting light transmission through the water column due to high sediment loads [Kirk, 1983]. Sea ice also impacts light transmission to the water column and plays a crucial role in determining the mixed layer depth (via increased stratification during ice melt and convective mixing during sea ice formation) that, along with the critical depth (depth at which photosynthesis is balanced by

respiration), dictates the onset and demise of the spring and summer phytoplankton blooms.

Unlike other oceans, the Arctic Ocean is almost completely landlocked, except for the very shallow Bering Strait (~50 m), that connects it to the Pacific Ocean, and the Fram Strait and Canadian Archipelago that allow exchange with the Atlantic Ocean. Associated with the extensive land margin is a broad continental shelf, $5x10^6$ km^2 in area that comprises about 53% of total Arctic Ocean. This is much higher than the 9.1 -17.7% characteristic of continental shelves in other oceans of the world [Menard and Smith, 1966; Jakobsson, 2003]. Ice-free continental shelves, such as those found in parts of the Chukchi Sea, often experience intense seasonal blooms of phytoplankton owing to their favorable nutrient and light conditions [Hill and Cota, 2005].

Another unique feature of the Arctic Ocean is the large amount of riverine discharge it receives (~4000 km^3 yr^{-1}) [Shiklomanov, 2000; Carmack and Macdonald, 2002], arising from both large rivers, like the Ob, Lena, Yenisey, and Mackenzie, and numerous smaller ones in both the Amerasian and Eurasian sectors. This large freshwater input affects both the salinity and nutrient concentration of the Arctic Ocean. Furthermore, it is predicted that precipitation in a warming climate will increase significantly [IPCC, 2006], thereby enhancing the already enormous fluxes of riverine sediment discharge (670 Mt yr^{-1}) and organic carbon (12.6 Mt yr^{-1}) from the land to the Arctic

Ocean [Macdonald et al., 1998], both of which will impact nutrient and light availability and hence, phytoplankton growth.

The circulation of the Arctic Ocean is comprised of both low salinity (<33) and nutrient-rich Pacific Ocean water and relatively nutrient-poor and more saline (~34.8) Atlantic Ocean water [Maslowski et al., 2004]. The denser Atlantic water is distributed via counterclockwise currents along the continental slope at the basin margins. The relatively less saline and warmer Pacific water enters the Arctic Basin through the Bering Strait between Cape Dezhnev and west Alaska, and exits through the Canadian Archipelago, the Fram Strait and the Nares Strait. Historically, the front separating the Atlantic and Pacific water has been located over the Lomonosov Ridge, but recently this front appears to have moved closer to the Alpha-Mendeleev Ridge. This shift in the location of the front has lead to the displacement of a large quantity of Pacific water that has been replaced by nutrient-poor water from the Atlantic [Macdonald, 1996], potentially reducing the amount of nutrients available for phytoplankton growth. The nutrient-rich water from the Pacific Ocean is generally restricted to the Chukchi Sea and the Amerasian Basin [Carmack et al., 1997].

Surface concentrations of nitrate, phosphate and silicic acid in Arctic waters approach detection limits after the spring bloom [Sakshaug, 2003], suggesting that annual primary production is generally controlled by nutrient

availability. The nitrate to phosphate ratio in these waters ranges from 11 to 16 (mol:mol) [Sakshaug, 2003], suggesting that much of the Arctic Ocean is nitrogen-limited (assuming that phytoplankton require nitrogen and phosphorus at the Redfield ratio of 16:1). Phosphorus limitation of phytoplankton is more likely in waters with a salinity of <25 [Sakshaug et al., 1983] due to low phosphate content of river waters that are otherwise rich in nitrate. The silicic acid to nitrate molar ratio is spatially variable, ranging from a high of 1.9-2.4 in the Chukchi Sea and Eastern Canadian Arctic to a low of 0.31 in the Eurasian basin [Codispoti, 1979; Harrison and Cota, 1991; Sakshaug, 2003].

Finally, sea ice dynamics are integral to the regulation of primary production in much of the Arctic Ocean. In winter, brine rejection due to ice formation destabilizes the mixed layer, leading to deep vertical mixing and replenishment of surface nutrient inventories. In spring, melting of ice results in strong surface ocean stratification, exposing the nutrient-rich waters to a light regime suitable for phytoplankton growth. The resulting spring ice edge bloom forms a significant component of the annual primary production [Niebauer et al., 1990; Falk-Petersen et al., 2000]. In the study presented here, we assess seasonal and interannual changes in the physical characteristics of the Arctic Ocean, including changes in irradiance, sea surface temperature, and sea ice distributions. In addition, we quantify the changes in

phytoplankton chlorophyll a (Chl a) and primary production that accompanied interannual differences in the physical environment of the Arctic Ocean within a number of different ecological provinces (e.g., pelagic, continental shelf, etc.). This is accomplished using a primary production algorithm parameterized for the Arctic Ocean with input data from a number of satellite remote sensing platforms. This approach has the advantage of providing estimates of Arctic primary production at relatively high temporal resolution over large geographic areas.

2. Methods

2.1. Primary Production Algorithm

Daily primary productivity (PP, mg C m-2 d-1) at each satellite pixel location was using the method as described in detail in Arrigo et al. [1998] and modified by Arrigo et al. [2008]. In its simplest form, the governing equation can be represented as:

$$PP = \int_{z=0}^{z1} \int_{t=0}^{t_{end}} Chl(z) \frac{C}{Chl} G(z,t)\, dt\, dz \qquad (1)$$

where $G(z,t)$ is the net biomass-specific phytoplankton growth rate (hr^{-1}) and C/Chl is the phytoplankton carbon to Chl *a* ratio (90 g:g, see below), z1=100 m, and t_{end}=24 hours. Surface Chl *a* concentrations determined from 8-day SeaWiFS L3 images are considered to be representative of concentrations throughout the mixed layer. Below the mixed layer, Chl *a* is assumed to

decrease exponentially with depth as described by *Arrigo et al.* [2008]. In the Arctic, the spring-summer mixed layer depth (MLD) is reported to vary between 15 m and 20 m [*McLaughlin et al.*, 2002]. In the present study, the MLD is assumed to be 20 m, similar to the value used by *Walsh et al.* [2005]. Sensitivity studies revealed that the algorithm is not sensitive to MLD; for example, increasing the MLD to 50 m increased the calculated depth-integrated primary production by only 10%. $G(z,t)$ is calculated each hour (t) and at each depth (z) as a function of the temperature-dependent upper limit to net growth and a light limitation term, L (dimensionless):

$$G(z,t) = G_0 \exp[rT(z)]\, L(z,t). \qquad (2)$$

where Go is the maximum microalgal net growth rate at 0°C (0.025 hr^{-1}) and r is a rate constant (0.0633 $°C^{-1}$) that determines the sensitivity of G to temperature, T (°C) [*Eppley*, 1972]. The light limitation term, L(z,t), is calculated for each depth and each hour as

$$L(z,t) = 1 - \exp\left(-\frac{PUR(z,t)}{E_k'(z,t)}\right) \qquad (3)$$

where $PUR(z,t)$ is photosynthetically usable radiation [*Morel*, 1978; 1987; 1991] and $E_k'(z,t)$ is the spectral photoacclimation parameter [*Arrigo and Sullivan*, 1994]. *PUR* is similar to photosynthetically active radiation (PAR, the total radiation between 400 and 700 nm), except that *PUR* is weighted by the

phytoplankton specific absorption spectra, as described by *Morel* [1978], and represents the subset of PAR that is readily absorbed by phytoplankton. $E_k'(z,t)$ varies with light history, simulating phytoplankton photoacclimation to a changing light regime. Downwelling spectral irradiance at the ocean surface was determined using the radiative transfer model of *Gregg and Carder* [1990], corrected for fractional cloud cover (from NCEP Reanalysis data) and specular reflectance [*Arrigo et al.*, 2008]. Downwelling spectral irradiance was propagated through the water column according to Beer's law as described in *Arrigo et al.* [1998] using the inherent optical properties typical of the Arctic ocean [*Wang and Cota*, 2003].

2.2. Algorithm Input Data

Chlorophyll a: Surface Chl *a* concentrations were determined from Level 3 (9 km resolution) SeaWiFS ocean color data (operational August 1997-present, distributed by http://oceancolor.gsfc.nasa.gov/) using the OC4v4 algorithm [*O'Reilly et al.*, 1998]. The OC4v4 Chl *a* algorithm is suitable for Case I waters (where the optical properties are dominated primarily by Chl *a*). However, we recognize that a large sediment load as well as CDOM (colored dissolved organic matter) from river discharge has the potential to alter these optical properties and impact Chl *a* retrievals. Hence, to account for the influence of

riverine sediments in coastal waters, primary production was quantified both by including and excluding questionable SeaWiFS pixels that were in proximity to the river discharge plumes (these pixels were flagged as being turbid in the SeaWiFS data). All results reported here have had river-influenced pixels removed. Exclusion of pixels associated with river discharge reduced the pan-Arctic primary production by less than 10% and therefore does not greatly affect the results.

In addition, SeaWiFS data for the Arctic Ocean are only available from March through September, after which the SeaWiFS sensor begins focusing its data collection and storage on more southerly waters. Because irradiance is minimal outside this data collection period, the lack of SeaWiFS data at other times of year is likely to result in only a slight underestimate of annual primary production (<10%).

Sea Surface Temperature: Sea surface temperature (SST) is based on the Reynolds Optimally Interpolated SST (OISST) Version 2 product [*Reynolds et al.*, 2002] obtained from NOAA (http://www.emc.ncep.noaa.gov/research/cmb/sst_analysis/).

Open Water Area: Open water area was estimated from Special Sensor Microwave Imager (SSM/I) 37 and 85 GHz bands using the Polynya Signature Simulation Method (PSSM) algorithm [*Markus and Burns*, 1995] which allows for the determination of sea ice presence/absence at 6.25 km resolution. A

given pixel is defined as being ice covered wherever the sea ice concentration is greater than approximately 10%.

All satellite remote sensing data were processed using Interactive Data Language (IDL). The primary productivity algorithm was encoded using Fortran 77. All computations were done at the High Productivity Technical Computing facility of Stanford's Center of Computational Earth and Environmental Science, which is composed of a Sun Sparc cluster running Solaris 10.

2.3. Defining Regions of Interest

The Arctic Ocean is defined as all waters north of the Arctic Circle (66° 33′ 39″). For the purpose of characterizing spatial differences, we divided the Arctic Ocean into eight geographic sectors and four open-water ecological regimes. The geographic sectors were demarcated by longitude (Fig. 1a) and include the Chukchi (180° to 160°W), Beaufort (160°W to 100°W), Baffin (100°W to 45°W), Greenland (45°W to 15°E), Barents (15°E to 55°E), Kara (55°E to 105°E), Laptev (105°E to 150°E), and Siberian (150°E to 180°) sectors.

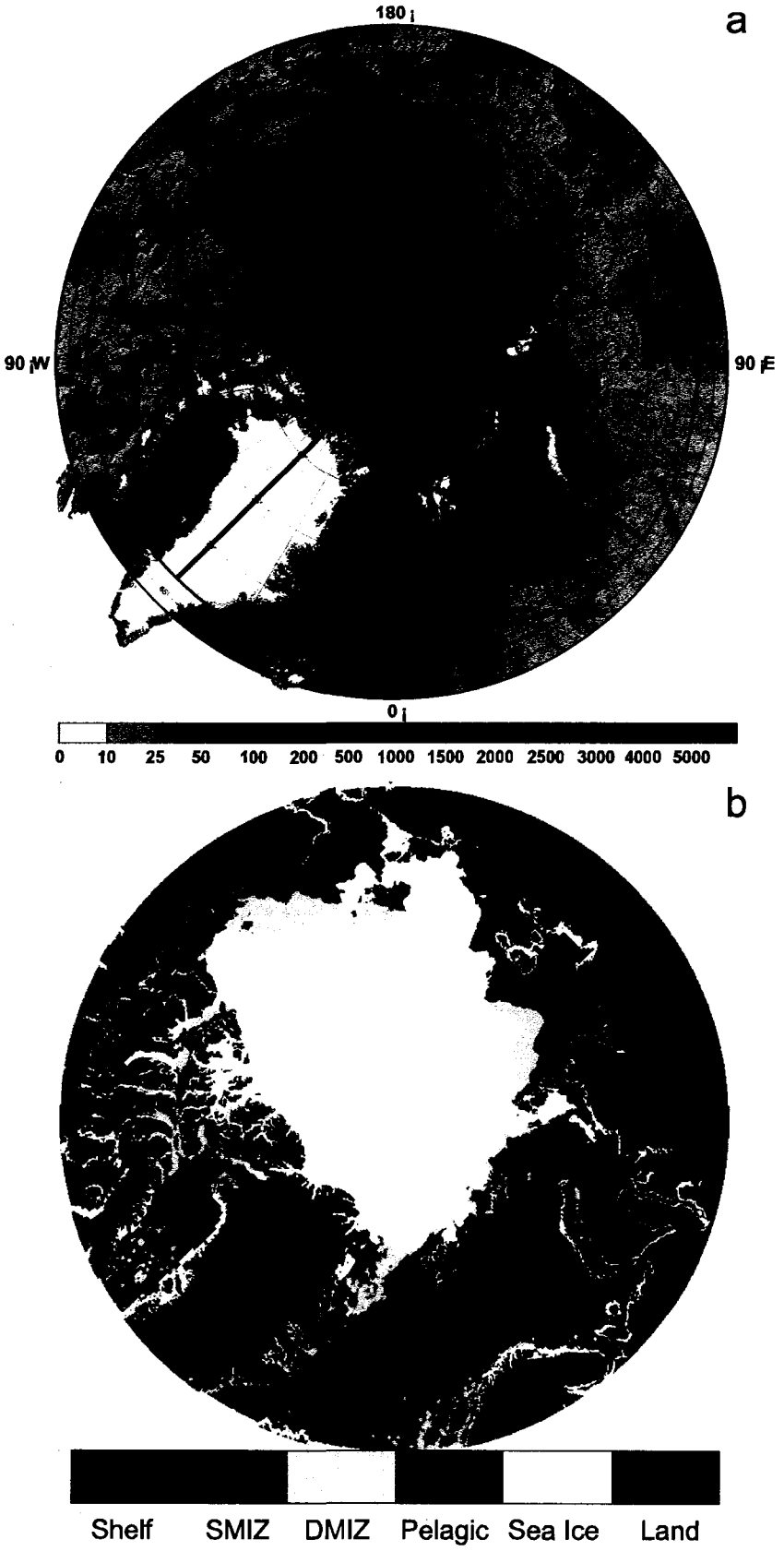

Figure 1. Map of the study area showing (a) bathymetry (in meters), the location of the Arctic Circle (shown in black), and the distribution of the eight geographic sectors (map adapted from the International Bathymetric Chart of the Arctic Ocean) and (b) an example of the locations of the four ecological provinces (September 1998).

The four ecological provinces include the pelagic, the shelf, the deep water marginal ice zone (DMIZ) and the marginal ice zone (MIZ) over the continental shelf (SMIZ). All provinces vary in size over time due to continual changes in sea ice extent (Fig. 1b). The ecological provinces were demarcated using a combination of sea ice distributions and bathymetric information. The pelagic and shelf provinces are defined as those waters with depths of >220 m and ≤220 m, respectively (in accordance with the definition of the Arctic continental shelf by *Walsh et al.*, 2005), and that have remained ice-free for >14 consecutive days. A pixel is considered part of the MIZ if it has been ice-free for ≤14 days [*Arrigo et al.*, 2008]. If an MIZ pixel is located on the shelf, then it is defined as belonging in the SMIZ, otherwise it is defined as being part of the DMIZ. The SMIZ and DMIZ together constitute the total Arctic Ocean MIZ.

2.4. Algorithm Validation

In the present study, we chose to use the surface Chl *a* concentrations produced from SeaWiFS data by the standard OC4v4 algorithm [*O'Reilly et al.*, 1998] rather than the regional Arctic algorithm of *Wang and Cota* [2003]. This decision was based on a recent assessment by *Matsuoka et al.* [2005], who used measurements of in-water apparent optical properties and Chl *a* to show that the standard OC4v4 Chl *a* algorithm used with SeaWiFS data performs as well or better in Arctic waters than the algorithm of *Wang and Cota* [2003]. The two

algorithms exhibited root mean square (RMS) errors between *in situ* and satellite-derived Chl *a* of 25% and 30%, respectively.

The best way to validate our primary production algorithm would be to compare algorithm-derived production with *in situ* estimates of primary production made at the same time and location. However, because of the small number of cloud-free images that correspond to available *in situ* measurements in the Arctic, this approach is not feasible. Thus, to validate our primary production algorithm we assumed that retrievals of surface Chl *a* by SeaWiFS were reliable (in waters not influenced by river runoff) and then compared regressions of daily primary production against surface Chl *a* produced by our algorithm to similar regressions generated from *in situ* Arctic data.

In situ measurements of primary production and concurrent surface Chl *a* concentrations used in this analysis were obtained from Phase I and II of the Shelf Basin Interaction (SBI) program [*http://www.eol.ucar.edu/projects/sbi/*] conducted in the Chukchi and Beaufort sectors of our study area during 2002-2004. The relationship between surface Chl *a* and daily primary production predicted by our algorithm for the SBI study region agrees well with the *in-situ* data, particularly in spring (Fig. 2a). In summer, there are clear cases where the algorithm underestimates daily production at low surface Chl *a* concentrations (Fig. 2b). These were stations with a particularly strong

subsurface Chl *a* maximum [*Hill and Cota*, 2005], which was not detected by the SeaWiFS sensor. Unfortunately, the prevalence of subsurface Chl *a* maxima in the Arctic Ocean is not well known so the significance of the problem cannot be adequately determined at this time.

The relationship between surface Chl *a* and computed primary production is sensitive to the value used for the C:Chl *a* ratio. A value of 90 produced the best agreement between algorithm-derived and *in situ* primary production. This is encouraging because 90 is similar to the C:Chl *a* ratio determined to be optimal for computing primary production in the Southern Ocean (88.5) using the same algorithm as that used here [*Arrigo et al.*, 2008]. It is also well within the range of 25-100 reported for *in situ* C:Chl *a* measurements from the Arctic [*Platt et al.*, 1982; *Buck et al.*, 1998; *Sakshaug*, 2003]. Although the paucity of Arctic data makes it difficult to validate our algorithm across the full range of surface Chl *a* values that have been measured, our algorithm has been validated over a much larger range of Chl *a* concentrations and rates of daily primary production in the Southern Ocean [*Arrigo et al.*, 2008], further supporting its use in northern polar waters.

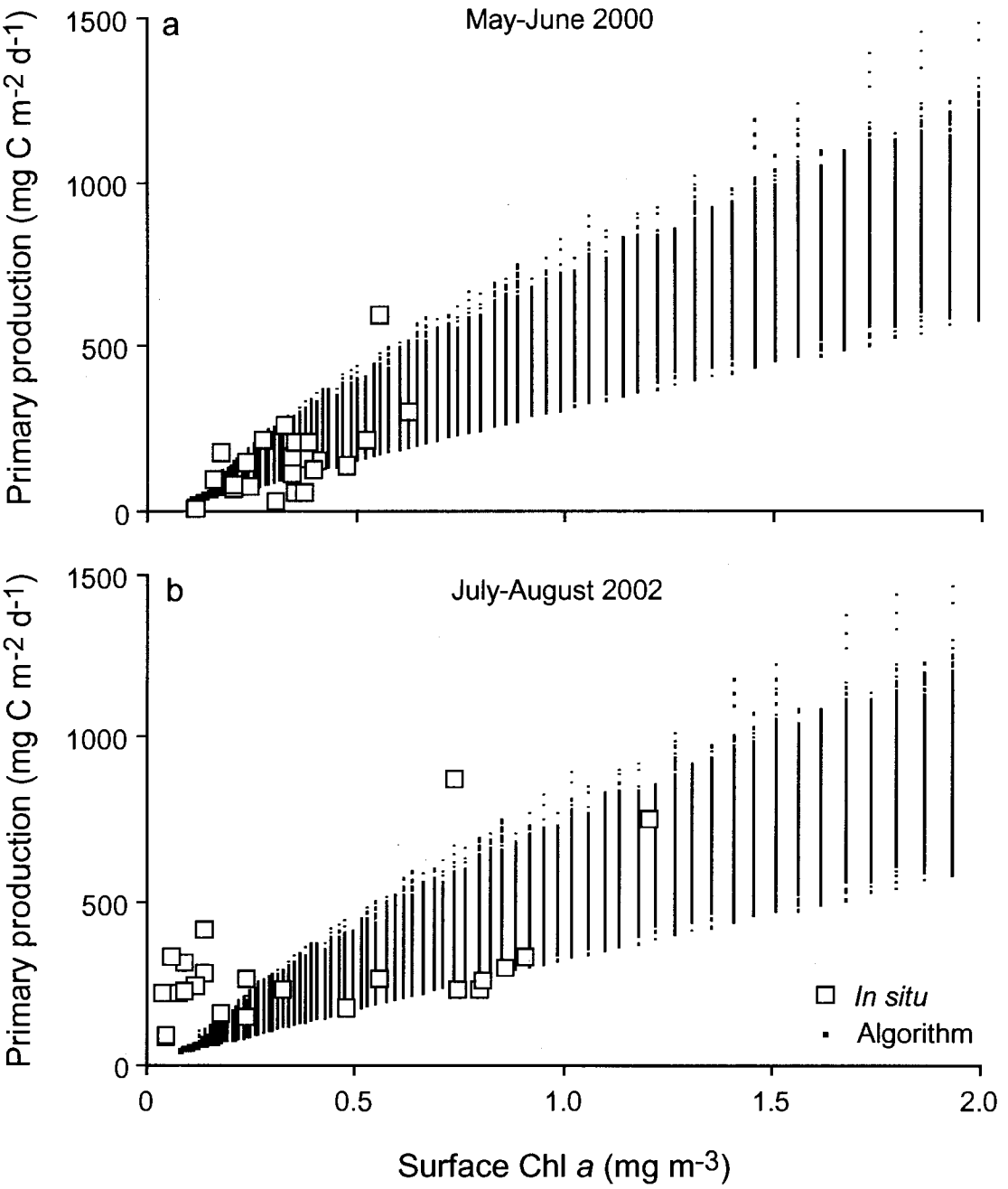

Figure 2. Plots of surface Chl *a* versus daily primary production estimated from our primary production algorithm and measured in situ at discrete stations from the Chukchi and Beaufort seas obtained during the Shelf Basin Interaction program during a) May-June 20 02 and b) July-August 2002. Algorithm output used in this analysis was restricted to those times and locations for which in situ data were available.

3. Results

3.1 Interannual Ice Dynamics

3.1.1. Pan-Arctic

During the 9-year period of interest (POI) of this study (1998-2006), the annual mean open water (ice-free) area in the Arctic Ocean exhibited a dramatic and statistically significant (as per regression analysis) upward trend (regression coefficient R^2=0.78, probability p= 0.002), increasing at the rate of ~0.07×10^6 km^2 yr^{-1} (Fig. 3a). This trend is consistent with earlier studies reporting a substantial loss of sea ice in recent decades, with Arctic ice cover decreasing by ~0.80×10^6 km^2 (7.4%) between 1978 and 2002 [*Johannessen et al.*; 1999; *Cavalieri et al.*, 2003]. Open water area during the POI was at its nine-year low in 1998, averaging ~3.8×10^6 km^2 over the year; the maximum annual mean open water area was attained in 2006, averaging 4.6×10^6 km^2. Although annual mean open water area in the Arctic increased by 19% between 1998 and 2006, this increase was not uniform throughout the year. For example, during August-September (the peak open water season, Fig. 4a), open water area averaged $6.9 \pm 0.03 \times 10^6$ km^2 during the POI, and increased by 11% between 1998 and 2006 (Fig. 3c).

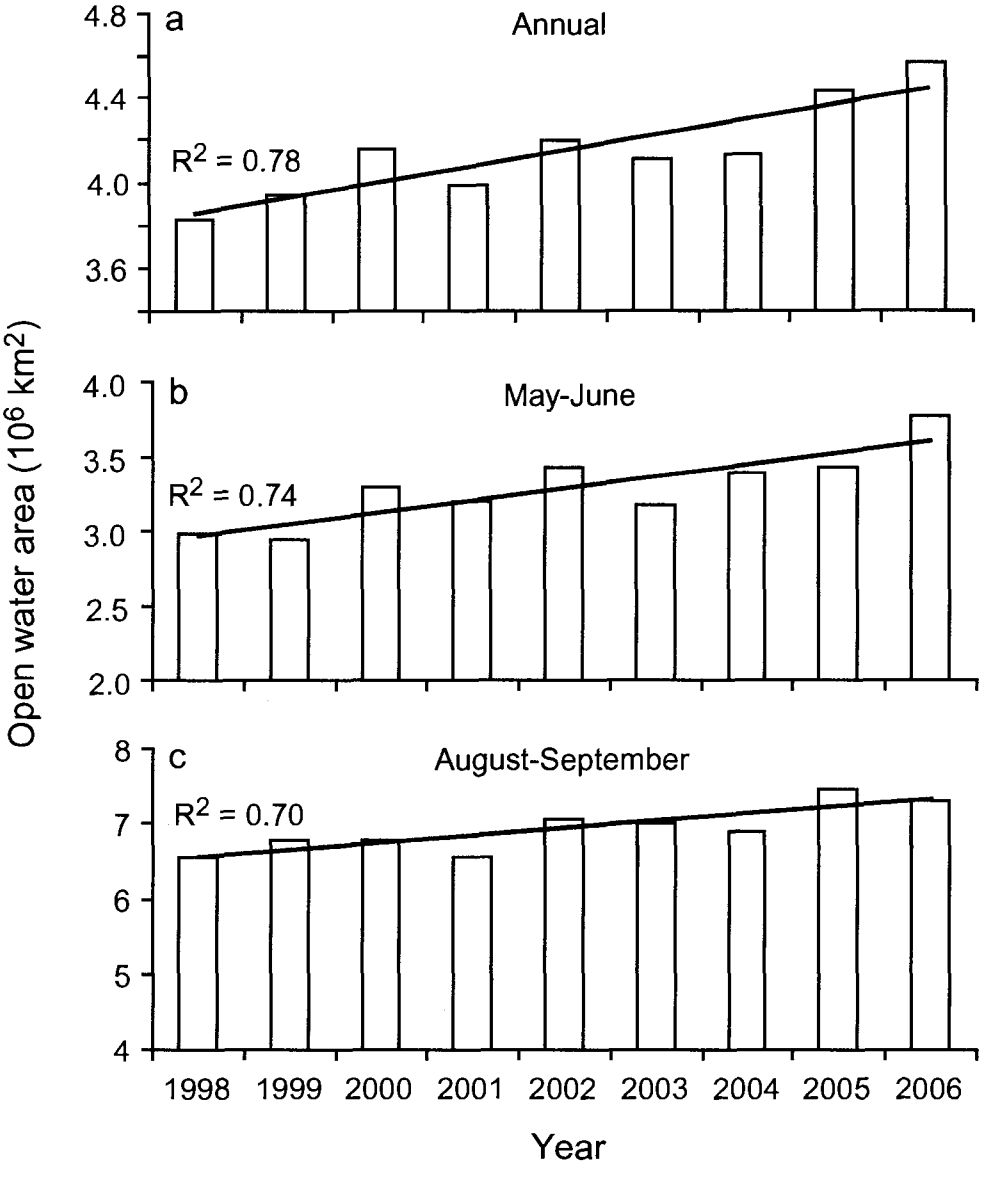

Figure 3. Open water area in the Arctic Ocean averaged over a) the entire year, b) the months of May-June (time of the a spring bloom), and c) the months of August-September (time of maximum open water). Also shown is the long-term trend in mean open water area.

However, during May-June (the peak of the spring phytoplankton bloom), open water area averaged only $3.3 \pm 0.02 \times 10^6$, but the change over time was more pronounced than in summer, increasing by 26% between 1998 and 2006 (Fig. 3b). This pattern reflects the fact that in recent years, Arctic sea ice has been retreating progressively earlier in the year.

Recent increases in annual mean open water area in the Arctic are the result of changes in both the timing of sea ice advance and retreat (earlier retreat and later advance will result in higher annual mean open water area) and the maximum amount of open water area attained during the year. For example, the relatively large annual mean open water area observed in 2002 and 2005 were due mainly to the extensive open water area in summer. On the other hand, open water area in the summer was actually lower in 2006 (the lightest sea ice year) than it was in 2005 (Fig 3c). However, the retreat of sea ice began relatively early in 2006 and the advance began later (Fig. 4a), more than compensating for the low summertime open water area. The early retreat of sea ice in recent years appears to be coupled with the higher early season SST, particularly in 2005 and 2006 (Fig. 4b). The annual mean SST in the Arctic Ocean increased from -0.07°C in 1998 to +0.26°C in 2006. Unfortunately, it is not clear from these data whether higher SST led to the increase in open water area or vice-versa. However, the peak in SST (Fig. 4b)

correlates well with the timing of peak open water area (Fig. 4a), with the latter lagging the annual SST peak by approximately 20 days.

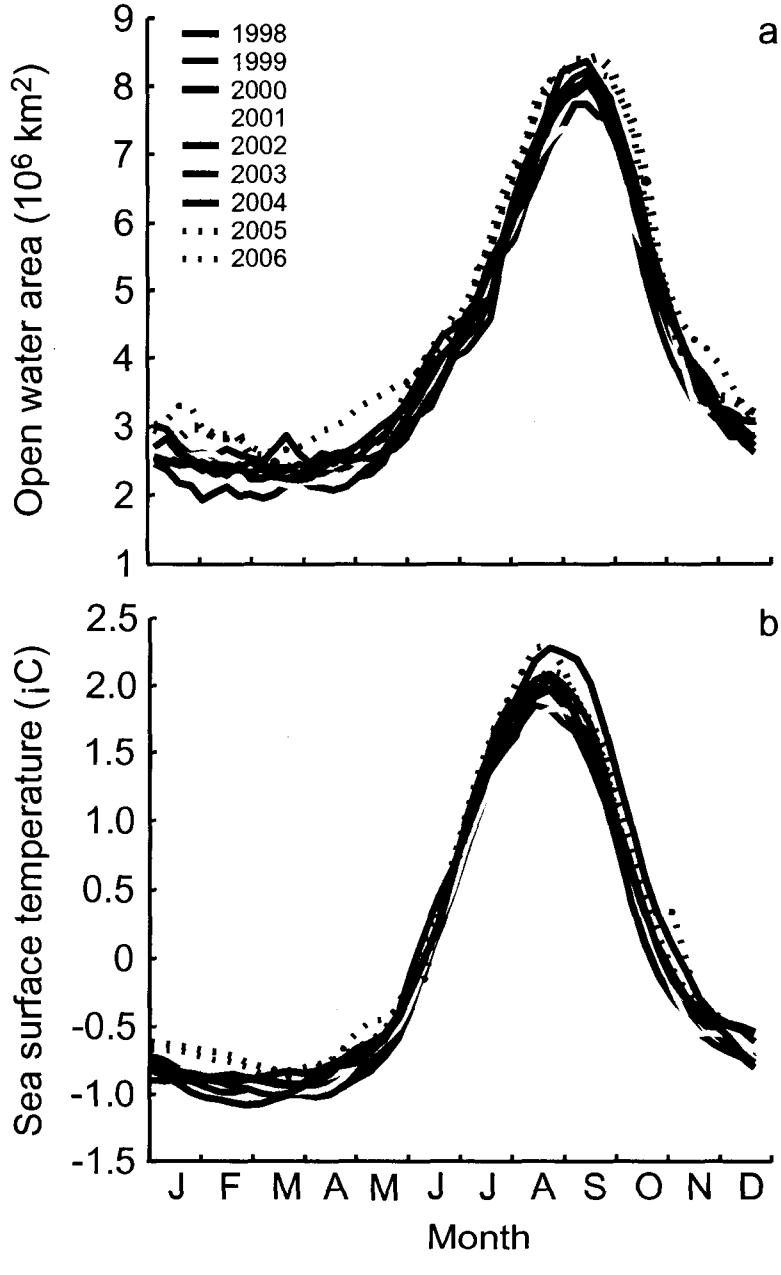

Figure 4. Weekly changes in a) open water area and b) sea surface temperature during 1998-2006.

3.1.2. Geographic Sectors

Among all geographic sectors, the Greenland and Barents had the largest annual mean open water area, averaging ~1.6±0.36 × 10^6 km^2 and ~1.1±0.11 × 10^6 km^2, respectively (Fig. 5) during the POI. Whereas open water area in most sectors was reduced to near zero in winter, the Barents and Greenland sectors had significant amounts of permanently open water (Fig. 12c), which appears to have increased in the Barents sector in recent years. The lowest annual mean open water area in the Arctic was observed in the Siberian and Laptev sectors, averaging only 0.18±0.06 × 10^6 km^2 and 0.22±0.06 × 10^6 km^2, respectively. Interannual differences in annual mean open water area were most dramatic in the Eurasian sectors, with the annual mean open water area in the Siberian, Laptev and Kara sectors being 276%, 134%, and 114% higher, respectively, in their lightest sea ice year than in their heaviest.

Over the POI, the rate of change in open water area varied substantially by geographic sector (Fig. 5). The Barents, Kara and Siberian sectors experienced greater absolute increases in open water area than any other sector, with the annual mean open water area increasing at a rate of 25,047 km^2 yr^{-1} (about 2% of the 1998 extent), 20,046 km^2 yr^{-1} (about 10% of the 1998 extent), and 14,416 km^2 yr^{-1} (about 30% of the 1998 extent), respectively, over the POI, although this increase was only statistically significant in the Siberian

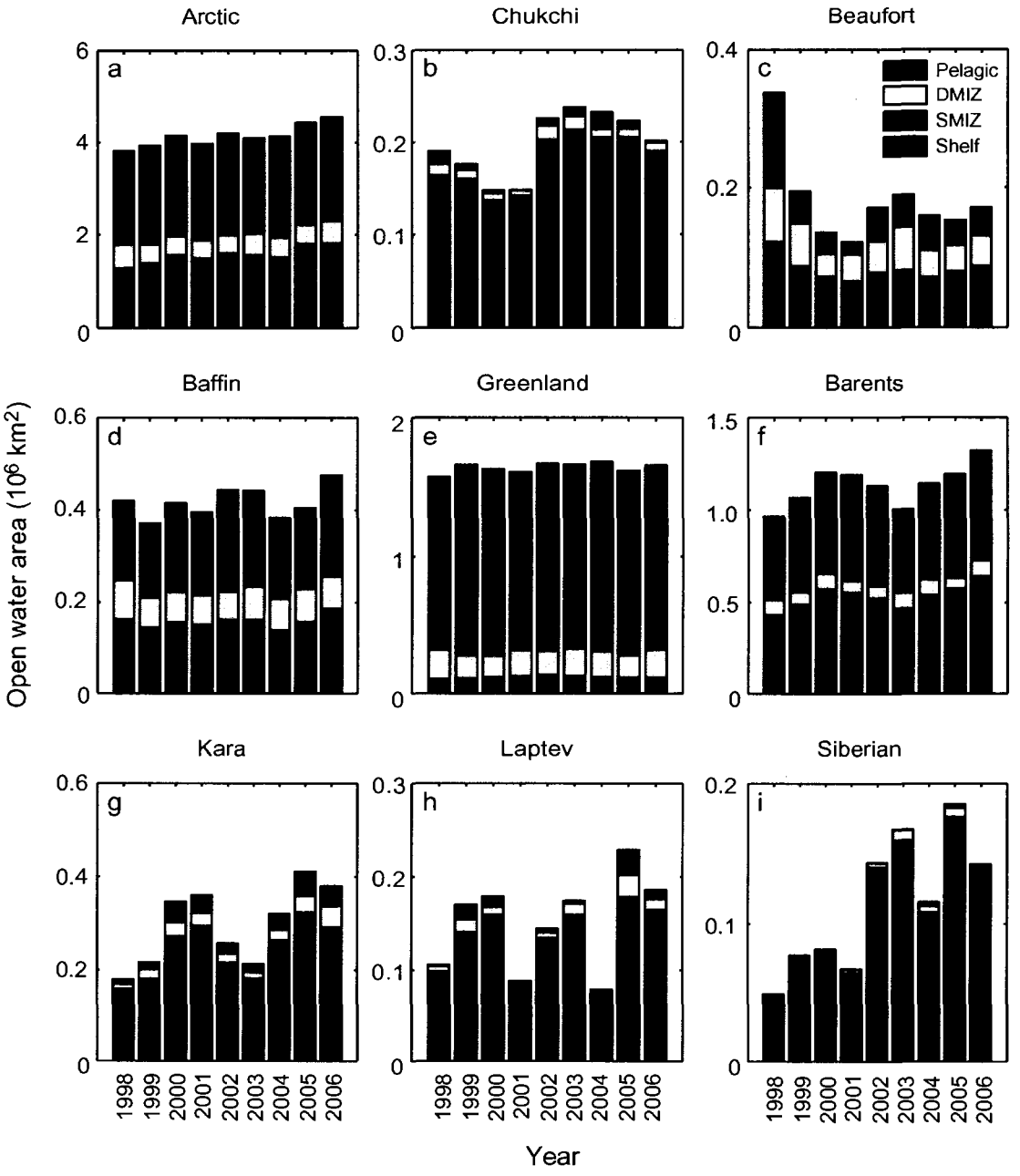

Figure 5. Annual mean open water area in the Arctic Ocean for each ecological province and geographical sector during 1998-2006.

sector. In other sectors, open water area increased at a rate of only ~5,000 $km^2\ yr^{-1}$ (except for the Beaufort, where open water area decreased over time). The relative increase in open water area was largest in the Siberian sector, increasing 276% between 1998 ($0.05\times 10^6\ km^2$) and 2005 ($0.19\times 10^6\ km^2$). In terms of absolute area, the Barents sector experienced the largest rise in open water area, increasing by $0.36 \times 10^6\ km^2$ between 1998 and 2006. Despite having the largest open water area of all the geographic sectors, changes in open water area in the Greenland sector were far less dramatic, with the minimum and maximum open water years (1998 and 2004, respectively) differing by only 7%. This small change is due to a large area of permanently open water within the pelagic province that has persisted throughout the POI. Interestingly, open water area in the Beaufort sector actually dropped during the POI, decreasing by 178% over the 9-year study period, from a maximum area of $0.38 \times 10^6\ km^2$ in 1998 to a minimum of $0.12 \times 10^6\ km^2$ in 2001. However, this trend was dominated by the large drop in ice cover between 1998 and 1999 (Fig. 5c). Since then, interannual changes in open water area in the Beaufort have been small.

3.1.2. Ecological Provinces

3.1.2.1. Annual Mean Open Water Area

Pelagic. The largest ecological province in the Arctic Ocean is the pelagic, encompassing an annual mean area of $2.16 \pm 0.07 \times 10^6$ km^2 during the POI (Fig. 5a). In the Greenland and the Barents sectors, the pelagic province comprises 82% (1.34×10^6 km^2) and 47% (0.53×10^6 km^2), respectively, of the total open water area in these sectors (Fig. 5e and f). The Baffin and Beaufort sectors also have significant pelagic provinces, covering 45% (0.18×10^6 km^2) and 25% (0.05×10^6 km^2), respectively, of their total area during the POI (Figs. 5c and d).

Shelf. The shelf province is the second largest ecological province in the Arctic Ocean with an annual mean open water area of $0.90 \pm 0.1 \times 10^6$ km^2 (Fig. 5a). The two geographic sectors with the largest shelf province (in absolute area) were the Barents and Chukchi (Fig. 5b and f), where open water area averaged 0.37×10^6 km^2 (32% of annual mean open water area in that sector) and 0.12×10^6 km^2 (59% of annual mean open water area in that sector), respectively, during the POI. Other geographic sectors with substantial shelf provinces were the Siberian, Laptev, and Kara sectors, where the shelf comprised 47% (0.05×10^6 km^2), 46% (0.07×10^6 km^2), and 39% (0.12×10^6

km^2), respectively, of total open water area in their respective sectors during the POI.

SMIZ. The area of the SMIZ province was slightly smaller than the shelf province, with an annual mean open water area of $0.70 \pm 0.04 \times 10^6$ km^2 (Fig. 5a). Geographic sectors with a relatively large SMIZ include the Siberian, Laptev, Kara and Chukchi sectors, where the SMIZ was nearly as large as the shelf province, averaging 49% (0.05×10^6 km^2), 44 % (0.06×10^6 km^2), 41% (0.12×10^6 km^2) and 31% (0.06×10^6 km^2), respectively, of total open water area during the POI. The largest SMIZ in terms of absolute area was in the Barents sector, averaging 0.16×10^6 km^2, although it comprised only 14% of the total open water area in that sector.

DMIZ. The DMIZ is the smallest of the four ecological provinces, averaging just $0.43 \pm 0.04 \times 10^6$ km^2 over the POI (Fig. 5a). The DMIZ was largest in the Greenland sector, where it averaged 0.19×10^6 km^2, nearly 50% of the total DMIZ area of the Arctic. This province was also relatively large in the Beaufort sector (0.08×10^6 km^2), where it comprised 27% of the open water area, and in the Barents (0.05×10^6 km^2) and Baffin sectors (0.07×10^6 km^2) where it comprised 17% of open water area.

3.1.2.2. Changes Over Time

Annual cycle. Open water area in the pelagic province of the Arctic Ocean typically increases from a winter low of 1.2-1.7 $\times 10^6$ km^2 (range reflects values for different years) to a peak of 3.2-3.6 $\times 10^6$ km^2 some time between late August and late October (Fig. 6).

Winter ice cover is much heavier in the other ecological provinces, such as the shelf, where open water area increased by an order of magnitude from a January minimum of only 0.12-0.30 $\times 10^6$ km^2 to a maximum of 2.4-3.4 $\times 10^6$ km^2 in early September to late October. The open water area in the SMIZ and DMIZ increased even more dramatically, rising seasonally by two orders of magnitude, from a low of 0.02-0.09 $\times 10^6$ km^2 and 0.01-0.07 $\times 10^6$ km^2, respectively, in January to a peak of 2.1-2.6 km^2 and 1.2-2.5 $\times 10^6$ km^2, respectively, during the peak open water period (mid-July to early September). The length of the open water period in the shelf, SMIZ, and DMIZ provinces were in general shorter than that of the pelagic province.

Interannual trends. The annual mean open water area in the pelagic province of the Arctic increased annually at a rate of 0.17 $\times 10^6$ km^2 yr^{-1} (R^2= 0.42) between 1998 and 2006, although this increase is not statistically significant (p=0.06, Table 1). Although smaller in area, the secular increase in annual mean open

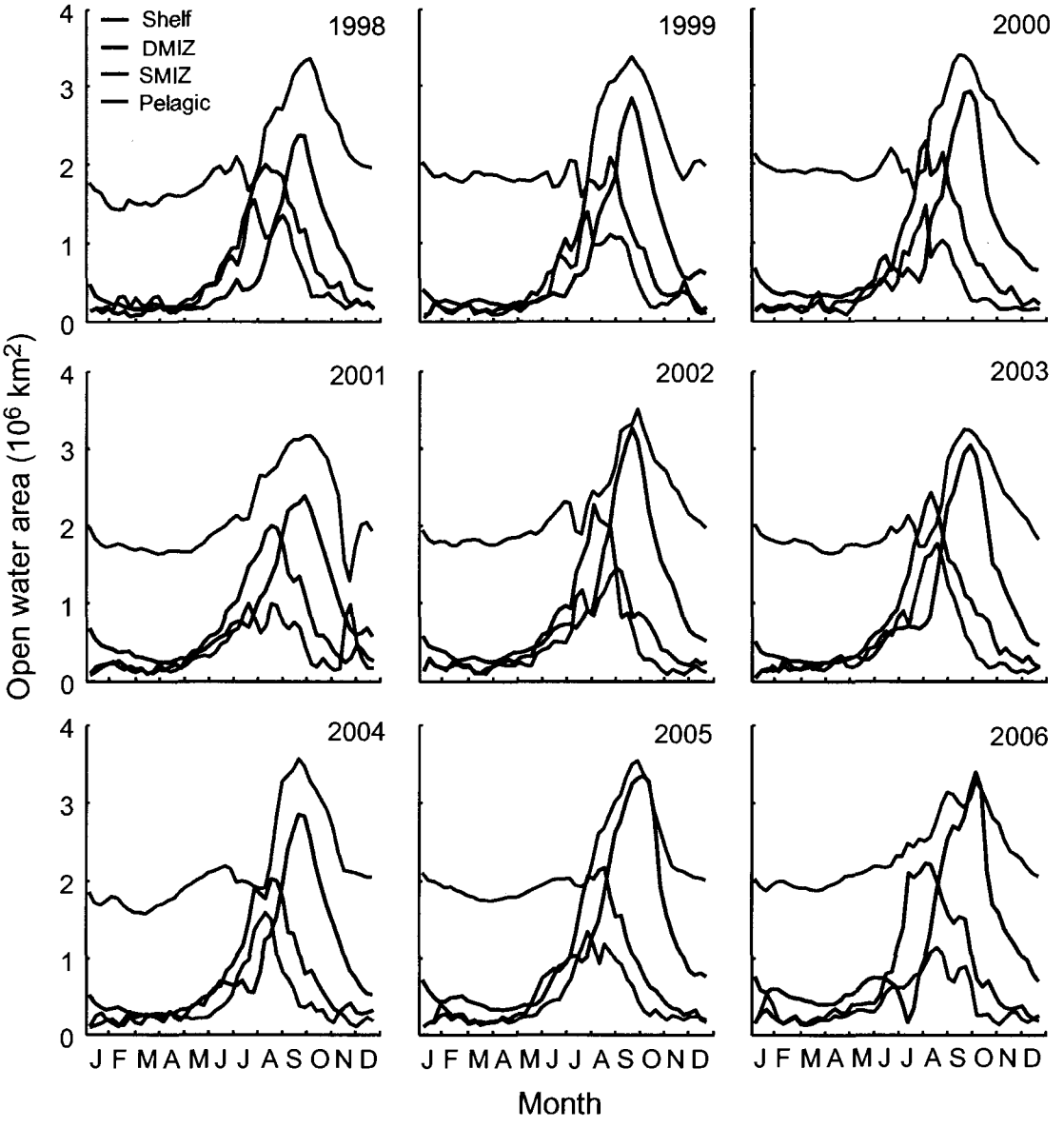

Figure 6. Weekly changes in open water area in the four ecological provinces of the Arctic Ocean during 1998-2006.

water area during the POI in both the shelf and the SMIZ provinces was significant, increasing annually at a rate of 0.05×10^6 km^2 yr^{-1} ($R^2 = 0.77$, $p=0.002$) and 0.01×10^6 km^2 yr^{-1} ($R^2 = 0.55$, $p=0.02$), respectively (Table 1). Secular increases in open water area were most dramatic in the shelf and the SMIZ zones of the Siberian sector (Table 1), increasing at a rate of 0.010×10^6 km^2 yr^{-1} ($R^2 = 0.64$, $p=0.01$) and 0.004×10^6 km^2 yr^{-1} ($R^2 = 0.75$, $p=0.02$), respectively, during the POI (Table 1). These changes in the Siberian sector represent a 9-fold increase in open water area (from a minimum of 0.012×10^6 km^2 in 1998 to maximum of 0.110×10^6 km^2 in 2005) in the shelf and a 2-fold increase (from a minimum of 0.033×10^6 km^2 in 1998 to maximum of 0.067×10^6 km^2 in 2005) in the SMIZ province between 1998 and 2006 (Fig 5i). Apart from these regions, there was no significant secular increase in open water area within the ecological provinces of any geographic sector of the Arctic during the POI (Table 1).

Table 1. Linear Regression of Open Water Area Against Year by Geographic Sector and Ecological Province.

		Chukchi	Beaufort	Baffin	Greenland
Shelf					
	Slope*	6131	-967	1762	898
	R^2	0.36	0.089	0.32	0.135
	p-value	0.087	0.435	0.113	0.33
SMIZ					
	Slope*	1328	-1425	19	102
	R^2	0.298	0.225	0	0.005
	p-value	0.128	0.197	0.984	0.85
DMIZ					
	Slope*	-24	-2966	-563	523
	R^2	0	0.284	0.049	0.006
	p-value	0.956	0.14	0.568	0.848
Pelagic					
	Slope*	-35	-5816	3872	4810
	R^2	0	0.216	0.237	0.101
	p-value	0.965	0.207	0.184	0.405
Total					
	Slope*	7399	-11174	5090	6333
	R^2	0.339	0.238	0.18	0.225
	p-value	0.1	0.183	0.256	0.197

*Slopes are in units of $km^2\ yr^{-1}$

Table 1 (continued). Linear Regression of Open Water Area Against Year by Geographic Sector and Ecological Province.

		Barents	Kara	Laptev	Siberian	Arctic
Shelf						
	Slope*	14190	9711	4552	**9841**	**46110**
	R^2	0.436	0.394	0.186	**0.635**	**0.768**
	p-value	0.053	0.07	0.246	**0.01**	**0.002**
SMIZ						
	Slope*	1398	4202	288	**3937**	**9848**
	R^2	0.145	0.336	0.007	**0.751**	**0.546**
	p-value	0.312	0.102	0.833	**0.002**	**0.023**
DMIZ						
	Slope*	332	2578	743	441	1063
	R^2	0.007	0.431	0.081	0.262	0.005
	p-value	0.832	0.055	0.459	0.159	0.85
Pelagic						
	Slope*	9138	3555	809	198	16529
	R^2	0.247	0.391	0.061	0.25	0.415
	p-value	0.174	0.072	0.52	0.17	0.061
Total						
	Slope*	25047	20046	6392	**14416**	**73550**
	R^2	0.39	0.425	0.12	**0.68**	**0.78**
	p-value	0.072	0.057	0.361	**0.006**	**0.002**

Bold denotes statistical significance at the 95% confidence level.
*Slopes are in units of $km^2\ yr^{-1}$

3.2. Primary Production

3.2.1. Pan-Arctic Primary Production

Phytoplankton dynamics in the Arctic Ocean are characterized by an initial spring bloom in April-May, and in some years, a subsequent summer bloom during July-August (Fig. 7a). Between these two blooms, mean surface Chl *a* concentrations in the Arctic remain relatively high, generally exceeding 1.5 mg m^{-3}. Surprisingly, the summer bloom was the more prominent of the two blooms during the first half of the POI (1998-2001), with the mean Chl *a* concentration during summer bloom being comparable to or even exceeding that measured during spring. Between 2002 and 2004, this pattern was reversed, with Chl *a* concentrations in spring exceeding those in both summer and autumn. However, in the two most recent years, the intensity of the summer bloom had again increased, with Chl *a* concentrations eclipsing those of the spring bloom in both 2005 (by a large margin) and 2006 (only slightly).

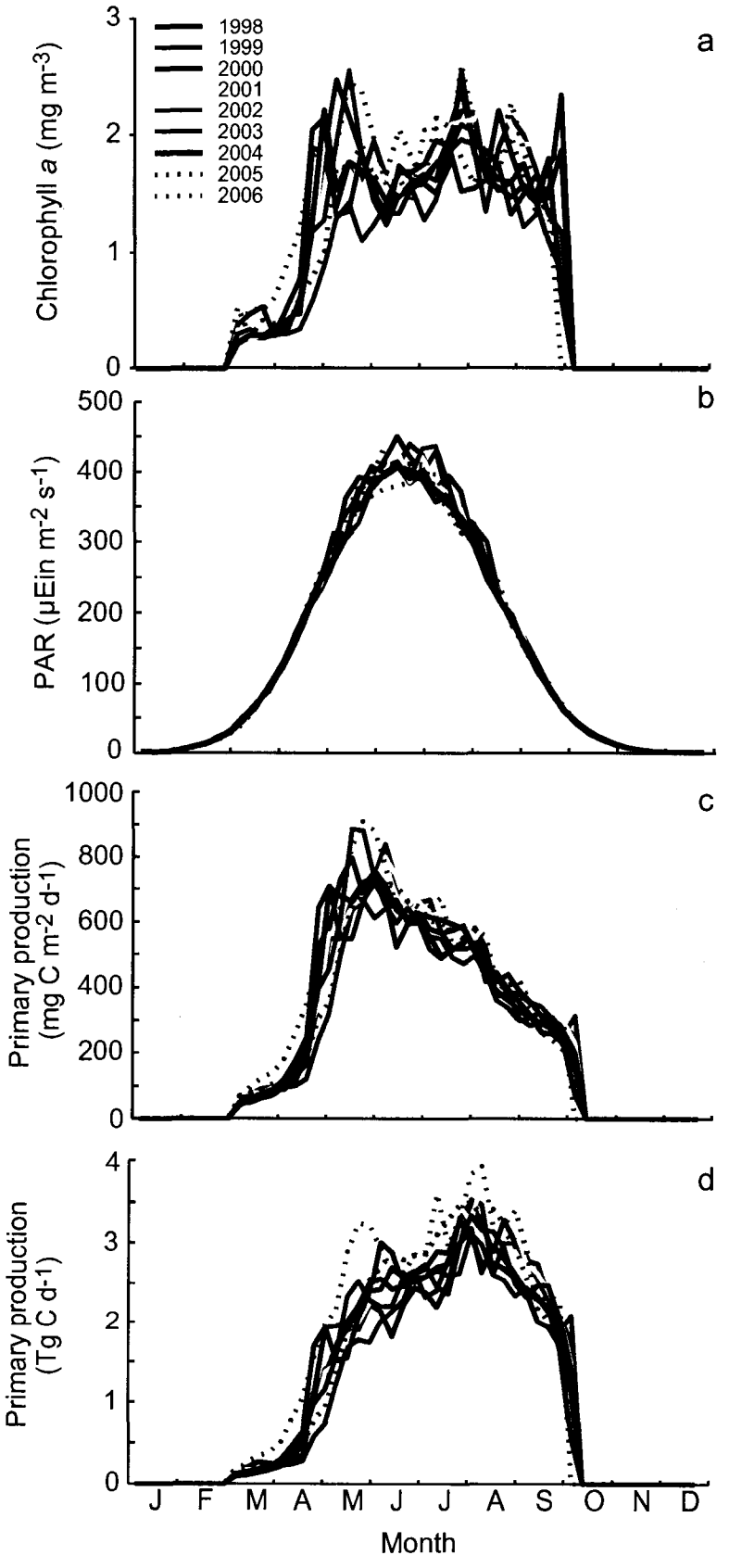

Figure 7. Weekly changes in a) mean surface Chl *a* concentration, b) mean daily photosynthetically active radiation (PAR) incident at the sea surface, c) mean area-normalized daily primary production, and d) annual primary production in the Arctic Ocean during 199 8-2006.

The daily rate of area-normalized production over the entire Arctic basin during the POI averaged 420±26 mg C m^{-2} d^{-1} during the phytoplankton growing season from March through September. Rates were highest in 2006 and 2001, averaging 474 and 447 mg C m^{-2} d^{-1}, respectively (Fig. 7a). The mean daily rate of area-normalized production was lowest in 1999 at 393 mg C m^{-2} d^{-1}. The daily rate of area-normalized production peaked during the May-June period (Fig. 7c), correlating well with surface Chl *a* (Fig. 7a) during the spring bloom when the amount of PAR incident on the sea surface is relatively high (Fig. 7b). Despite occasionally high Chl *a* concentrations (Fig. 7a), daily area-normalized rates of production (Fig. 7c) were consistently lower during the summer months because of the dwindling irradiance characteristic of this time of year (Fig. 7b).

Although daily production in August-September (360±33 mg C m^{-2} d^{-1}) was lower than in May-June (659±39 mg C m^{-2} d^{-1}), the August-September values have a disproportionate impact on annual primary production (Fig. 7d) because they coincide with the annual peak in open water area (Fig. 4a). For instance, 2001 exhibited the highest August-September rates of area-normalized production of any year except 2006 (Fig. 7c). Because this high rate of area-normalized production coincided with the annual peak in open water area, annual production in 2001 was among the highest of any year during the POI (Fig. 8a), even though open water area was below average

(Fig. 3a). On the other hand, high rates of area-normalized production in May-June do not necessarily translate into high annual area-integrated production. For example, in 2003, a high daily rate of area-normalized production during May led to high total production during this month (Fig. 7d), but the annual production was still relatively low (Fig. 8a) because of depressed August-September values (Fig. 7c). In 2006, the relatively high open water conditions earlier in the year (Fig. 4a), coupled with a high area-normalized primary production rate (Fig. 7c), led to high total production throughout the productive period of the year (Fig. 8b), and therefore the highest annual production (Fig. 8a) during the POI.

Annual pan-Arctic primary production averaged 419±33 Tg C yr^{-1} during 1998-2006 (Fig. 8a), with an interannual variability of 26% [(max-min)/mean]. Annual production peaked in 2006 at 483 Tg C yr^{-1} and was lowest in 1998 at 375 Tg C yr^{-1}. Overall, total Arctic primary production increased during 1998-2006, but not significantly (R^2=0.4, p=0.07), increasing each year by an additional 7.62 Tg C yr^{-1}. The relatively low coefficient of determination (R^2) between annual primary production and year is due to a period of decreased production between 2001 and 2003. This transient decrease in annual production is largely attributable to a drop in productivity during the months of August-September between 2001 and 2004 (Fig. 8c).

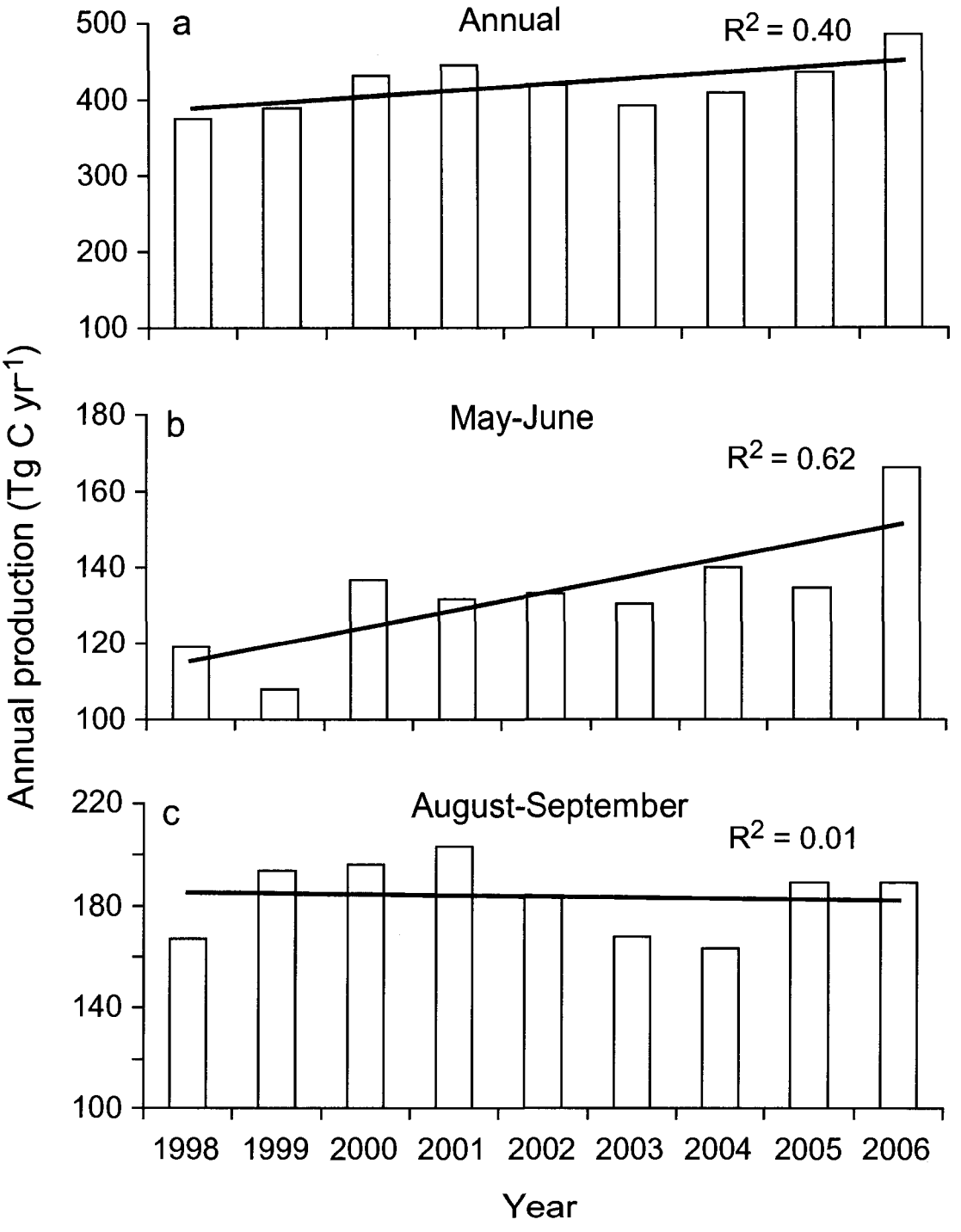

Figure 8. Total primary production computed for a) the entire year, b) the months of May-June, and c) the months of August-September. Also shown is the long-term trend in primary production.

While total production during the two months of the spring bloom (May-June) (Fig. 8b) exhibited a markedly increasing temporal trend, rising at the rate of 4.57 Tg C yr^{-2} (R^2=0.6, p=0.01), there was no significant interannual trend in production during the period of maximum open water area (August-September) (Fig. 8c).

3.2.2. Geographic Sectors

Annual primary production in the Arctic varied widely between geographic sectors (Fig. 9). The two largest sectors, the Greenland and Barents, also were the most productive (Figs. 9e and f), averaging ~133 Tg C yr^{-1} and 108 Tg C yr^{-1}, respectively. Even though the Greenland and Barents sectors did not have the highest area-normalized production rate, the large seasonal and perennial open water area in these regions (Fig. 5) resulted in high total annual production. Most of the other geographic sectors exhibited much lower rates of annual production during the POI, generally in the range of 25-50 Tg C yr^{-1}. Annual production was lowest in the Siberian sector, which averaged only ~17.8 Tg C yr^{-1} during the POI (Fig. 9i).

The degree of interannual variability in annual primary production also was quite high between sectors (Fig. 9). The Greenland sector exhibited the least amount of variability (Fig. 9e), as determined from its low coefficient of

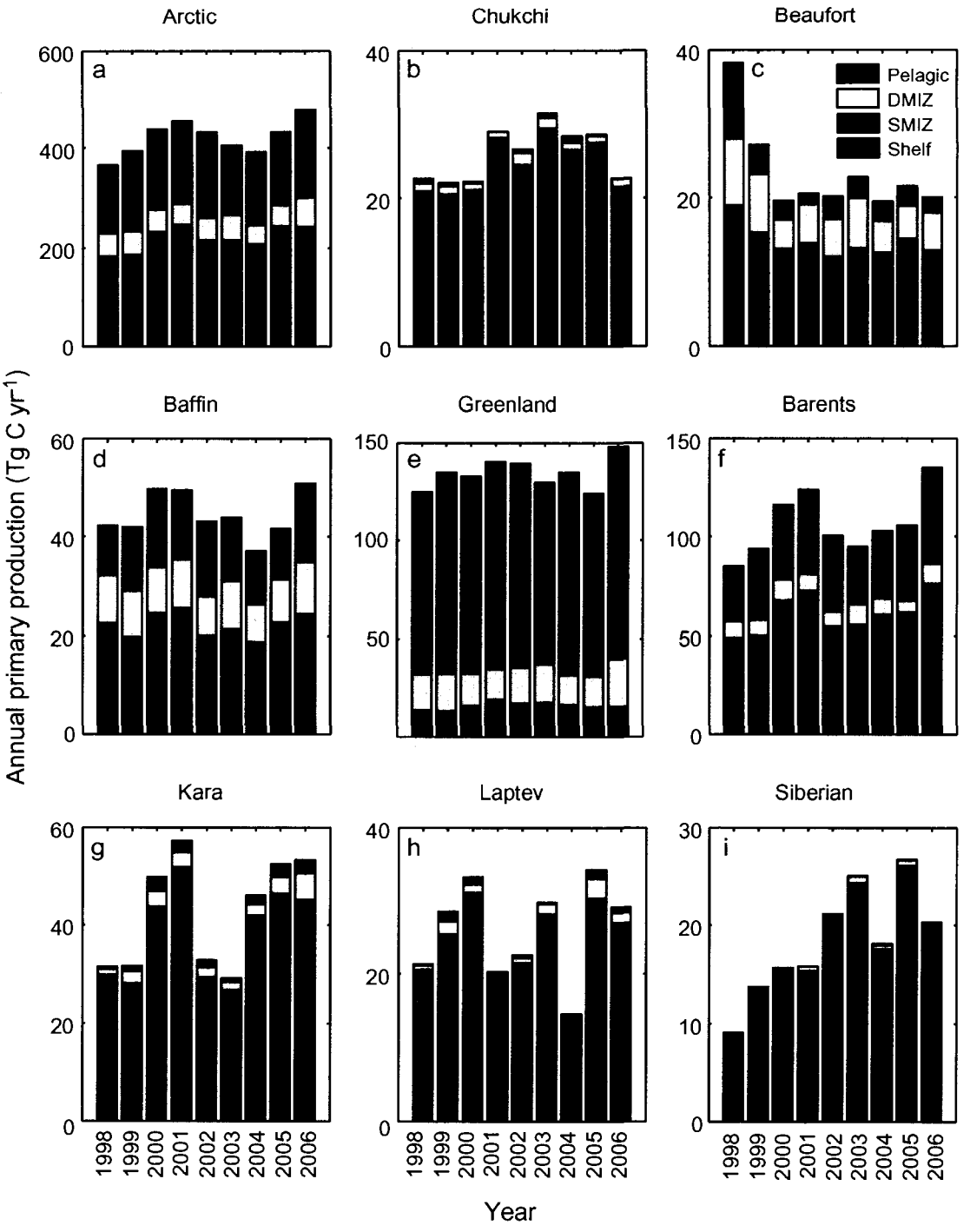

Figure 9. Annual primary production in the Arctic Ocean for each ecological province and geographical sector during 1998-2006.

variation (CV=standard deviation/mean) of 0.05. The Baffin, Barents, and Chukchi sectors exhibited an intermediate amount of interannual variability, with CVs for annual primary production all ranging from 0.10 to 0.15. The highest amount of interannual variability was observed in the Beaufort, Kara, Laptev, and Siberian sectors, which had CVs in the range of 0.24-0.29. In most sectors, yearly changes in annual primary production (Fig. 9) can be explained by interannual changes in sea ice cover (Fig. 5), with most geographic sectors exhibiting a significant correlation between these two quantities (Table 2). In fact, the sectors with the highest correlation between annual production and open water area (Beaufort, Barents, Kara, Laptev, and Siberian) were also the sectors with the highest degree of interannual variability in annual primary production. The unusually slight variation in annual production in the Greenland sector and the lack of a relationship with open water area was most likely due to the presence of a large area of permanently open water that varied little interannually.

The Siberian was the only Arctic sector that exhibited a significant increase in annual primary production during the POI ($R^2 = 0.6$, $p=0.009$), rising at the rate of 1.7 Tg C yr^{-2} (Table 3). Most other sectors displayed either no obvious temporal trend between 1998 and 2006 or a slight, but non-significant increase (Fig. 9). The Beaufort was the only sector where annual production actually decreased during the POI, falling at a

Table 2. Linear Regression of Annual Primary Production Against Open Water Area by Geographic Sector

	Chukchi	Beaufort	Baffin	Greenland
Slope*	5.33	**9.17**	6.75	9.84
R^2	0.269	**0.895**	0.24	0.15
p-value	0.153	**<0.001**	0.181	0.304

	Barents	Kara	Laptev	Siberian	Arctic
Slope*	**13.4**	**12.7**	**12.4**	**11.3**	**12.1**
R^2	**0.866**	**0.893**	**0.896**	**0.942**	**0.617**
p-value	**<0.001**	**<0.001**	**<0.001**	**<0.001**	**0.012**

Bold denotes statistical significance at the 95% confidence level.
*Slopes are in units of (10^7 g C yr^{-1}) km^{-2}

Table 3. Linear Regression of Annual Primary Production Against Year by Geographic Sector and Ecological Province.

		Chukchi	Beaufort	Baffin	Greenland
Shelf					
	Slope*	0.28	-0.183	0.000	0.17
	R^2	0.087	0.278	0.000	0.22
	p-value	0.442	0.145	0.998	0.203
SMIZ					
	Slope*	0.308	-0.289	0.002	0.041
	R^2	0.266	0.397	0.000	0.011
	p-value	0.155	0.069	0.992	0.788
DMIZ					
	Slope*	-0.009	-0.389	-0.029	0.314
	R^2	0.007	0.39	0.008	0.08
	p-value	0.833	0.072	0.822	0.46
Pelagic					
	Slope*	-0.01	-0.593	0.071	0.592
	R^2	0.012	0.373	0.007	0.054
	p-value	0.781	0.081	0.83	0.549
Total					
	Slope*	0.576	-1.445	0.076	1.188
	R^2	0.193	0.421	0.002	0.122
	p-value	0.237	0.059	0.906	0.357

Bold denotes statistical significance at the 95% confidence level.
*Slopes are in units of (Tg C yr^{-1}) yr^{-1}

Table 3 (continued). Linear Regression of Annual Primary Production Against Year by Geographic Sector and Ecological Province.

		Barents	Kara	Laptev	Siberian	Arctic
Shelf						
	Slope*	1.783	0.539	0.204	0.673	3.466
	R^2	0.365	0.099	0.031	0.5	0.438
	p-value	0.085	0.409	0.65	0.033	0.052
SMIZ						
	Slope*	0.077	0.917	0.057	0.924	2.038
	R^2	0.004	0.22	0.004	0.738	0.205
	p-value	0.87	0.203	0.875	0.003	0.221
DMIZ						
	Slope*	-0.005	0.281	0.078	0.038	0.278
	R^2	0	0.399	0.07	0.245	0.016
	p-value	0.98	0.068	0.491	0.175	0.747
Pelagic						
	Slope*	1.173	0.178	0	0.007	1.417
	R^2	0.239	0.268	0	0.141	0.08
	p-value	0.182	0.153	0.999	0.319	0.461
Total						
	Slope*	3.066	1.938	0.352	1.648	7.892
	R^2	0.279	0.218	0.021	0.647	0.334
	p-value	0.144	0.205	0.709	0.009	0.103

Bold denotes statistical significance at the 95% confidence level.
*Slopes are in units of (Tg C yr^{-1}) yr^{-1}

rate of 1.5 Tg C yr^{-2} (R^2 =0.4, p=0.059). However, this negative trend was not statistically significant, being driven primarily by large decreases in production during the first two years of the POI (Fig. 9). Between 2000 and 2006, annual production in the Beaufort remained relatively constant.

3.2.3. Ecological Provinces

3.2.3.1. Pelagic

Among the ecological provinces of the Arctic, total annual production was highest in the pelagic province (Fig. 9a), averaging 154 ± 13 Tg C yr^{-1} during the POI, which constituted 34-40% of pan-Arctic annual primary production. The high annual production in this province is due to its large open water area, accounting for ~52% of the average open water area in the entire Arctic basin over a year. The pelagic province was the dominant contributor to annual production in the Greenland and the Barents sectors (Figs. 9e and f), where it accounted for 75% (98 Tg C yr^{-1}) and 35% (37 Tg C yr^{-1}), respectively, of total annual production. There was no significant temporal trend in annual production in the pelagic province, either for the entire Arctic Ocean or within individual geographic sectors. The area-normalized production rate in the pelagic province was lower than that of the shelf and the SMIZ provinces (Fig. 10), averaging 348±22 mg C m^{-2} d^{-1}, and exhibiting no

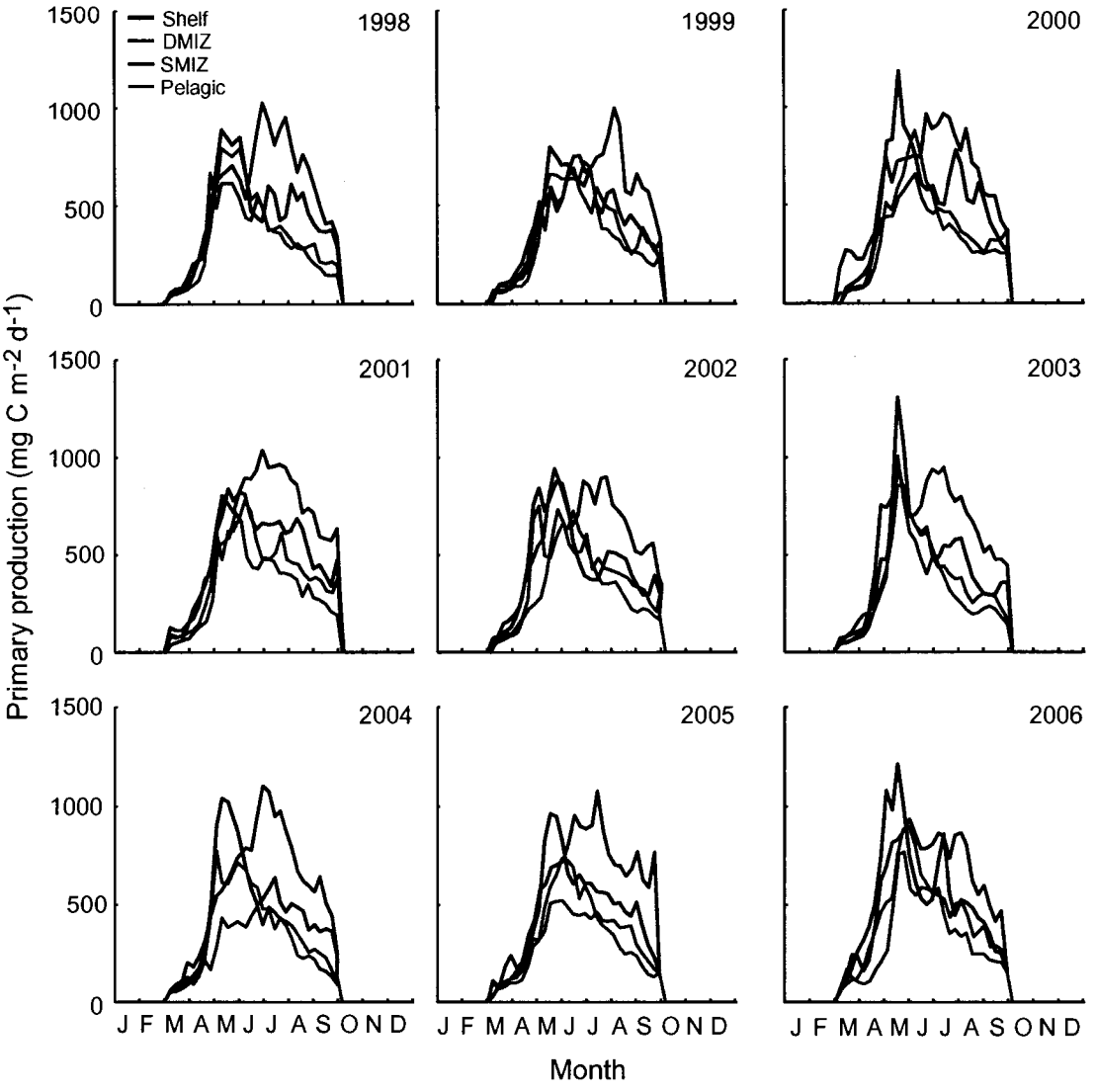

Figure 10. Weekly changes in daily area-normalized primary production in each ecological province of the Arctic Ocean during 1998-2006.

interannual trend during the POI. The area normalized production rate in the pelagic province reached its yearly maximum of 781-1016 mg C m^{-2} d^{-1} between April and mid-July (Fig. 10).

3.2.3.2. Shelf

Annual primary production in the shelf province averaged 86 ± 14 Tg C yr^{-1} during the POI (Fig. 9a), contributing 16-24% of pan-Arctic production. The shelf province was particularly important in the Barents, Kara, and Chukchi sectors (Fig. 9), where it accounted for 31% (33±8 Tg C yr^{-1}), 32% (12±4 Tg C yr^{-1}), and 41% (10±2 Tg C yr^{-1}), respectively, of annual primary production in these sectors.

The shelf exhibited the largest temporal increase in annual production of all the ecological provinces over the POI (R^2= 0.44, p=0.052), increasing each year by an average of 3.5 Tg C yr^{-1} (Fig. 11a). Although the 9-year trend was not statistically significant, increases in primary production were particularly dramatic for the last two years of the POI, exceeding 1998 levels by 70% and 63%, respectively, in 2005 and 2006. This increase was primarily due to a large and statistically significant (Table 1) increase in open water area in this province but also to a smaller (but not significant) increase in the daily area-normalized rate of production (Fig. 11a). Open water area in the shelf

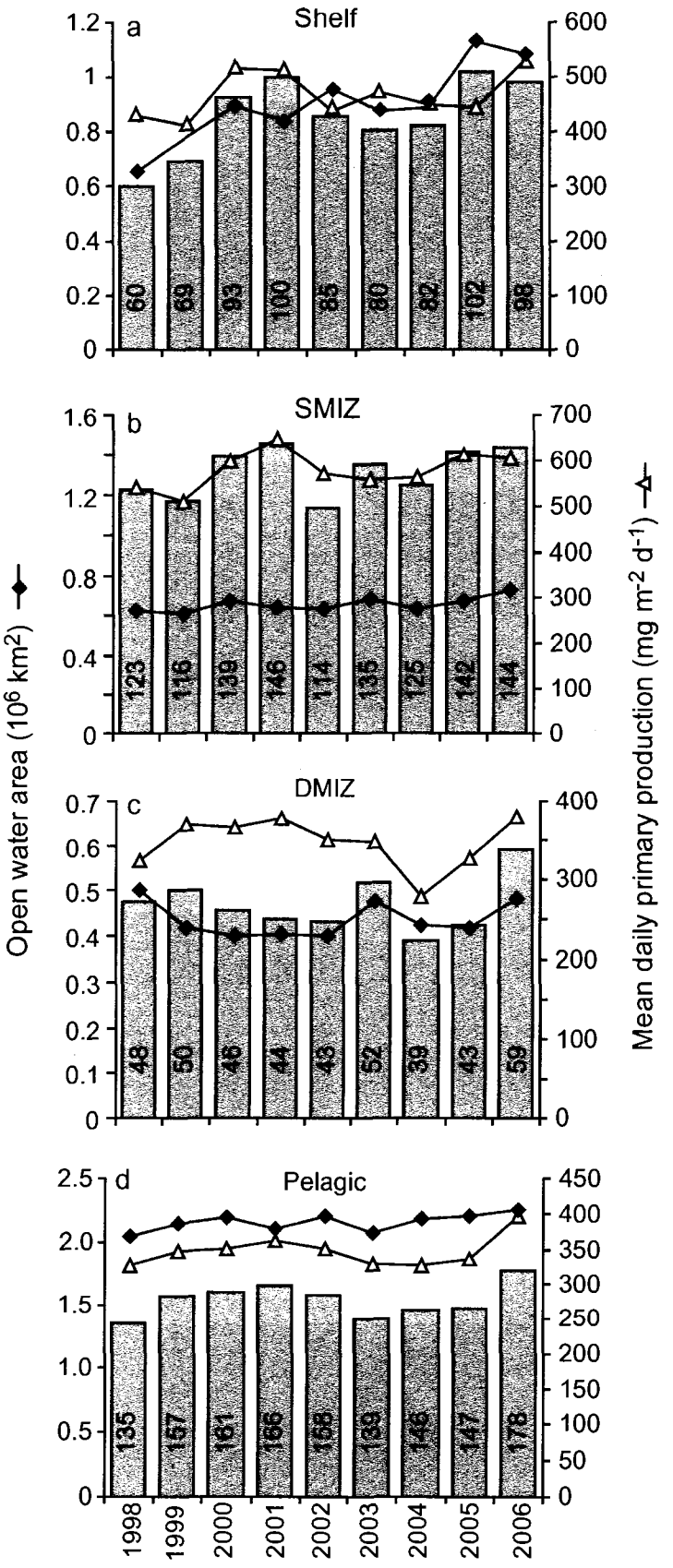

Figure 11. Total annual primary production (grey columns, Tg C yr^{-1}), annual mean open water area and annual mean area-normalized primary production in the a) shelf, b) SMIZ, c) DMIZ, and d) pelagic provinces of the Arctic Ocean during 1998-2006.

province increased from 0.66×10^6 km^2 in 1998 to 1.13×10^6 km^2 (in 2005) and 1.09×10^6 km^2 (in 2006), an increase of 71% and 64%, respectively. In contrast, the area-normalized production rate increased by 3.5% in 2005 and 24% in 2006, relative to the 1998 value. The area-normalized rate of production in the shelf province during the spring bloom was the highest of all the other ecological provinces, ranging from 790-1308 mg C m^{-2} d^{-1} (Fig. 10).

3.2.3.3. SMIZ

Total annual production in the SMIZ was the second largest of all the ecological provinces (Fig. 9a) and was comparable to that in the pelagic province, averaging 132 ± 6.0 Tg C yr^{-1} during the POI and representing 28-33% of the Arctic Ocean annual primary production. This was despite the fact that the SMIZ comprised on average only ~16% of the open water in the Arctic Ocean over a year. There was no significant interannual trend for total annual production in the SMIZ over the POI (R^2= 0.2, p=0.21, Table 3). The SMIZ province was particularly important in the Kara, Laptev and Siberian sectors, where it contributed >60% (>15 Tg C yr^{-1}) of annual primary production (Fig. 9). The SMIZ was the dominant province in the Chukchi, Beaufort, and Baffin sectors as well, accounting for 53% (14 Tg C yr^{-1}), 48% (10 Tg C yr^{-1}), and 35% (16 Tg C yr^{-1}) of sector-wide production, respectively.

The high total annual production in the SMIZ resulted from an area-normalized production rate that was higher than in any other ecological province, averaging 579± 42 mg C m^{-2} d^{-1} over the POI and reaching as high as 982-1174 mg C m^{-2} d^{-1} during the peak of the spring bloom (Fig. 10). The dominance of SMIZ persisted for most of the year, except during April-May when it was eclipsed by the daily production rate in the shelf province. The area-normalized production rate was highest in 2001 and 2006, averaging 650 and 606 mg C m^{-2} d^{-1}, respectively.

3.2.3.4. DMIZ

Annual production in the DMIZ was the lowest of all the ecological provinces (Fig. 9) and displayed no significant temporal trend during the POI (Table 3). With annual production rates averaging 47 ± 12 Tg C yr^{-1} (Fig. 9a), the DMIZ contributed just 9.6-13% of annual primary production in the Arctic Ocean. This low value was due more to a small amount of open water area in this province than to low area-normalized production rates, which were similar to those in the pelagic province, averaging 347 ± 32 mg m^{-2} d^{-1} over the POI. Rates of area-normalized production were highest in 2001 and 2006, exhibiting values of 377 and 379 mg m^{-2} d^{-1}, respectively (Fig. 10).

The DMIZ province was most productive in the Greenland sector (Fig. 9), contributing 18 Tg C yr^{-1} or 14% of total annual production in this sector. Although the DMIZ accounts for a higher proportion of annual production in the Beaufort (25%) and Baffin (21%) sectors, total DMIZ production there (5 and 9 Tg C yr^{-1}, respectively) was considerably less than in the Greenland sector.

3.2.3.5. Total Shelves

Despite accounting for only 30-40% of total open water area, the combined annual production of the two provinces associated with the shallow waters of continental shelf, the shelf and SMIZ provinces, had almost equal contribution to annual primary production in the Arctic as the Pelagic and DMIZ combined (Fig. 9). Over the entire Arctic Ocean, the annual mean production in the waters of the shelf and SMIZ combined (217 Tg C yr^{-1}) exceeded the production of the offshore waters of the pelagic and the DMIZ provinces (201 Tg C yr^{-1}). Primary production on the continental shelves was particularly important in the Chukchi, Siberian, Laptev, and Kara sectors, where the SMIZ+shelf accounted for 90% or more of annual production.

3.2.4. Controls of Primary Production

In general, the spatial pattern of annual primary production (Fig. 12a) most closely mimics that of Chl *a* over most of the Arctic Ocean (Fig. 12b). Of course the high correlation between primary production and Chl *a* concentration (Fig. 13a) is to be expected, given that our algorithm computes primary production from Chl *a* and an estimate of the phytoplankton growth rate (Eq. 2). While SST also plays an important role, the large amount of spatial and temporal variability exhibited by Chl *a*, which can range over four orders of magnitude, far outweighs the relatively smaller variability characteristic of SST. For example, primary production anomalies (Fig. 14), calculated as the difference between the annual mean for a single year and the nine-year mean (Fig. 12a), are largest (±80 g C m^{-2} yr^{-1}) in waters with high Chl *a* variability (Fig. 15).

Because phytoplankton blooms require ice-free surface waters in order to obtain sufficient light for net growth, primary production also is positively correlated with open water area in most sectors of the Arctic Ocean (Fig. 13b). The higher rates of primary production in the Arctic in recent years are reflected in large and widespread positive primary production anomalies, particularly in 2005 and 2006 (Fig. 14), that correspond to strong positive open water anomalies (Fig. 16). In 2006, annual primary production was

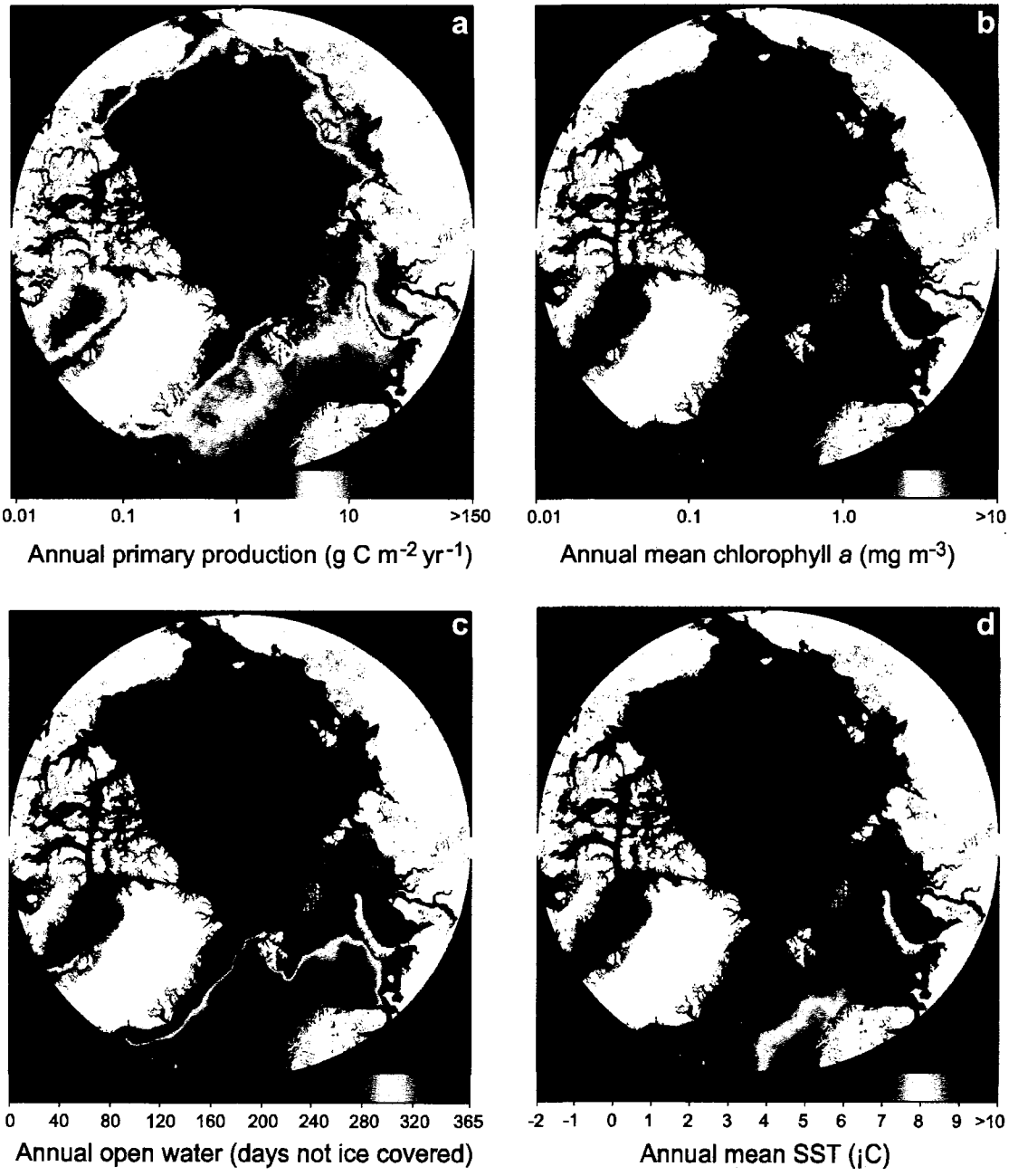

Figure 12. Climatologies (1998-2006) for a) annual primary production, b) annual mean surface Chl a, c) annual mean open water (number of ice-free days per year), and d) annual mean sea surface temperature.

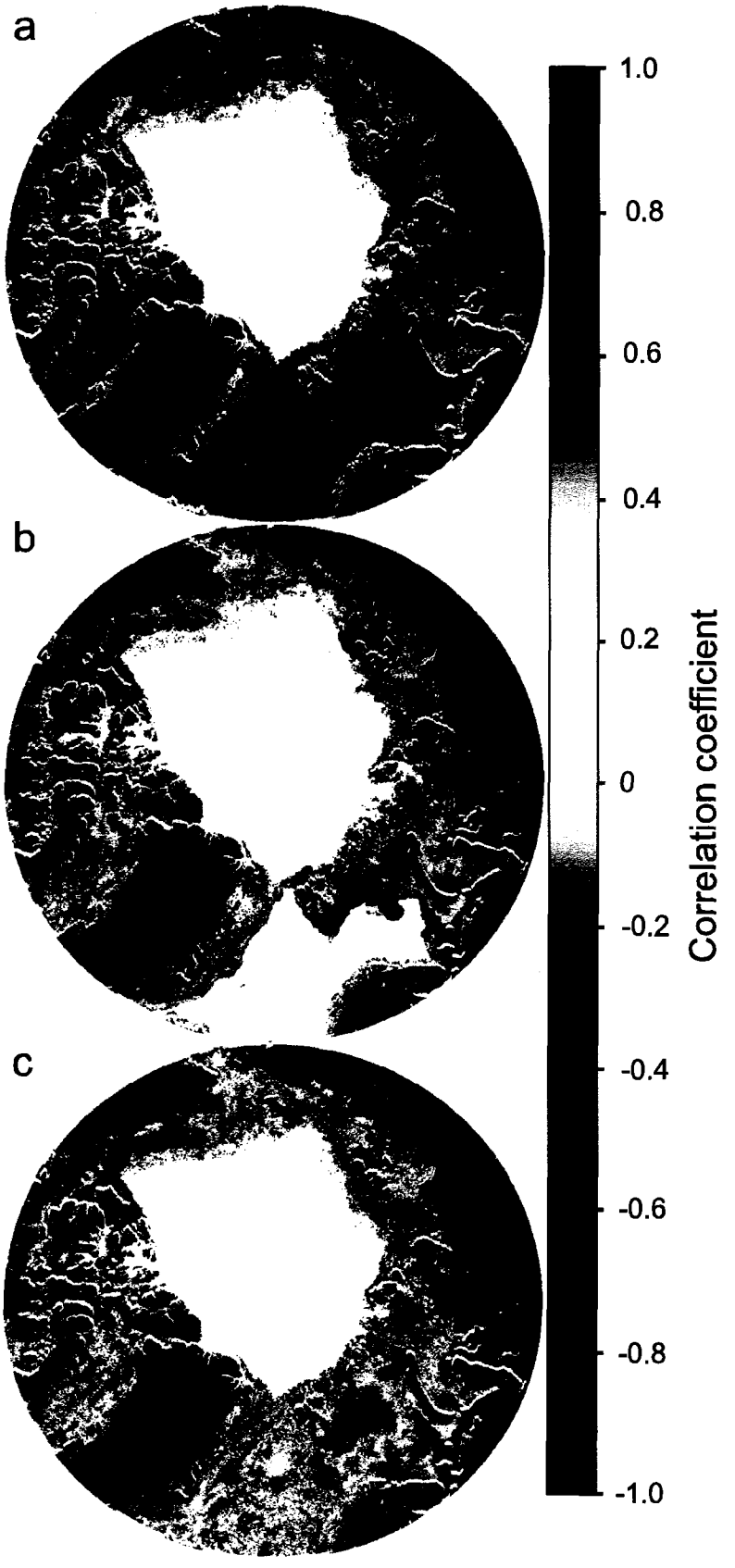

Figure 13. Maps of the correlation coefficient for the regression of annual mean primary production against a) annual mean surface Chl a, b) annual mean open water area (only in regions where open water is present for ≤350 days), and c) annual mean sea surface temperature for the nine years of our study. Only pixel locations where data are available for all nine years are shown in color.

>60 g C m^{-2} yr^{-1} higher than the 9-year average (Fig. 12a) in some parts of the Barents, Kara, and Greenland sectors. While anomalously high rates of production in 2005 and 2006 were due in part to unusually high Chl *a* concentrations (Fig. 15), open water conditions in some regions persisted for >150 days longer than average (Fig. 16), greatly extended the length of the phytoplankton growing season. In the Siberian sector, where open water area increased significantly during the POI, the changes in production also were positive, although modest (20-40 g C m^{-2} yr^{-1}), especially since 2002. This increase resulted from both higher Chl *a* concentrations and open water area in these waters after 2003. The negative primary production anomalies (<-60 g C m^{-2} yr^{-1}) in the Barents and Kara sectors in 2003 were mainly due to anomalously low Chl *a* concentrations, since open water area in these regions differed little from other years.

Primary production was positively correlated with SST (Fig. 13c) in all sectors except the Greenland. The positive correlation of SST with primary production is due both to direct effects of SST on phytoplankton growth rates (Eq. 2) and possibly indirect effects of SST on surface water stratification, impacting both light and nutrient availability. It is interesting to note that the correlation between SST and annual primary production (Fig. 13c) is spatially similar to the correlation between open water area and annual primary

production (Fig. 13b), indicating that the correlation between the SST and open water area is also high.

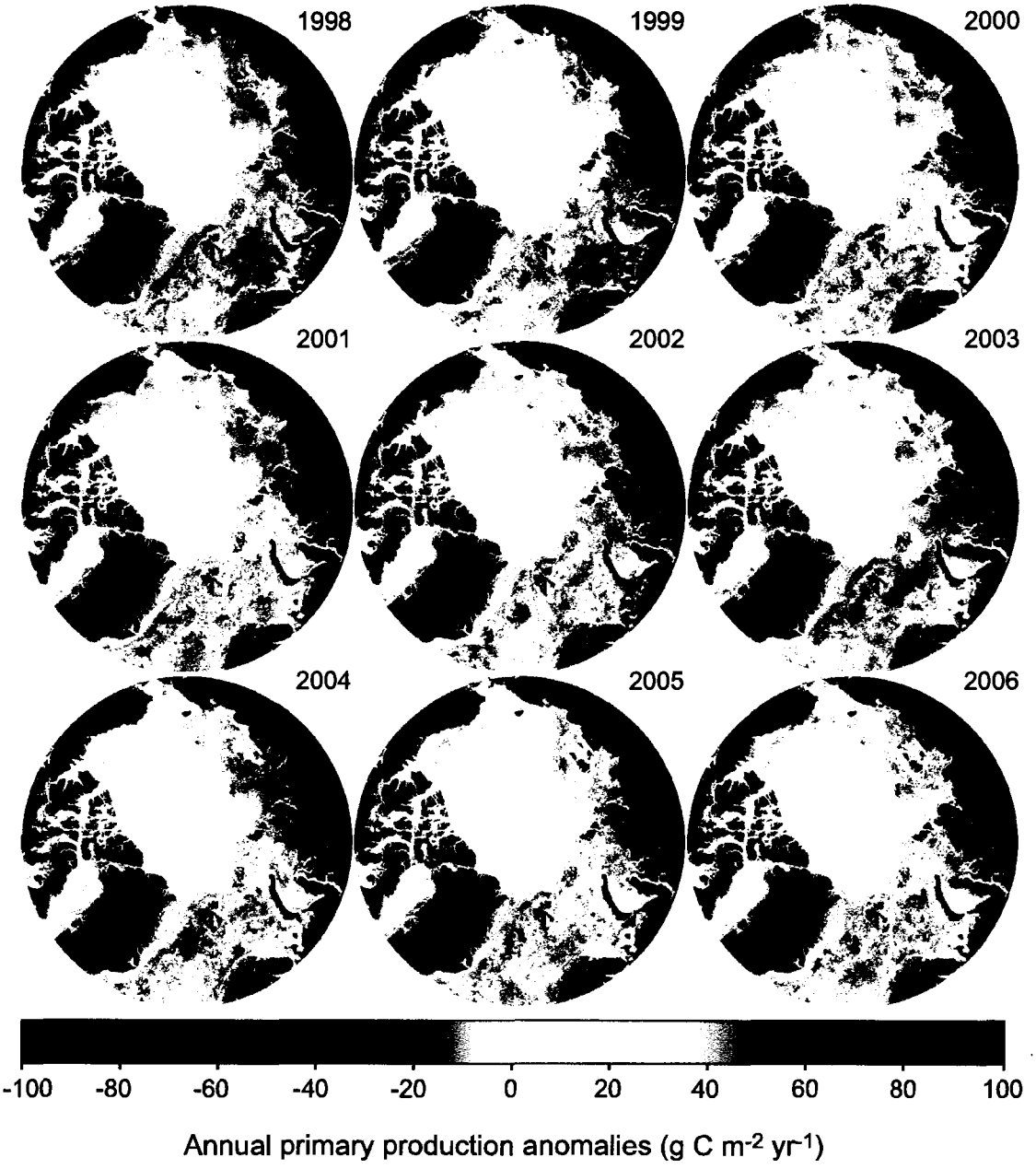

Figure 14. Anomaly maps of annual primary production for each of the nine years of this study. Colors represent change from the climatological mean shown in Fig. 12a.

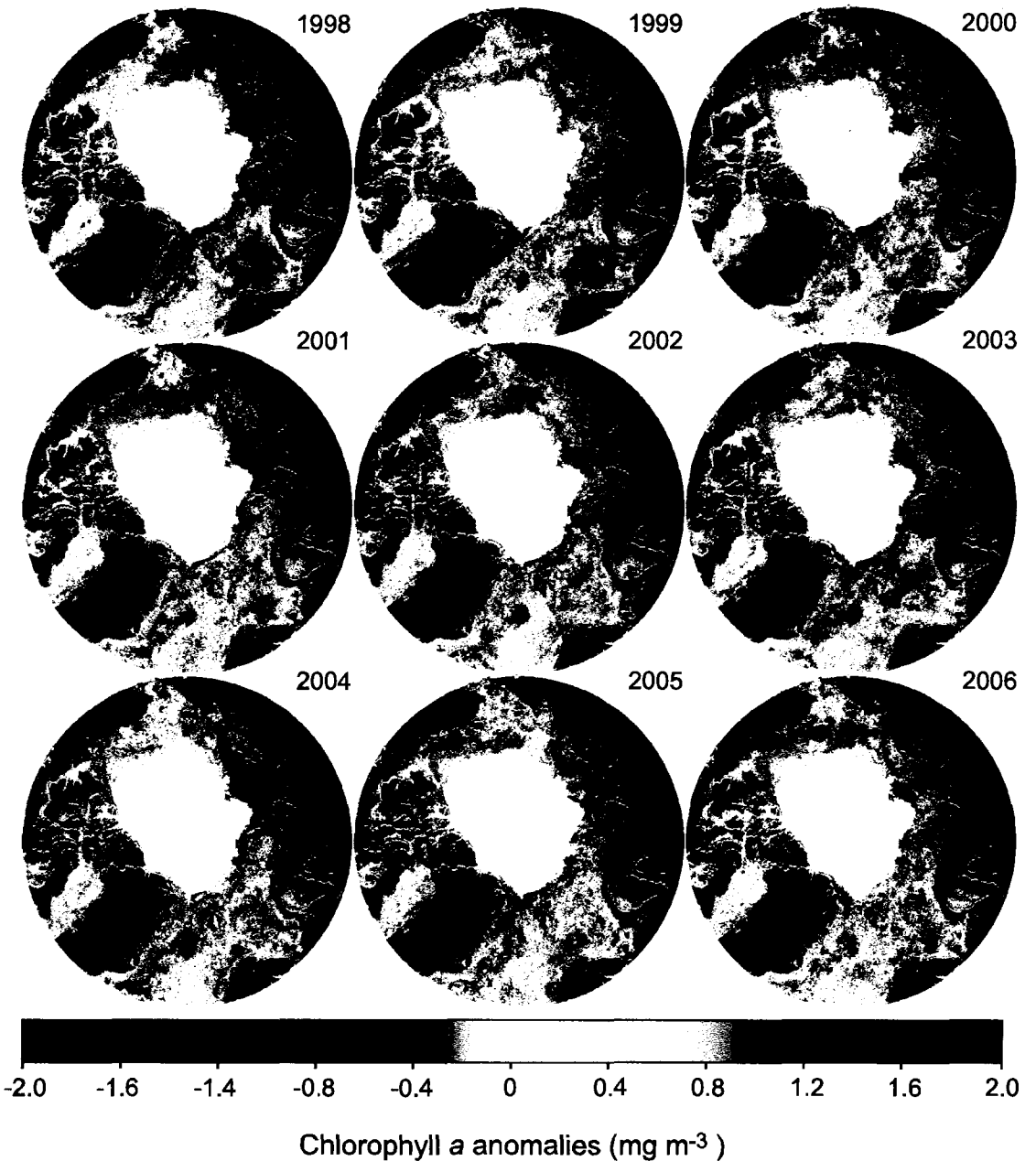

Figure 15. Anomaly maps of surface Chl a for each of the nine years of this study. Colors represent change from the climatological mean shown in Fig. 12b.

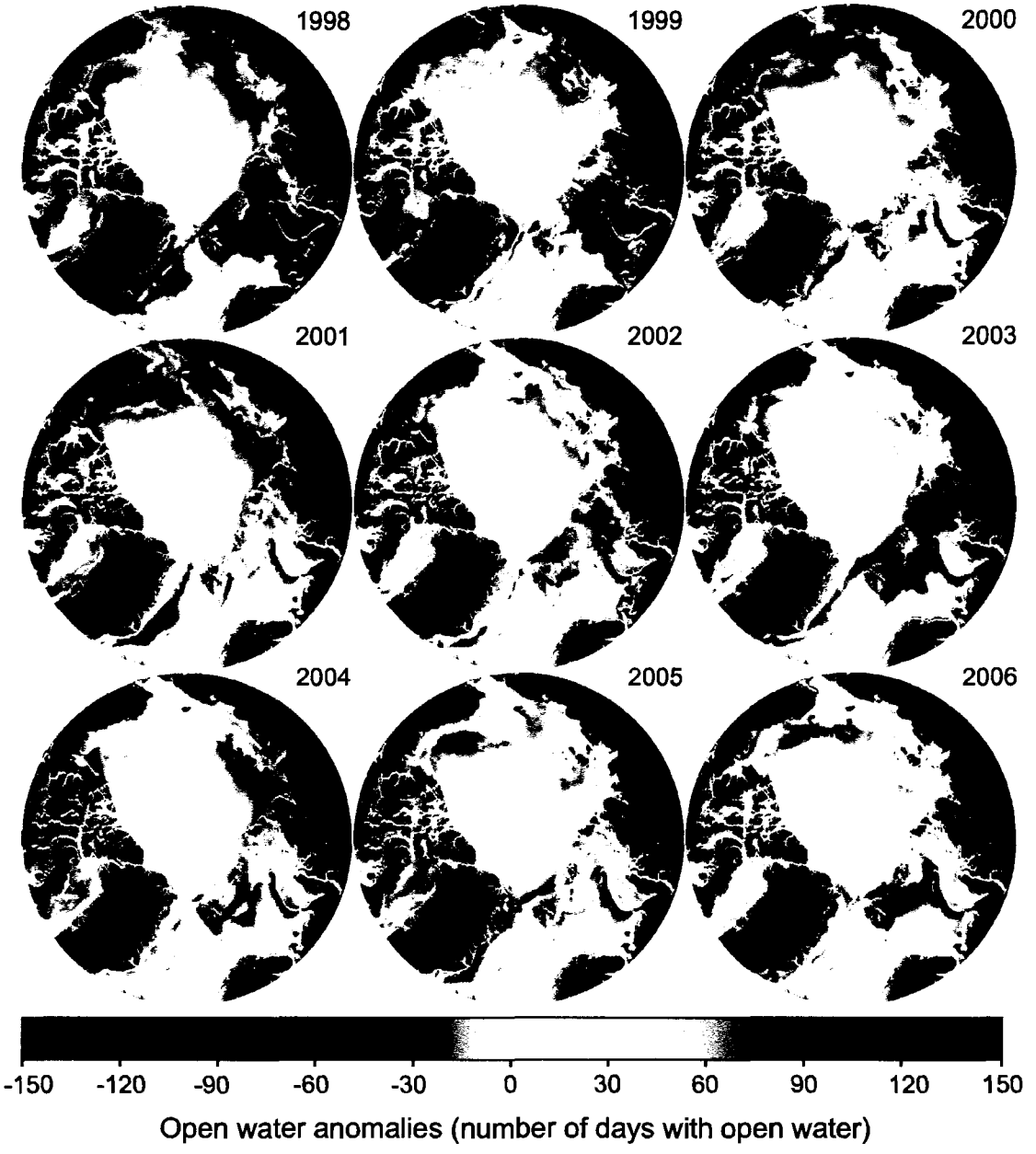

Figure 16. Anomaly maps of open water area for each of the nine years of our study. Colors represent change from the climatological mean shown in Fig. 12c.

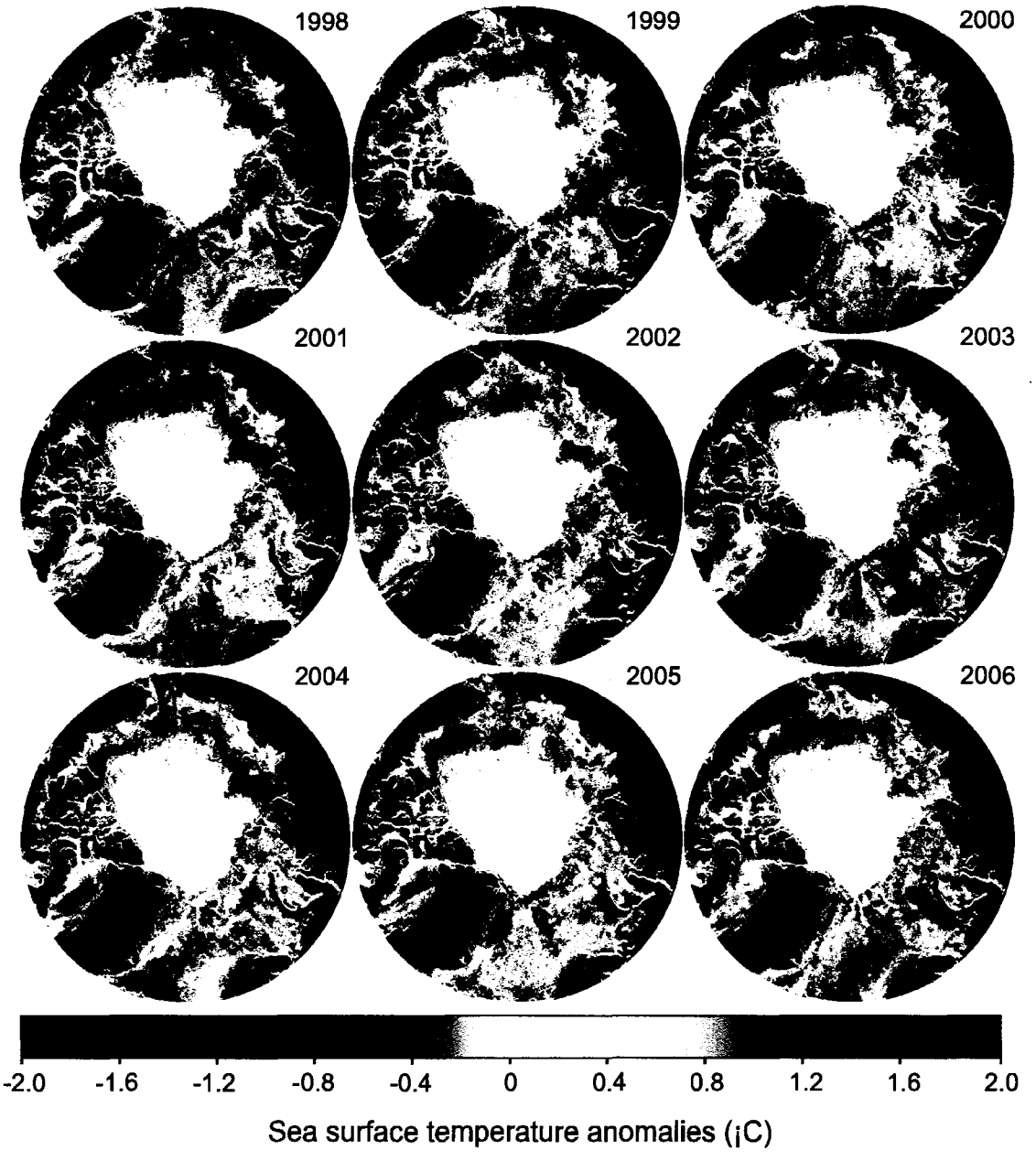

Figure 17. Anomaly maps of sea surface temperature for each of the nine years of our study. Colors represent change from the climatological mean shown in Fig. 12d.

4. Discussion

4.1. Comparison with Previous Results

Unfortunately, there are very few historical estimates of pan-Arctic primary production with which to compare our results. *Subba Rao and Platt* [1984] estimated that the annual rate of Arctic-wide primary production for all waters north of 65°N was 206 Tg C yr^{-1}, approximately half the mean value estimated here (419 Tg C yr^{-1}). Because the study region in *Subba Rao and Platt* [1984] was slightly larger area than that used here, the primary reason for the discrepancy between the two values is that their estimate of mean area-normalized production for the Arctic (9-27 g C m^{-2} yr^{-1}) was considerably lower than ours (44 g C m^{-2} yr^{-1}). However, our value is in much better agreement with the much more recent pan-Arctic productivity estimate of 329 Tg C yr^{-1} made by *Sakshaug* [2003], which was based on a compilation of both historical measurements and model results. The computed annual primary production in the early years of our study is within 10% of the estimate of *Sakshaug* [2003]. This early period should bear a greater similarity to the historical observations compiled by *Sakshaug* [2003], which were made prior to the rapid increase in open water area observed recently. In later years (e.g., 2006), our estimate of production is 50% higher than that of *Sakshaug* [2003],

due mostly to the dramatic increases in open water area but also to the slight increase in daily area-normalized production rates.

Annual rates of primary production computed here are likely to be underestimates of actual rates because, due to insufficient spatial resolution of satellite data, we are unable to quantify primary production in the leads and melt ponds within the Arctic sea ice zone that are known sinks for atmospheric CO_2 [*Semiletov et al.*, 2004]. Furthermore, the primary production algorithm does not account for production by phytoplankton growing under sea ice and by sea ice algae, although this is likely to represent only a small fraction of total Arctic primary production. Most importantly, calculated rates of primary production in the summer may be low because of the subsurface chlorophyll maximum (SCM) that occasionally develops offshore and is unresolved by SeaWiFS [*Falk-Peterson et al.*, 2000; *Hill and Cota*, 2005; *Matrai et al.*, 2007]. In some areas, productivity is highest at the ocean surface despite the presence of a SCM [e.g. *Matrai et al.*, 2007], suggesting that these SCMs were the result of an increase in phytoplankton Chl *a* per cell with depth, rather than an actual subsurface peak in phytoplankton abundance. In these waters, our algorithm should still work quite well. However, in those situations where the depth of the SCM corresponds to the depth of the productivity peak [e.g. *Hill and Cota*, 2005], depth-integrated water column production calculated by our algorithm is well below the *in situ* estimate. For

example, *Hill and Cota* [2005] observed numerous stations with a SCM in the western Arctic. Surface Chl *a* at these stations averaged 0.4 mg m^{-3}, while the Chl *a* concentration at the depth of the SCM averaged 2.5 mg m^{-3}. The depth-integrated primary production for these stations averaged approximately 600 mg C m^{-2} d^{-1}, well above the range of values produced by our algorithm for a surface Chl *a* concentration of 0.4 mg m^{-3} (Fig. 2b). The prevalence of subsurface productivity maxima missed by SeaWiFS and their impact on annual primary production estimates is unclear. Approximately 25% of the July-August stations shown in Fig. 2b exhibited a significant subsurface productivity maximum that was not accounted for by our algorithm. Given that July and August account for approximately 40% of annual primary production (Fig. 7d), if our algorithm underestimated primary production over 25% of the Arctic Ocean during these two months by as much as a factor of two, then the actual annual production would be only 10% higher than we have estimated here.

4.2. Temporal Changes in Primary Production

Between 1998 and 2006, annual primary production in the Arctic Ocean increased by ~30%, in sharp contrast to lower latitudes where primary production appears to have declined in recent years [*Behrenfeld et al.*, 2006]. Changes in primary production in the Arctic also differed markedly from

trends observed in the Southern Ocean, where rates of annual production between 1997 and 2006 were ~5-fold higher than those estimated here, but with much less interannual variability (11% versus 26% for the Arctic) and no significant temporal trend.

However, the change in annual primary production in the Arctic between 1998 and 2006 was not monotonic (Fig. 8a), increasing in the early years of the POI (1998 to 2001), decreasing thereafter until 2003, and then rising again to the maximum value attained during the POI in 2006 (483 Tg C yr^{-1}). Because of this irregular temporal pattern, the secular trend in annual primary production was not statistically significant (R^2=0.4, p=0.07). In contrast, the amount of open water area, which is a major factor controlling annual primary production, did exhibit a statistically significant increase between 1998 and 2006 (Fig. 3a). This difference suggests that the temporal trends observed in primary production were driven in large part by interannual changes in the rate of area-normalized production, rather than by changes in sea ice extent. For example, the local maximum in annual primary production in 2001 was the result of both higher than normal phytoplankton biomass and higher area-normalized rates of production during the late summer bloom of that year, despite open water area being relatively low (Fig. 3a). The cause for this increase can clearly be seen by closer inspection of the primary production anomaly in 2001 (Fig. 14), which shows that elevated production in the

Barents and Kara sectors coincided with a highly positive Chl *a* anomaly in these regions (Fig. 15), but with no discernable changes in the open water area (Fig. 16) or SST (Fig. 17). Similarly, the drop in annual production between 2001 and 2003, despite a slight increase in open water area, was closely tied to a coincident drop in area-normalized production in all four of the ecological provinces in the Arctic Ocean (Fig. 11). Thus, changes in total production in the Arctic were not simply a consequence of increased open water area in recent years; changes in phytoplankton biomass and area-normalized production also played important roles. This was especially true in 2005 and 2006 when both the area-normalized rate of production and open water area were at or near their nine-year highs, elevating 2006 to the most productive year of the POI.

Although the precise cause of the observed interannual variation in area-normalized production is not clear, changes taking place in the Greenland Sea, particularly from 2004-2006, may provide some clues. This is of interest because the waters in the western Greenland Sea is strongly influenced by the cold fresh Polar surface waters [*Sutherland and Pickart*, in press]. Over most of the Arctic, we observed a strong positive correlation between annual mean SST and annual primary production (Fig. 13c). The major exception to this pattern is found in those parts of the Greenland Sea that remain ice-free all year (red areas in Fig. 12c). In these waters, positive SST anomalies (Fig. 17)

coincided with negative primary production anomalies (Fig. 14), resulting in an atypical negative correlation between SST and annual primary production (Fig. 13c). The temperature of these waters is known to be especially sensitive to the phase of the Arctic Oscillation (AO) [*Wanner et al.*, 2001]. As the AO becomes more positive, westerly winds strengthen, northward advection of North Atlantic waters increases, and waters in the western Greenland Sea cool [*Thompson and Wallace*, 1998]. As can be seen in our study, a cooler Greenland Sea is associated with enhanced Chl *a* concentrations in these waters and positive annual primary production anomalies. This pattern is particularly evident from 2004 through 2006, when cooling of the open waters of the Greenland Sea (Fig. 17) was associated with a marked increase in both Chl *a* (Fig. 16) and primary production (Fig. 14). Although the mechanism behind the elevated production in a cooler Greenland Sea is not presently known, the increased northward advection of North Atlantic water during positive phases of the AO may enhance the flux of nutrients into the Greenland Sea that stimulate the growth of phytoplankton and increase annual primary productivity.

It should be noted, however, that the temporal pattern of annual pan-Arctic primary production was not well correlated with the AO index (data from the NOAA climate monitoring center,

http://www.cpc.ncep.noaa.gov/products/precip/CWlink/daily_ao_index/a

o_index.html), averaged either annually (R^2=0.016, p=0.74) or only over the more critical winter months (November-April, R^2=0.013, p=0.77). However, the AO is most highly correlated with annual primary production in the Greenland Sea, by far the most productive sector of the Arctic Ocean (Fig. 9), although even there it explains only 29% of the interannual variability (p=0.12) between 1998 and 2006. This lends support to the notion that increased advection of waters into the Greenland Sea during a positive phase of the AO could play an important role in enhancing phytoplankton productivity. It must be remembered, however, that the AO is complex and does not actually exist in two quasi-stable states (positive or negative), as was suggested by the simple description given above. Instead, the AO is highly dynamic and can vary markedly on monthly time scales. Thus, it is not surprising that the correlation between annual primary production and the AO is relatively weak, even in the Greenland Sea where its impacts are expected to be most apparent.

4.3. Recent Loss of Sea Ice

The results presented in this study show that during 1998-2006, the loss of sea ice (and increase in open water area) was not uniform across the Arctic, being more pronounced in some geographic sectors than in others. Open water area increased most rapidly in the Barents and Kara sectors, and most

significantly in the Siberian sector. The observed decrease in sea ice in these sectors is consistent with the previously documented decreasing trend in ice thickness between 1987 and 1999 by *Rothrock et al.* [2003]. The dramatic loss of sea ice in the Siberian sector is particularly alarming because model results demonstrate that changes in the Siberian Sea can be a precursor to basin-wide changes in sea ice thickness [*Rothrock et al.*, 2003; *Ukita et al.*, 2007]. Our study shows that the rate of loss of sea ice in these waters has been accelerating in recent years, particularly since 2003.

The accelerated changes of sea ice extent and thickness in the Arctic are due to multiple factors. Foremost is the loss of ice due to wind stress changes that increase the advection of sea ice out of the Arctic [*Zhang et al.*, 2000; *Holloway and Sou* 2002]. This impact can be amplified by increased melting and a longer melt-season, resulting in a positive feedback on sea ice loss [*Smith*, 1998; *Laxon et al.*, 2003]. The rate of sea ice melt also may be accelerated by the observed increase in water temperature in recent years. This temperature increase has been attributed to a combination of warmer Pacific waters entering through the Bering Strait [*Fukasawa et. al.*, 2004; *Shimada et al.*, 2006] and a rise in downward longwave radiation [*Francis and Hunter*, 2006] resulting from increase in liquid-water clouds relative to ice clouds [*Zuidema et al.*, 2005; *Francis and Hunter*, 2006]. Consistent with this viewpoint, *Serreze et. al.*[2003] suggested that the recent changes in Arctic sea

ice cover, particularly the low sea ice extent in 2002, were due to increased advection of atmospheric heat into the Arctic Ocean during spring, coupled with high temperature and low pressure in summer that was affected by the enhanced storm activity along northeastern Eurasia. In contrast, *Rigor et al.* [2002] and *Rigor and Wallace* [2004] argue that anomalous changes in sea ice are due to winter wind anomalies associated with the high-index AO conditions that increase the advection of ice away from the Eurasian and Alaskan coasts. Regardless of the relative importance of meteorological conditions in the winter and spring, losses of Arctic ice have been extensive in recent years, exemplified by the dramatic 30% decrease between 2006 and 2007 in the extent of perennial sea ice during the summer [*Comiso et al*, 2008].

4.4. Other Environmental Changes in the Arctic

Primary production in the Arctic is likely to vary in response to changes in a number of other environmental factors that influence the onset and development of phytoplankton blooms, including PAR at the upper ocean surface, nutrient inventories, and freshwater content. For example, mean Arctic-wide PAR exhibited a slow but steady decrease during the POI, dropping each year by an average of 0.7 μEin m^{-2} s^{-1} (R^2=0.74). PAR was highest in 1999 (annual mean of 201 μEin m^{-2} s^{-1}) and lowest in 2006 (annual mean of 195 μEin m^{-2} s^{-1}). Using our primary production algorithm, we

calculate that the observed 3% decrease in PAR between 1999 and 2006 should translate into in a 1% decrease in annual primary production.

More importantly, there has been a significant rise in freshwater content in the Arctic due to melting of sea ice and glaciers, excess precipitation, and increasing river discharge [*Peterson et. al.*, 2002]. The rise in river discharge is due primarily to increased runoff from Asian rivers, which currently adds 2560 km^3 of freshwater to the Arctic Ocean each year, an increase of 5% over the mean from the previous 20 years [*Richter-Menge et. al.*, 2006]. Discharge from the Yukon and Mackenzie rivers in recent years also was higher than normal [*Richter-Menge et. al.*, 2006], most likely due to an increase in net excess precipitation over evaporation (P-E) at high latitudes [*Peterson et al.*, 2002]. Enhanced melting of glaciers [*Dyurgherov and Carter*, 2004] and the Greenland ice sheet [*Box et al.*, 2004] further contributed to the recent increase in freshwater content of the Arctic. Finally, the contribution of freshwater from melting sea ice in the Arctic increased from 8000 km^3 in 1980 to 17,000 km^3 in 1997 [*Peterson et al.*, 2006]. These changes in Arctic freshwater input, especially from river runoff (which also contributes substantial amounts of sediment and organic matter), alter the availability of both nutrients and light necessary for phytoplankton growth. Increasing freshwater content intensifies surface stratification, thereby decreasing the thickness of the upper mixed layer, increasing light availability and partially offsetting the drop in

irradiance due to increased turbidity and decreases in incident PAR. On the other hand, increased stratification would likely reduce the supply of nutrients from the deeper waters beneath the mixed layer, decreasing phytoplankton growth and productivity.

While increasing air temperature appears to have governed the processes of excess river discharge and accelerated sea ice melt in recent years, the P-E anomaly seems to be more closely tied to the changes in the AO [*Peterson et al.*, 2006]. *Steele and Ermold* [2004] report considerable freshening of the western Siberian shelf sea (White Sea and Kara Sea) and salinification of the eastern Siberian shelf seas. Fresh water tends to accumulate in the Arctic Ocean during the negative phase of the AO and subsequently exits to the North Atlantic during the positive AO phase [*Dickson*, 1999]. However, the poor correlation we report between the AO index and both phytoplankton biomass and primary production in the Arctic suggests that these oceanographic manifestations of the AO may be very localized or may operate on timescales or at times of year that reduce their impact on phytoplankton productivity in the Arctic. The AO seems to exert its greatest influence during the coldest part of the year (November-April), when low light conditions preclude phytoplankton growth. The extent to which stratification intensified by a negative AO persists into the spring and summer may ultimately determine its impact on rates of primary production.

4.5. Future Changes in Arctic Ocean Phytoplankton Productivity

The increase in the flux of CO_2 from the atmosphere into the Arctic Ocean has tripled over the last 3 decades (from 24 to 66 Tg C yr^{-1}) [*Bates et al.*, 2006]. This increase is attributed to the recent loss of sea ice that facilitated both increased primary production and sea-air CO_2 exchange. The recent increase in primary production reported here should further enhance this exchange, due to the reduction in surface water pCO_2 during the conversion of inorganic CO_2 to organic carbon by phytoplankton that eventually sinks below the thermocline. Although it has been calculated that outgassing of CO_2 will increase by 8 g C m^{-2} yr^{-1} for every 1°C increase in sea surface temperature [*Anderson and Kaltin*, 2001], the biologically-mediated decrease in surface pCO_2 should partially offset the increased outgassing of CO_2 expected as Arctic surface waters warm in upcoming years. In fact, it has been suggested that when anticipated changes in CO_2 solubility (due to changes in both temperature and salinity) and phytoplankton production are taken into account, the potential for the Arctic Ocean to act as a sink for atmospheric CO_2 will increase in the future [*Anderson and Kaltin*, 2001]. However, longer-term observations are required to understand the extent to which primary production will be either intensified or weakened by the many concurrent environmental changes ongoing in the Arctic Ocean (e.g., declines in sea ice cover, increased SST, increased freshwater fluxes, changes in nutrient and

light availability). In addition, although our study quantifies large-scale changes in the primary production of northern polar seas, it is unable to address any ongoing taxonomic changes within the phytoplankton community within the Arctic Ocean [*Booth and Horner*, 1997] as a consequence of observed environmental changes. Finally, further studies are required to quantify the extent to which the negative feedback between losses of sea ice and increased biological CO_2 uptake in the Arctic (which would reduce atmospheric warming) will be countered by the increased CO_2 outgassing resulting from surface ocean warming due to reduced sea ice albedo [*Morales Maqueda et al.*, 1999]. This understanding is particularly critical given the unprecedented acceleration of sea ice loss observed in the Arctic in recent years.

References:

Arctic Climate Impact Assessment (ACIA) (2005), Cambridge University Press, Cambridge, United Kingdom and New York, NY, USA.

Anderson, L. G., and S. Kaltin (2001), Carbon fluxes in the Arctic Ocean - potential impact by climate change, Polar Res., 20(2), 225-232.

Arrigo, K. R., and C. W. Sullivan (1994), A high resolution bio-optical model of microalgal growth: Tests using sea ice algal community time-series data, Limnol. Oceanogr., 39(3), 609-631.

Arrigo, K. R., D. Worthen, A. Schnell, and M. P. Lizotte (1998), Primary production in Southern Ocean waters, J. Geophys. Res., 103, 15587-15600.

Arrigo, K. R., G. L. van Dijken, and S. Bushinsky (in press), Primary production in the Southern Ocean, 1997-2006, J. Geophys. Res.

Bates, N. R., S. B. Moran, D. A. Hansell, and J. T. Mathis (2006), An increasing CO2 sink in the Arctic Ocean due to sea ice loss, Geophys. Res. Lett., 33(23), L23609, doi:10.1029/2006GL027028.

Behrenfeld, M. J., R. T. O'Malley, D.A. Siegel, C. R. McClain, J. L. Sarmiento, G. C. Feldman, A. J. Milligan, P. G. Falkowski, R. M. Letelier, and E. S. Boss (2006), Climate-driven trends in contemporary ocean productivity, Nature, 444(7120), 752-755.

Boetius, A. and E. Damm (1998), Benthic oxygen uptake, hydrolytic potentials and microbial biomass at the Arctic continental slope, Deep-Sea Res., Part I, 45(2-3), 239-275.

Booth, B. C. and R. A. Horner (1997), Microalgae on the Arctic Ocean Section, 1994: species abundance and biomass, Deep-Sea Res., Part II, 44(8), 1607-1622.

Box, J. E., D. H. Bromwich, and Le-Sheng Bai (2004), Greenland ice sheet surface mass balance 1991-2000: application of Polar MM5 mesoscale model and in situ data, J. Geophys. Res., 109, D16105, doi:10.1029/2003JD004451.

Buck, K. R., T. G. Nielsen, B. W. Hansen, D. Gastrup-Hansen, and H. A. Thomsen (1998), Infiltration phyto- and protozooplankton assemblages in the annual sea ice of Disko Island, West Greenland, spring 1996, Polar Biol., 20(6), 377-381.

Carmack, E. C., K. Aagaard, J. H. Swift, R. W. MacDonald, F. A. McLaughlin, E. P. Jones, R. G. Perkin, J. N. Smith, K. M. Ellis, and L. R. Killius (1997), Changes in temperature and tracer distributions within the Arctic Ocean: results from the 1994 Arctic Ocean Section, Deep-Sea Res., Part II, 44(8), 1487-1502.

Carmack, E. C., and R. W. Macdonald (2002), Oceanography of the Canadian shelf of the Beaufort Sea: A setting for marine life, Arctic, 55, 29-45.

Cavalieri, D. J., C. L. Parkinson, and K. Y. Vinnikov (2003), 30-year satellite record reveals contrasting Arctic and Antarctic decadal sea ice variability, Geophys. Res. Lett., 30(18), 1970, doi:10.1029/2003GL018031.

Chapman, W. L., and J.E.Walsh (2003), Observed climate change in the Arctic, updated from Chapman and Walsh, 1993: Recent variations of sea ice and air temperatures in high latitudes, Bull. Am. Met. Soc., 74(1), 33-47.

Codispoti, L. A. (1979), Arctic Ocean processes in relation to the dissolved silicon content of the Atlantic, Mar. Sci. Commun., 5(6), 361-381.

Comiso J. C., C. L. Parkinson, R. Gersten, L. Stock (2008), Accelerated decline in the Arctic sea ice cover, Geophys. Res. Lett., 35, L01703, doi:10.1029/2007GL031972.

Dickson, B. (1999), Oceanography - All change in the Arctic, Nature, 397(6718), 389-391.

Dyurgerov, M. B., and C. L. Carter (2004), Observational evidence of increases in freshwater inflow to the Arctic Ocean, Arctic Antarctic and Alpine Research, 36(1), 117-122.

Eppley, R. W. (1972), Temperature and phytoplankton growth in the sea, Fishery Bull. (Washington D C), 70(4), 1063-1085.

Falk-Petersen, S., H. Hop, W. Budgell, E. Hegseth, R. Korsnes, T. Loyning, J. Orbaek, T. Kawamura, and K. Shiras

Chapter 4

Air-Sea Flux of CO_2 in the Arctic Ocean, 1998-2003

Abstract

The Arctic Ocean is experiencing an unprecedented reduction in sea ice. As more ocean water come in direct contact with the atmosphere, the air-sea flux of CO_2 is likely to be affected. This study provides high resolution basin scale estimates of air-sea flux of CO_2 (FCO_2) in the Arctic Ocean. For this purpose, multiple linear regression relationships with sea surface temperature, chlorophyll and salinity measured from in-situ measurements were developed to compute dissolved inorganic carbon (DIC) concentration. Partial pressure of carbon dioxide was computed using this DIC concentration as input. This enabled the computation of air-sea flux of CO_2 which is a function of wind speed. For basin-wide application, a combination of remotely sensed and modeled data was applied to obtain interannual estimates air-sea flux of CO_2 in the Arctic Ocean and its regional seas for the years 1998-2003. Longer open water periods in the Atlantic dominated Greenland and Barents sectors led to the highest annual flux in these sectors relative to other sectors, although the area-normalized FCO_2 was low in these sectors. The Arctic Ocean was found to be a net sink to atmospheric CO_2 with the spatially integrated annual FCO_2

being 169±9 Tg C yr^{-1}. Pan-Arctic estimates of FCO_2 exhibited no significant increase during 1998-2003. Among the geographic sectors, only the Siberian sector exhibited significant increase in annual FCO_2 due to corresponding increase in ice-free water.

1. Introduction

Recent changes in global climate have been attributed to an increase in atmospheric carbon dioxide (CO_2), a major greenhouse gas which has increased from a pre-industrial value of 280 ppm to 379 ppm in 2005 [IPCC, Fourth assessment report, 2007]. Current atmospheric concentrations exceed the natural range over the last 650,000 years (180-300 ppm) and have resulted in a 20% increase in radiative forcing between 1995-2005. Because of the powerful effects of CO2 on global climate, it has been of interest to assess its sources and sinks.

The ocean is a significant reservoir of CO_2 [*Siegenthaler and Sarmiento,* 1993], including of post-industrial anthropogenic CO_2 [*Sabine et al.,* 2004]. There is regional variability in the uptake of CO_2 by the oceans with the latitudes of 40°-60° in both hemispheres being the most significant sinks [*Takahashi et al.,* 2002]. However, few studies have quantified the role of Arctic Ocean as a sink or source to atmospheric CO_2 due to its relative inaccessibility and perennial ice cover. However, recent changes in the Arctic as a result changing climate have brought in a renewed interest in quantification of the carbon uptake capacity of the Arctic Ocean.

The most visible change occurring in the Arctic is the shrinking of sea ice cover [*Comiso et al.*, 2008, *Pabi et al.*, 2008] with the mean annual ice decreasing by 19 % during 1998-2006. These changes in sea ice could have a number of biogeochemical implications. Decreasing sea ice cover should increase the air-sea flux of carbon dioxide into or out of the Arctic Ocean. Furthermore, increased freshwater flux from the melting of sea ice affects seawater chemistry by changing the salinity and the solubility of CO_2. Melting sea ice also affects the physical structure of the water column via increased stratification, reducing entrainment of CO_2 from depth. Finally, by increasing light availability, reduced sea ice cover can enhance primary production and the uptake of CO_2 [*Bates et al.* 2006].

The significant rise in the rate of sea ice melt, along with increased precipitation and river discharge, has lead to a rise in the freshwater content in the Arctic [*Peterson et. al.*, 2002]. Enhanced melting of glaciers further contributed to the freshwater content of the Arctic [*Dyurgerov and Carter*, 2004]. The freshwater flux from melting sea ice in the Arctic increased from 8000 km^3 in 1980 to 17,000 km^3 in 1997 [*Peterson et al.*, 2006]. River discharge currently adds 2560 km^3 of freshwater to the Arctic Ocean each year, an increase of 5% over the mean from the previous 20 years [*Richter-Menge et. al.*, 2006]. These changes in Arctic freshwater input, especially from river runoff (which also contributes substantial amounts of sediment and organic matter),

alter the availability of both nutrients and light necessary for phytoplankton growth, affecting the biological pump and carbon sequestration.

The biological pump is driven by primary production, a process that reduces surface DIC concentration as phytoplankton convert inorganic carbon to organic matter during photosynthesis. Some of the organic carbon is converted back to CO2 due to community respiration and microbial remineralization. While photosynthesis is limited to the euphotic depth, respiration and remineralization occurs throughout the water column. Eventually, about 1% of the biologically derived organic matter is exported to deep water where it remains for thousands of years.

The solubility pump works to transport CO_2 from the surface of the ocean to it's interior. The high capacity of the ocean to take up CO_2 is because of the reaction of CO_2 with water to form carbonic acid (H_2CO_3), bicarbonate (HCO_3^-) and carbonate ions (CO_3^{2-}) ions, which collectively constitutes DIC. Although the relative concentration of these species is dependent on the pH of the water, the majority of DIC exists as bicarbonate. As a result the ocean water is usually undersaturated in dissolved CO_2. The physical process of sinking of cold and high salinity water in the poles, transfers this DIC from the surface waters towards the ocean bottom where it remains for hundred of years. Furthermore, CO_2 solubility increases at the colder temperatures

characteristic of deep waters, so CO_2 tends to move from the warm surface ocean into the colder deep ocean.

The Nordic seas of the Arctic Ocean are important sites of intermediate and deep-water formation [*Swift and Aagaard*, 1981] and play a crucial role in meridional overturning circulation [*Broecker and Peng*, 1992]. As the denser water sinks, it also carries with it the inorganic and organic carbon from the surface [*Broecker and Peng*, 1992, *Skjelvan et al.*, 2005]. Because of this process, large quantities of anthropogenic CO_2 penetrate to intermediate and abyssal depths [*Sabine et al.*, 2004]. The increased freshening of Arctic Ocean could affect deep-water formation [*Aagaard and Carmack*, 1989], potentially reducing the transport of CO_2 into the deep ocean.

Given the unprecedented reduction in Arctic sea ice and its implications for the oceanic CO_2 pool, it is imperative that we quantify the pan-Arctic air-sea CO_2 flux and estimate its interannual variability. Previous estimates of the Arctic CO_2 sink were based either on extrapolation of regional measurements or by mass balance calculation [*Bates et al.*, 2006b, *Anderson et al.*, 1998]. The objective of this study was to assess CO_2 dynamics throughout the Arctic Ocean and estimate the spatial and temporal variability in the net air-sea CO_2 flux. For this purpose, we used chlorophyll (Chl *a*) and sea ice observations along with modeled sea surface temperature (SST), sea surface salinity (SSS),

and wind speed to obtain the total air-sea CO_2 flux over the Arctic Ocean during the period 1998-2003.

2. Methods

The approach we took was to first calculate surface water pCO_2 and estimate the air-sea flux of CO_2 (FCO_2) from the pCO_2 difference between the ocean and atmosphere (ΔpCO_2), the CO_2 solubility in seawater, and wind speed. Spatial and temporal variations in pCO_2 were calculated daily from estimates of SST, SSS, dissolved inorganic carbon (DIC) concentration, and alkalinity, derived either from model output or from satellite data.

2.1. Estimates of DIC and alkalinity

2.1.1. DIC

A multivariate linear relationship was formulated to predict surface DIC concentrations from observations of Chl *a*, SST, and SSS. This approach is similar to that used to determine pCO_2 in the Arabian Sea and Pacific Ocean [*Sarma et. al.*, 2006]. The relation was of the form:

$$DIC = A_0 + A_1 SST + A_2 Chl\ a + A_3 SSS \qquad (1)$$

Because the Greenland and Barents seas are dominated by Atlantic waters, the relationship between SST and SSS in these regions differs from that of the rest of the Arctic, which are dominated by Pacific waters flowing in through

the Bering Strait [Fig 1]. The waters of the North Atlantic Ocean are in general warmer and saltier than the waters originating from the Pacific Ocean. Therefore, one set of coefficients was used to define the relationship between DIC and SST, SSS, and Chl *a* for the Greenland and Barents seas while a different set was used for rest of the Arctic Ocean (Table 1). Data collected near the surface in the Greenland Sea by *Wallace et al.* [1995] were used to derive these coefficients for Atlantic-dominated waters (e.g., Greenland and Barents seas); the result is shown in Fig. [2]. For regions dominated by Pacific water (e.g., Chukchi, Beaufort, Baffin, Kara, Laptev and East Siberian seas), data from the recent Shelf-Basin Interaction (SBI) project were used [*Bates et al.*, 2006a , *Hill and Cota*, 2005]. Because SBI collected data in both the spring and summer, two separate relationships for these seasons were derived [Fig. 3], the coefficients for which can be found in Table 1. We found that when the spring and the summer data were combined, the relationship between DIC and SST, SSS, and Chl *a* was not as strong as when two different seasonal relationships were used.

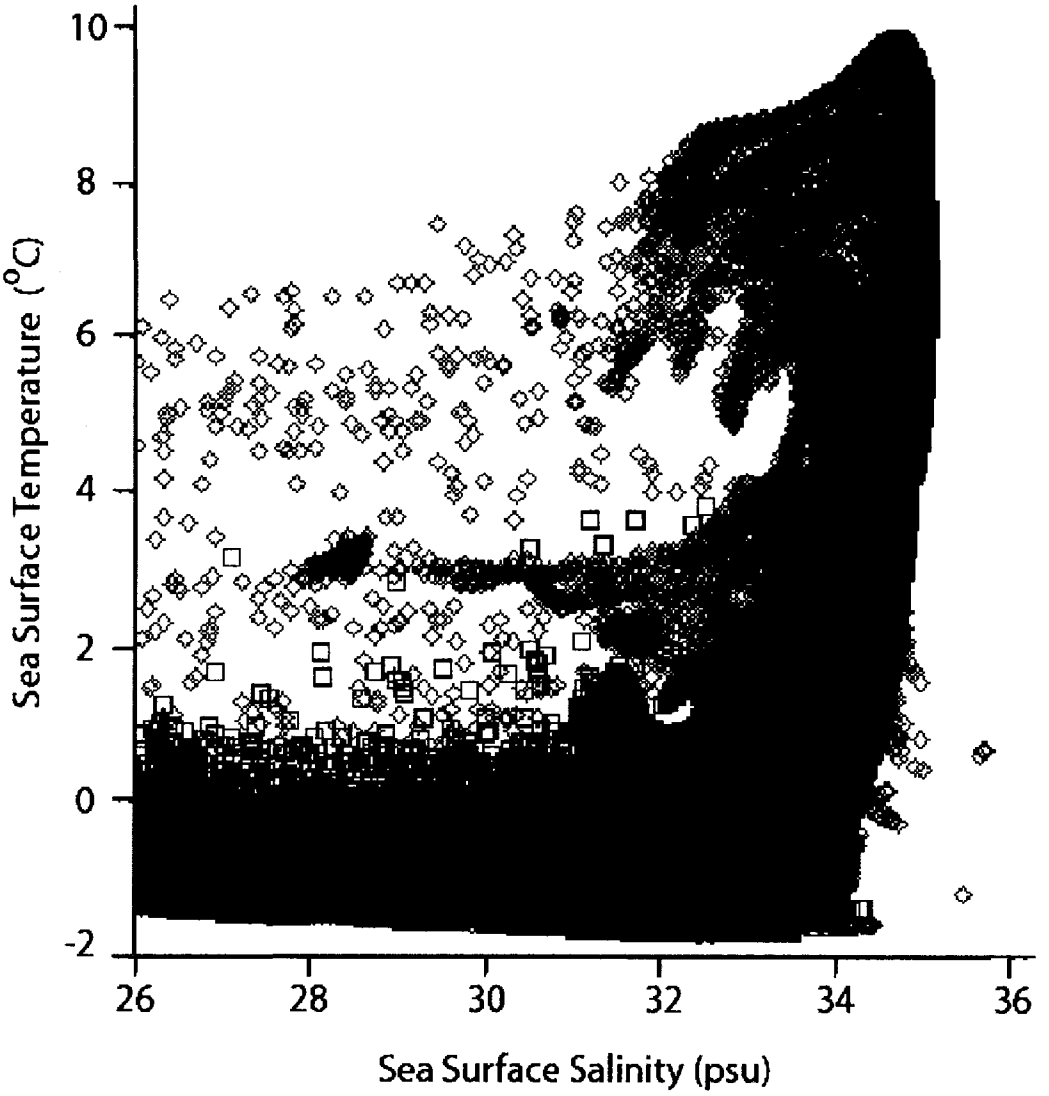

Figure 1. SST vs. SSS for Atlantic (black symbols) and Pacific (Red symbols) dominated waters that were demarcated based on geographic sectors.

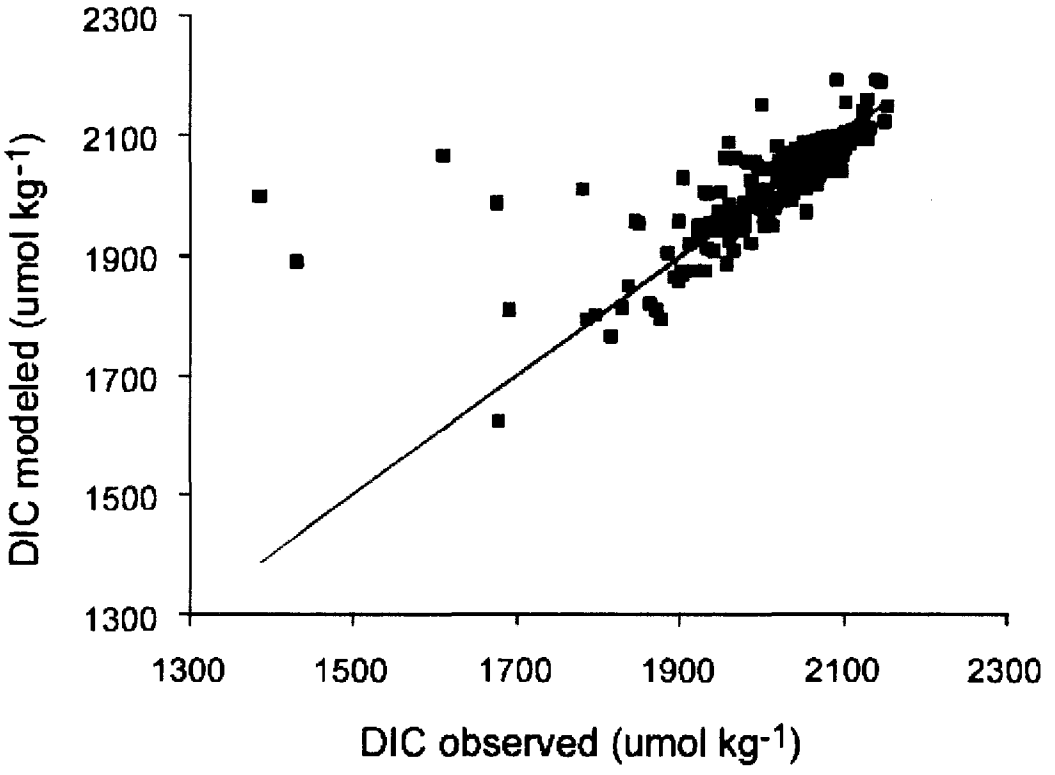

Figure 2. Modeled vs. measured DIC in Atlantic dominated waters. The 1:1 line is provided for reference

Table 1: Coefficients for the best fit of Eq. 2 derived for Atlantic and Pacific-dominated Arctic waters.

	Pacific-spring	**Pacific-summer**	**Atlantic**
A_0 (µmol kg^{-1})	473.01	278.9011	-4.8762
A_1 (µmol kg^{-1} $°C^{-1}$)	-44.319	-16.4536	-5.139
A_2 (µmol kg^{-1} mg^{-1} m^3)	-13.505	-2.3763	-4.0197
A_3 (µmol kg^{-1} psu^{-1})	49.646	56.3991	64.7901
R^2	0.9	0.92	0.62

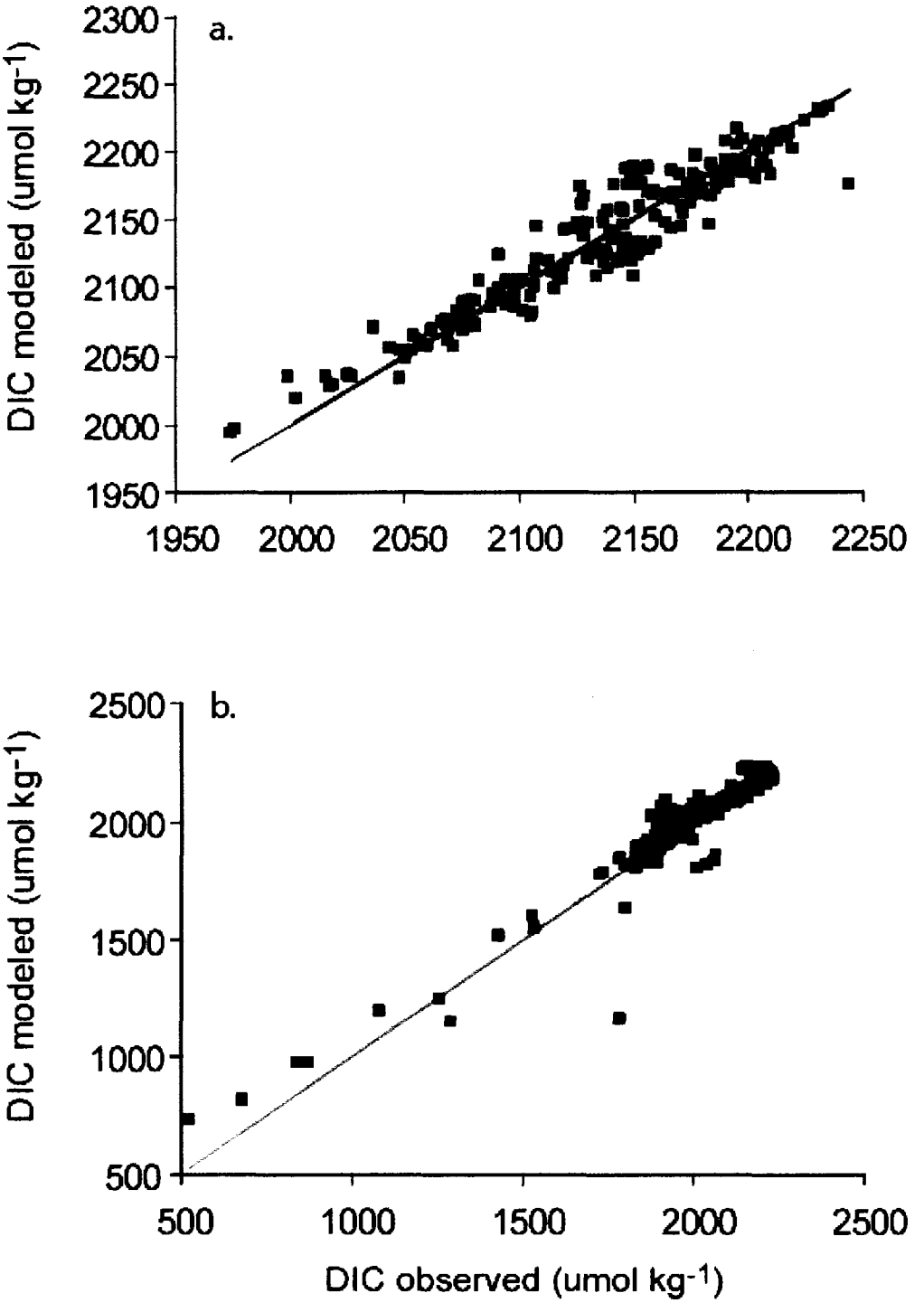

Figure 3. Modeled vs. measured DIC for Pacific-dominated waters in a) spring and b) summer. The 1:1 line is provided for reference.

2.1.2. Total Alkalinity

Total alkalinity (TA) in Arctic surface waters was calculated from SST and SSS, similar to the approach used by *Lee et al.* [2006] to derive TA in the Atlantic, Pacific, Indian and Southern Oceans. In the Atlantic-dominated sectors of the Arctic Ocean, TA was calculated as

$$TA = 200.13 + 4.42\ SST + 63.06\ SSS \qquad (2)$$

using data from *Wallace et al.* [1995]. The relationship between measured TA and TA calculated from SST and SSS is shown in Fig 4 (R^2=0.55, $p<0.001$). In the Pacific-dominated sectors, we used the TA relationship derived by *Kaltin and Anderson* [2005]

$$TA = 47.2\ SSS + 688.6. \qquad (3)$$

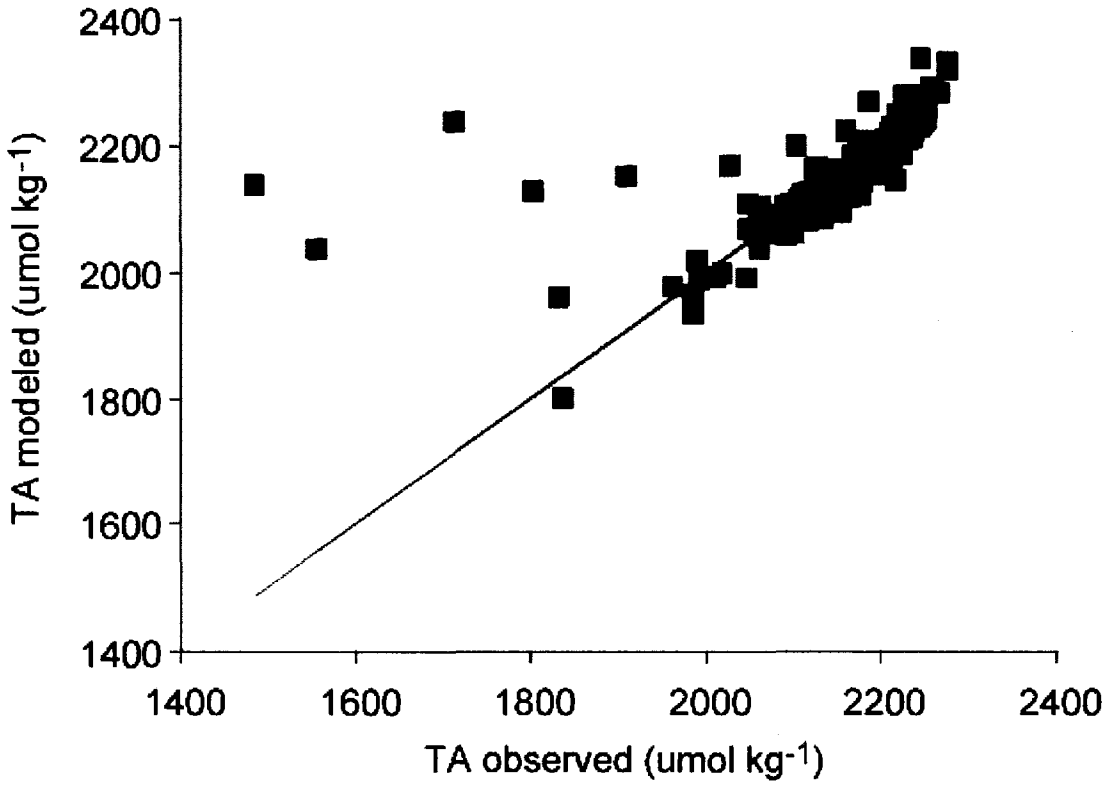

Figure 4. Modeled vs. measured total alkalinity for Atlantic-dominated waters. The 1:1 line is provided for reference.

2.2. Partial Pressure of CO_2 (pCO_2)

The pCO_2 was calculated from DIC, TA, SST, and SSS using the iterative formulations described in the Ocean Carbon Cycle Model Intercomparison Project protocols [*Najjar and Orr*, 1999], which used carbonic acid dissociation constants by *Mehrbach et al.* [1973] that were refitted by *Dickson and Millero* [1987]. The pH was computed using a combination of Newton-Raphson and Bisection iterative methods to solve for hydrogen ion concentrations.

2.3. Air-sea CO_2 flux (FCO_2)

The net air sea CO_2 flux was determined from the relationship

$$FCO_2 = k\sigma(\Delta pCO_2) \qquad (4)$$

where k, the gas transfer (or piston) velocity, determines the rate of air-sea CO_2 exchange, σ is the CO_2 solubility, and ΔpCO_2 is the air-sea difference in pCO_2. Atmospheric pCO_2 was set at 380 μatm for this study which was the highest . The sign of ΔpCO_2 determines the direction of CO_2 exchange; negative values will lead to a flux of CO_2 from the atmosphere into the ocean. The gas transfer velocity is determined from *Wanninkhof* [1992]

$$k = 0.39 * W_{10}^2 (Sc/660)^{-0.5} \qquad (5)$$

where W_{10} is the wind speed (m s^{-1}) computed from daily mean wind fields at 10 m above sea level obtained from the NCEP/NCAR Reanalysis project [*Kalnay et al.*, 1996] and Sc is the Schmidt number, which varies as a function of temperature

$$Sc = 2073.1 - 125.62\ SST + 3.627\ SST^2 - 0.043219\ SST^3 \qquad (6)$$

The solubility of CO_2 (σ) was computed as a function of temperature (T, Kelvin) and salinity (S) [*Weiss and Price*, 1980]

$$\sigma = \exp[(-162.8301 + 218.2968\left(\frac{100}{T}\right) + 90.9241\ln\left(\frac{T}{100}\right) - 1.47696\left(\frac{T}{100}\right)^2$$
$$+ S(0.025695 - .025225\left(\frac{T}{100}\right) + 0.0049867\left(\frac{T}{100}\right)^2)]$$

2.4. Arctic-wide application

For Arctic-wide calculation of FCO_2, data for SSS, SST, and Chl *a* are required at high temporal and spatial resolution over the entire basin. Satellite data best fulfills this criterion and is available for both Chl *a* and SST. However, no satellite data are yet available for SSS measurements. The next best option was to use SSS derived from a coupled ice-ocean Arctic Ocean {*Maslowki et al.*, 2000; 2002]. This model has a horizontal resolution of 9 km with 45 vertical layers and is well-validated using buoy-derived sea ice motion (International Arctic buoy data program) and satellite-derived sea ice concentration. Both SSS and SST were obtained for model runs simulating Arctic Ocean dynamics for the years 1998-2003. Validation of both SSS and SST were done as discussed in *Steiner et al.*, [2004].

We obtained surface Chl *a* concentrations from Level 3 SeaWiFS ocean color data (distributed by http://oceancolor.gsfc.nasa.gov/) using the OC4v4 algorithm [*O'Reilly et al.*, 1998], which is of the same 9 km resolution as the model-derived SSS and SST fields.

To calculate the CO_2 flux for the Arctic Ocean, only open water areas (ice free water) were considered. Open water area was determined from Special Sensor Microwave Imager (SSM/I) 37 and 85 GHz bands using the Polynya Signature Simulation Method (PSSM) algorithm [*Markus and Burns*, 1995], which allows determination of sea ice presence/absence at 6.25 km resolution. A given pixel is defined as being ice covered if the sea ice concentration is greater than approximately 10%.

All the input data have temporal resolution of 1 day with the exception of SeaWiFS Chl *a*, which were 8-day means for improved data coverage. All data were projected onto a common grid (polar stereographic). The resulting outputs (DIC, pCO_2 and FCO_2) were computed on a daily basis and mapped onto the same projection. All data were processed using Interactive Data Language (IDL) and all analysis and visualization was done using Matlab. Computation of pCO_2 and FCO_2 was done using FORTRAN 77. All computations were done at the High Productivity Technical Computing facility of Stanford's Center of Computational Earth and Environmental Science, which is composed of a Sun Sparc cluster running Solaris 10.

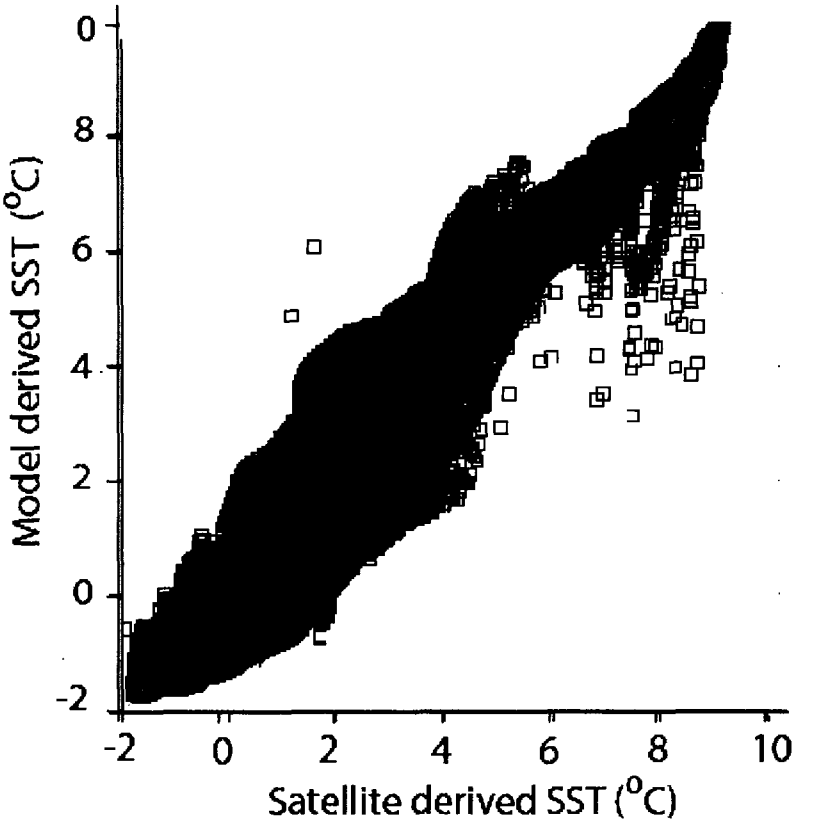

Figure 5. Modeled versus satellite-derived SST. The 1:1 black is provided for reference.

2.5. Defining Regions of Interest

The Arctic Ocean was defined as all waters north of the Arctic Circle (66° 33′ 39″). For the purpose of characterizing spatial differences, we divided the Arctic Ocean into eight geographic sectors demarcated by longitude [Fig. 6a]. These include the Chukchi (180° to 160°W), Beaufort (160°W to 100°W), Baffin (100°W to 45°W), Greenland (45°W to 15°E), Barents (15°E to 55°E), Kara (55°E to 105°E), Laptev (105°E to 150°E), and East Siberian (150°E to 180°) sectors.

3. Environmental Conditions

3.1. Salinity

The spatial distribution of salinity in the Arctic Ocean is influenced by the inflow of higher salinity (~34.8) waters from the Atlantic Ocean through the Fram and Nares straits as well as by Pacific waters of lower salinity (~32.5) entering through the Bering Strait [Fig. 6b]. Salinity is also highly influenced by the river waters flowing in from both the western and eastern Arctic; the effect of these freshwater inputs can be seen in Fig. [6b] as low salinity waters along the coast of the Beaufort, Laptev, Kara and East Siberian seas. During the course of a year, the salinity is highest in the months of April-May and then falls to its minimum value during the August-September period. Seasonal variability is highest in the Pacific-influenced waters due to variable river flow compared to that in the Atlantic-influenced sectors. In the Pacific sectors the salinity varies by as much as 3 psu compared to less than 1 psu variability in the Atlantic dominated sectors. During the period 1998-2003, the average annual salinity of the Arctic Ocean decreased at the rate of 0.01 per year (R^2=0.69, p=0.04).

3.2. Sea Surface Temperature

The SST of the Greenland and the Barents sectors of the Arctic Ocean is influenced by the influx of warm Atlantic Ocean as evidenced by the elevated

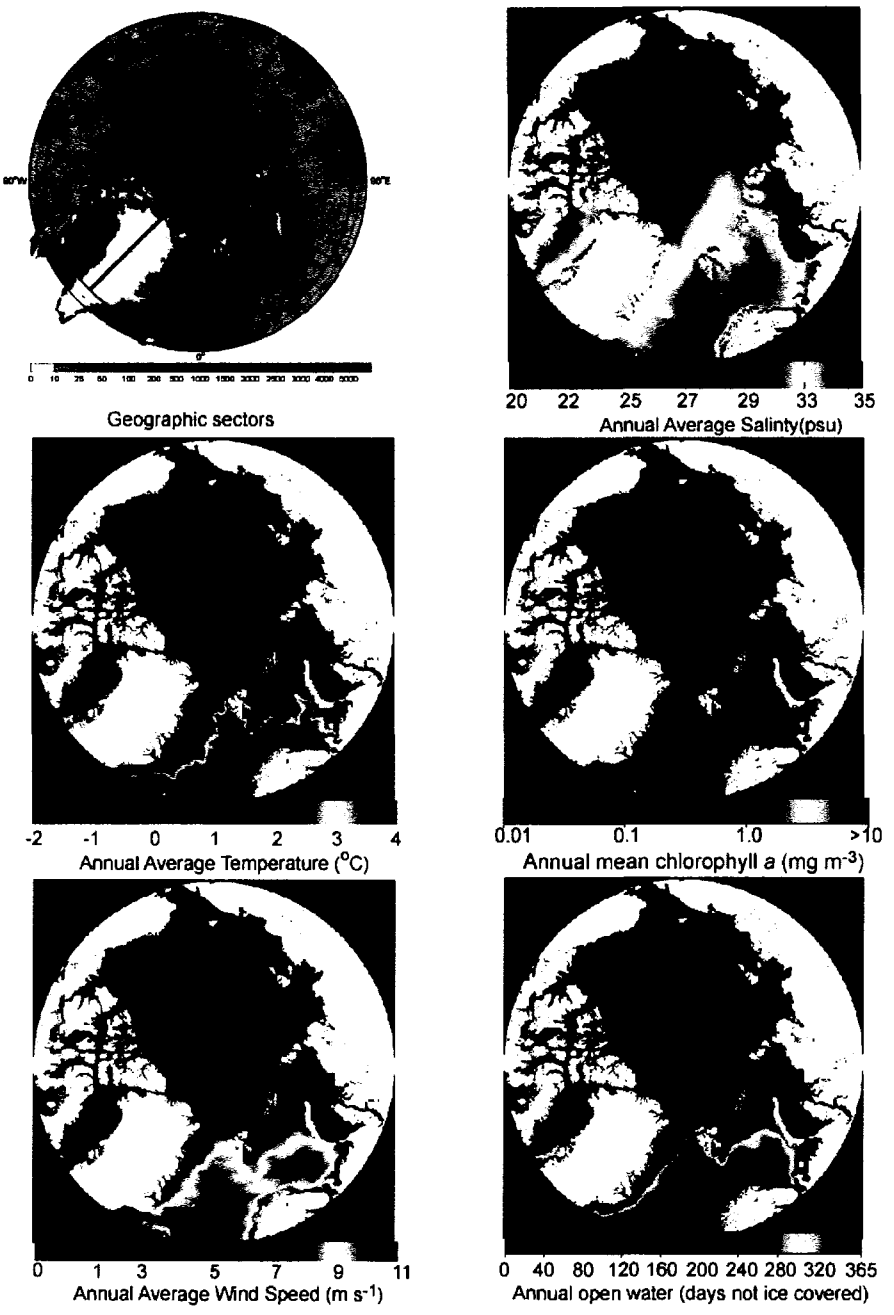

Figure 6. Maps of a) Arctic sectors and annual means for b) SSS, c) SST, d) number of days per year with open water, e) Chl *a*, and f) wind speed.

SST shown in Fig. [6c]. The seasonal pattern of open water is almost the opposite of salinity with the maximum temperature and greatest open water area found during the months of August-September. SST was highest in the Greenland sector followed by the Barents sector with an annual average temperature of 2.8°C and 2.2°C, respectively. The lowest temperature was found in the Laptev and East Siberian sectors (annual average -1.3°C at both the sectors). During the period 1998-2003 there was a significant (R^2=0.7, p=0.03) increase in SST in the whole of the Arctic increasing at the rate of 0.04°C per year.

3.3. Chlorophyll a

The spatial distribution of Chl *a* is marked by higher values on the shelf compared to deeper waters [Fig 6], reflecting higher nutrient concentrations and rates of primary production. The annual cycle of Chl *a* is characterized by an initial spring bloom in April-May, and in some years a subsequent summer bloom during July-August. Between these two blooms, mean surface Chl *a* concentrations in the Arctic Ocean remain relatively high, generally exceeding 1.5 mg Chl *a* m^{-3}. There is no significant secular trend in Chl *a* in any of the sectors or in the pan-Arctic basin during the period 1998-2003.

3.4. Wind

The spatial pattern of wind speed [Fig 6] shows distinctly high speeds over the Greenland and Barents sectors and lower values elsewhere. The annual cycle in wind speed is similar Arctic-wide, with high winds (4.9 m s^{-1}) during October-March that decrease in intensity from April to September (3.7 m s^{-1}). Seasonal variability in wind speed was highest in the Barents and Greenland sectors, with amplitudes of 5.5 and 4.7 m s^{-1}, respectively, from an annual average wind speed of 5.6 m s^{-1} and 5.2 m s^{-1}, respectively. Variability in the other sectors ranged from 2-4 m s^{-1}, with the lowest variability observed in the Laptev sector.

3.5. Open water area

The sectors with greatest amount of open water area during 1998-2003 were the Atlantic influenced sectors of the Barents and the Greenland seas [Fig 6] where open water persisted for >320 days per year, except for the northeastern Greenland coast and northern Barents sector. In the Chukchi and Baffin Bay sectors, open water lasts for approximately 160-200 days per year. Open water area is greatest during the months August-September, lagging the SST peak by about 20 days. More detailed changes in open water area can be found in *Pabi et al.* [2008]. There was no secular trend in open water area in the Arctic Ocean during 1998-2003.

4. Results

4.1. DIC

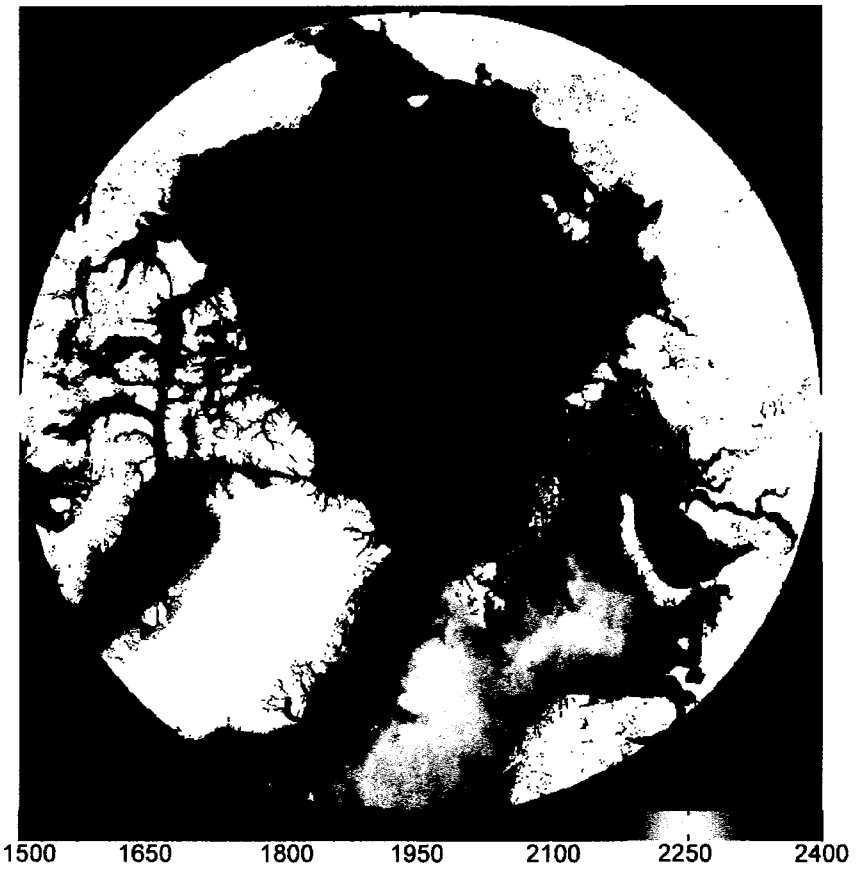

Figure 7. Map of annual average DIC concentration (μmol kg^{-1}) in the Arctic Ocean.

The spatial pattern of mean annual surface DIC concentrations calculated using Eq. 1 exhibits a great deal of spatial variability within the Arctic Ocean [Fig 7]. Mean surface DIC was highest in Atlantic waters of the Greenland and Barents sectors, ranging from 1581 to 2242 μmol kg^{-1}. Areas of high DIC concentration were also found in the Baffin and Beaufort sectors, although, on

average, values were substantially lower than regions dominated by Atlantic waters. The lowest surface DIC was found in the Chukchi, East Siberian, Laptev, and coastal regions of the Kara sectors. These DIC distributions are consistent with *in-situ* measurements made previously [*Bates et al.*, 2006; *Miller et al.*, 1999; *Kaltin et al.*, 2002; *Omar et al.*, 2003]. DIC also was lower in areas influenced by freshwater sources from rivers, consistent with observations made by *Hansell et al.* [2004] in the Beaufort Gyre.

The temporal trend in DIC is similar for all Arctic sectors during the open water season. The highest values for DIC are found in the spring, particularly in regions of deep water, due to entrainment of DIC-rich deep waters into the surface layer during deep mixing in winter. As the season progresses, increased light availability stimulates phytoplankton production and a marked drawdown of DIC. In highly productive sectors, such as the Chukchi, DIC can fall from a spring maximum of 2100 μmol kg^{-1} to 1850 μmol kg^{-1} [Fig. 8]. At the same time, increased surface temperatures increases pCO_2 and accelerates the loss of CO_2 from the ocean to the atmosphere, diminishing surface DIC. In river-dominated sectors such as the Beaufort, Laptev, Kara, and East Siberian, the seasonal amplitude in DIC is further exaggerated by dilution of surface waters by low-DIC water from rivers, which reach peak discharges in spring and early summer [*Pavelsky and Smith*, 2004].

By late summer and early autumn, surface DIC concentrations begin to increase again as surface waters cool, wind speeds increase, and mixed layers begin to deepen, entraining higher DIC water into the surface. This is most easily seen in the Greenland and the Barents sectors, due to their relatively long open water seasons [Fig 6]. As sea ice begins to form in the other Arctic sectors, salinization of surface waters also aids in vertical mixing and restoring surface DIC concentrations to the early spring values. However, because of the large freshwater fluxes in many regions of the Arctic (due primarily to river flow), surface waters remain stratified for much of the year [*Harms et al.*, 2000; *Dmitrenko et al.*, 2001], resulting in little entrainment of DIC-rich deep waters into the surface layer and relatively low DIC concentrations in surface waters that persist throughout the winter (e.g. Laptev, East Siberian).

The temporal trends observed here [Fig 8] are consistent with previous measurements of DIC in Arctic waters. Our estimates of surface DIC concentration for the Chukchi sector vary from 2073 to 2166 μmol kg^{-1} in spring and 997 to 1930 μmol kg^{-1} in summer, similar to measurements made by *Bates et al.* [2006] for the same seasons (2100-2200 μmol kg^{-1} in spring and 526-1900 μmol kg^{-1} in summer). In the Barents sector, we estimated a mean DIC concentration in July between 1998 and 2003 of 2105 μmol kg^{-1}, with a value of 2130 μmol kg^{-1} in July of 1999.

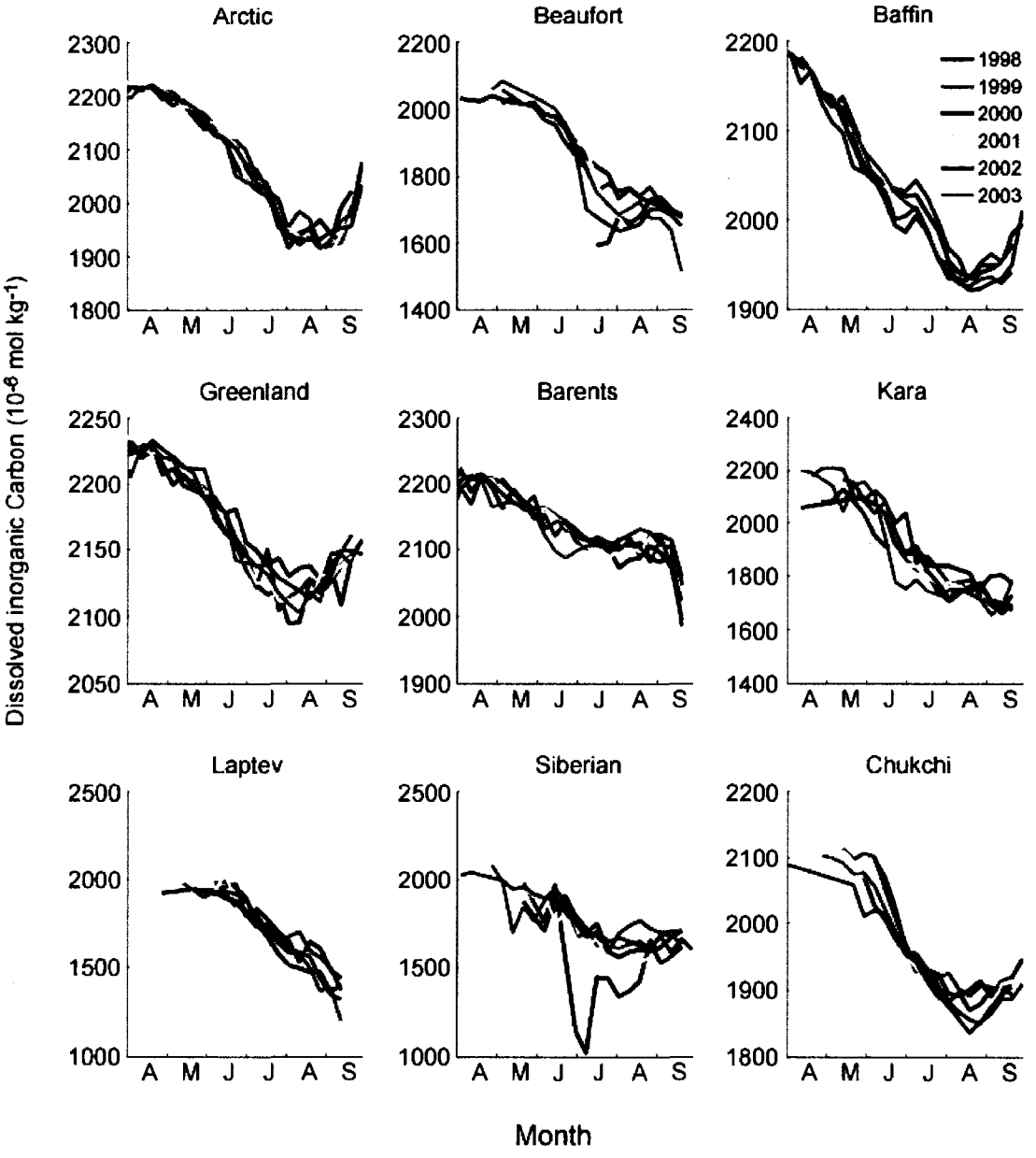

Figure 8. Time series of DIC (μmol kg^{-1}) in the Arctic Ocean and its geographical sectors.

This is in excellent agreement with the July 1999 measurements of DIC in the Barents Sea of 2136 μmol kg^{-1} [*Kaltin et al.*, 2002]. In the Beaufort sector, measurements of DIC made during September of 2008 were within 3% of our estimate of 2044±42 (2044± standard deviation) μmol kg^{-1} averaged over the same time period [*H. Thomas, pers. comm.*]. Finally, in the Greenland sector during the period 1993-1995, DIC concentrations dropped from a mean of 2143 μmol kg^{-1} in spring to 2064 μmol kg^{-1} in summer, but remained as high as 2100 μmol kg^{-1} in several regions [*Miller et al.*, 1999]. In our study, the average DIC concentration in the Greenland sector during the spring and summer of 1998-2003 was 2186±23 μmol $kg^{-1}$and 2119±23 μmol kg^{-1}, respectively. The slightly higher values in our study for the Greenland sector may be due to an increase in dissolution of DIC from the atmosphere since 1995 [*Sabine et al.* 2004]. A similar anthropogenic increase in DIC was reported for the Barents sector by *Omar et al.* [2003] between the years 1967 and 2000-2001.

4.2. Partial Pressure of CO_2 (pCO_2)

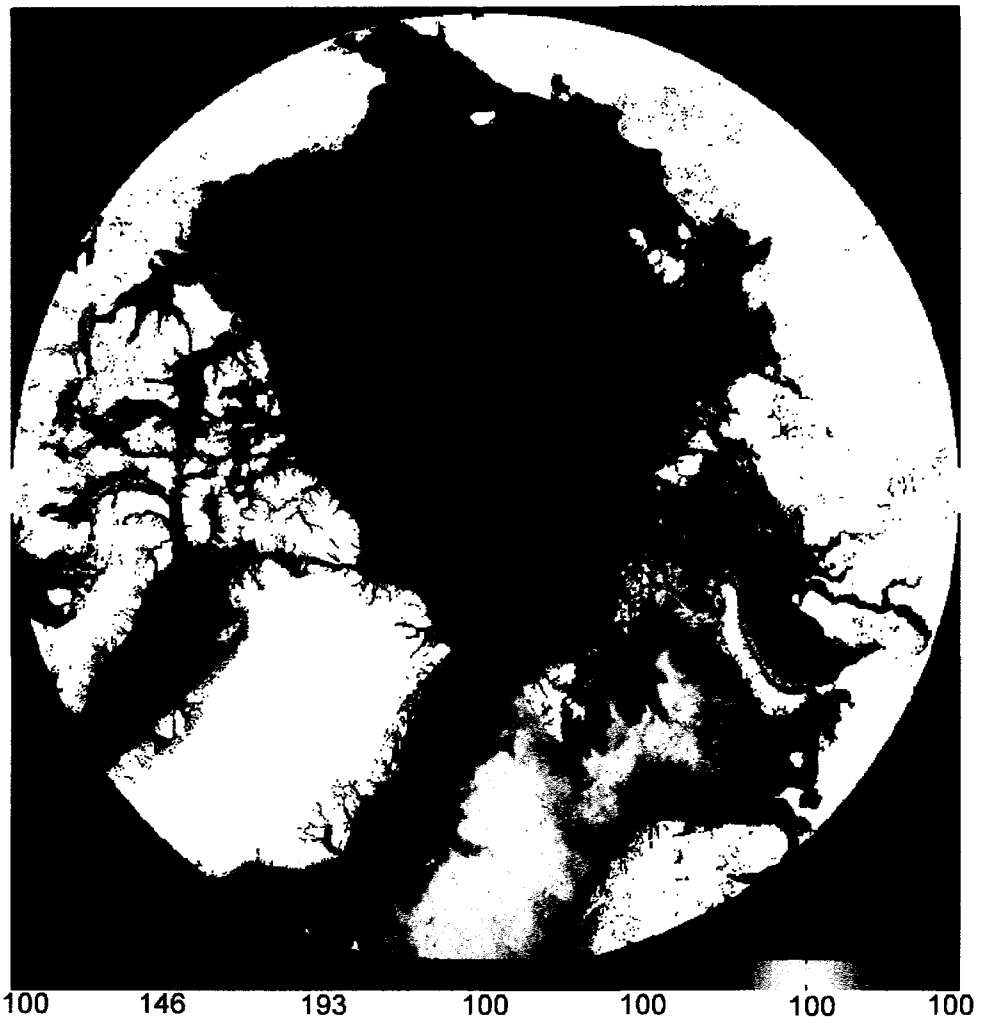

Figure 9. Map of annual average pCO_2 (μatm) in the Arctic Ocean.

The spatial pattern of pCO_2 broadly mimics the spatial pattern of DIC, with higher pCO_2 in the regions dominated by Atlantic waters and relatively lower values in the other sectors. This is consistent with observation by *Kaltin and Anderson* [2005] that of the flux of atmospheric CO_2 into the Atlantic-

influenced Barents Sea was about half that in the Chukchi Sea. The relatively high pCO_2 in surface waters close to the deeper central basin is due to a combination of deep mixing entraining high DIC and reduced surface alkalinity from dilution by sea ice melt.

In the Chukchi sector, pCO_2 was higher over the central Chukchi shelves than in coastal waters of the western Beaufort Sea [Fig 9], similar to the spatial pattern reported by *Bates et al.* [2006]. Also in agreement with *Bates et al.* [2006], we found low pCO_2 [Fig 9] along the coast in the vicinity of freshwater discharge from the Mackenzie River. In the Greenland sector, the average pCO_2 was 313±151 μatm during 1998-2003. Measurements archived by *Takahashi et al.* [2002] suggest that the average pCO_2 measured in this region was 282±31 μatm in 1995. The relatively higher values of pCO_2 in this study is most likely due to equilibration of the ocean water in this region with increasing atmospheric CO_2 values since 1995. This is supported by an increase in pCO_2 of 28±21 μatm from 1994 to 2001 in the Greenland Sea reported by *Nakaoka et al.* [2006].

The temporal trend of pCO_2 also is similar to that of DIC, with high pCO_2 in early spring that decreases throughout the spring and summer [Fig 10]. Also like DIC, pCO_2 increases in early autumn in several sectors of the Arctic Ocean, including the Greenland, East Siberian, and Chukchi. The

correspondence between the temporal trends in DIC and pCO_2 demonstrates that pCO_2 in these Arctic waters during spring and summer is controlled more by decreases in DIC concentration than by decreases in CO_2 solubility that result from increasing temperatures (which would increase pCO_2). The relatively small impact of SST on pCO_2 is probably due to low seasonal variability of SST in these polar waters compared to the large seasonal changes in DIC.

In the Pacific-dominated waters of the Chukchi Sea, we calculated surface pCO_2 ranging from a high of 346±132 μatm in May-June and dropping to 222±152 μatm in July-August and 209±125 μatm in September [Fig. 10]. Similarly, *Bates et al.* [2006] reported high pCO_2 in the Barrow Canyons region and western Beaufort Sea during May-June (~300-350 μatm) that fell to 180-220 μatm in July-August. Also sampling the Chukchi along the Central Channel west of Cape Lisburne to Barrow Canyons, both *Pipko et al.* [2002] and *Murata and Takizawa* [2003] reported somewhat higher pCO_2 levels in late September, ranging from 280-320 μatm and of 290-350 μatm. However, *Murata and Takizawa* [2003] reported lower pCO_2 values in this region in September of 1999 (240-280 μatm) and 2000 (180-220 μatm), similar to values calculated here. In the Atlantic-dominated waters of the Greenland sector, our results show that pCO_2 is highest in April (335±1 μatm) and decreases

thereafter until reaching its seasonal minimum (297±11 µatm) in July-August [Fig. 10]. This seasonal difference of 38 µatm agrees well with the range of 42 µatm calculated from observed seasonal pCO_2 changes in the Greenland Sea between April and July (*Takahashi et al.*, 2002).

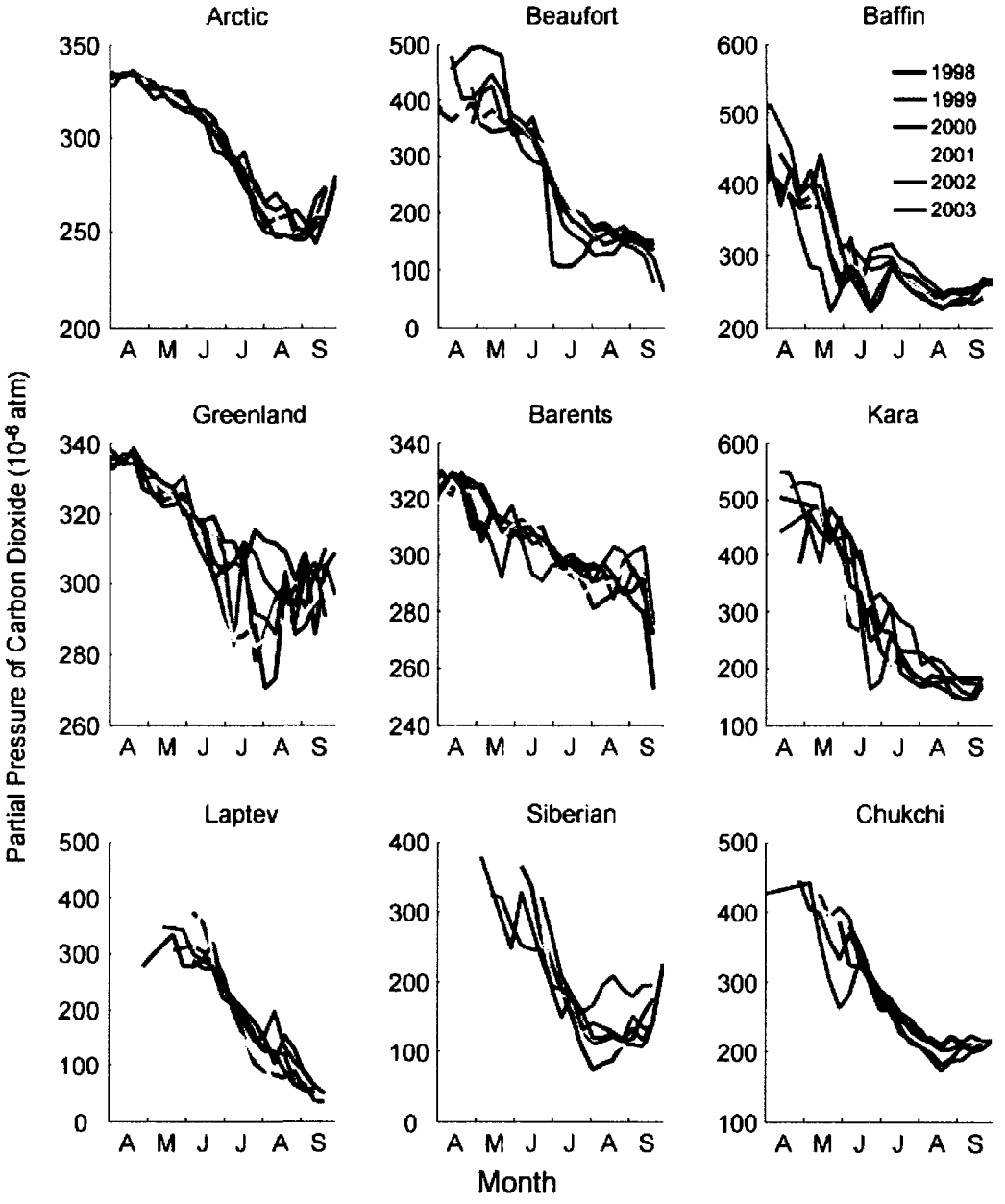

Figure 10. Time series of pCO_2 (μatm) in the Arctic Ocean and its geographical sectors.

4.3. Air-sea flux of CO_2 (FCO_2)

FCO_2 is primarily influenced by ΔpCO_2 as well as wind speed that drives turbulence in the marine atmospheric boundary layer. Consequently, the spatial pattern of mean annual FCO_2 was broadly similar to that of the mean annual pCO_2 [Fig. 11]; the Pacific-influenced waters exhibited a higher FCO_2 from the atmosphere into the ocean (more negative FCO_2) than the other sectors. It is notable that the mean FCO_2 was negative in most places, showing that the Arctic Ocean is on average a net sink of atmospheric CO_2.

The temporal pattern of FCO_2 illustrates that most sectors experience outgassing in the beginning of the year. This is most likely due to a combination of high pCO_2 conditions under the retreating the sea ice [Fig. 10], coupled with high wind-speed characteristic of this period and low primary production that is limited by light. In the Pacific-dominated sectors, the influx of Pacific waters supersaturated in CO_2 [*Kaltin and Anderson*, 2005] also would enhance outgassing of CO_2 in this region. In the subsequent months, the increase in both freshwater content and primary production in ice-free waters leads to depletion of CO_2 in the surface layers [*Kaltin and Anderson*, 2005]. Consequently, the flux of CO_2 into the surface ocean increases.

In contrast, no outgassing of CO_2 was observed in the beginning of the year in the Barents and Greenland sectors since surface waters in these sectors

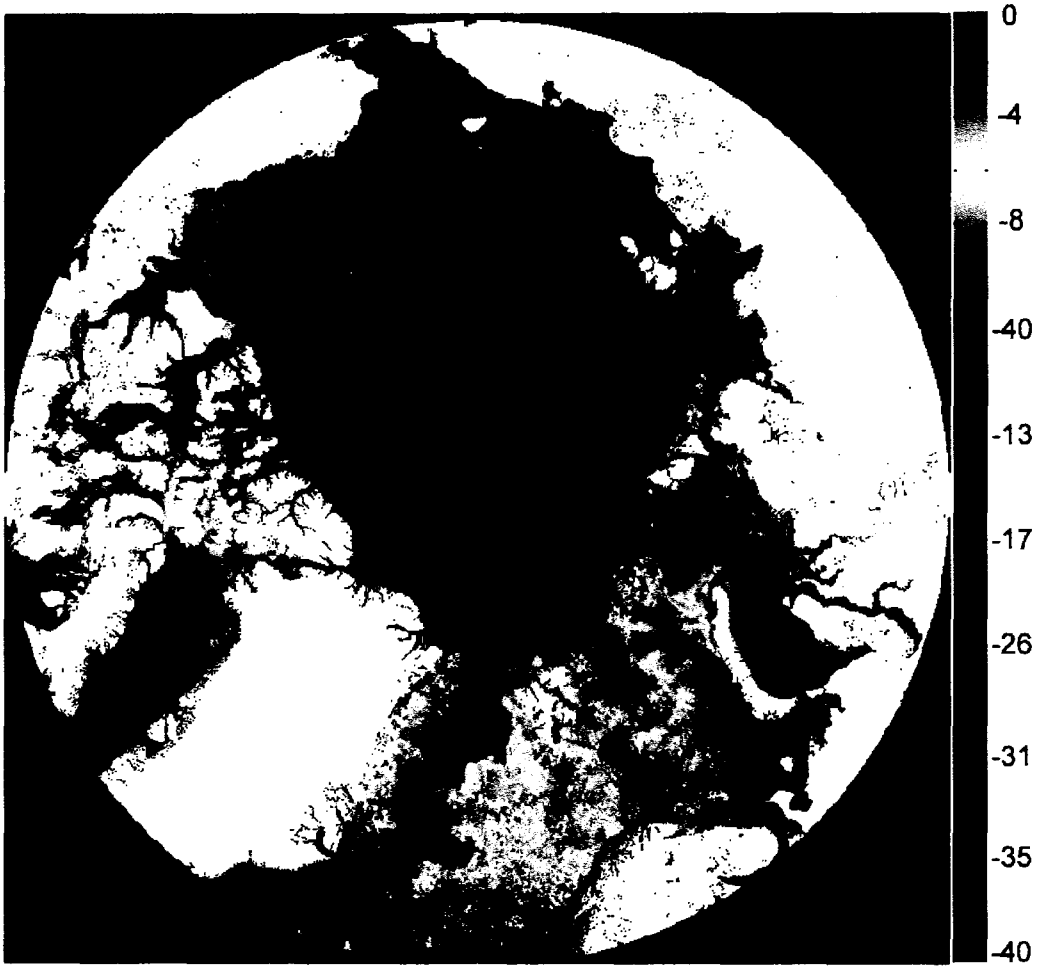

Figure 11. Map of mean daily FCO_2 (mmol m^{-2} d^{-1}) in the Arctic Ocean.

remained under-saturated in CO_2 throughout the year. Unlike in other sectors, the air-sea flux of CO_2 into surface waters in the Barents and Greenland sectors decreased during the middle of the year [Fig 12]. This is

due to a steep decrease in wind speed in these sectors combined with low seasonal variability of pCO_2 relative to other sectors. However, the flux of CO_2 into the ocean intensified in September as the wind speed increased at a time when pCO_2 in these waters was still quite low. This pattern matches that derived by *Nakaoka et al.* [2006] for the Greenland and the Barents Sea, who also emphasize the effect of wind on the air-sea CO_2 flux. The Arctic-wide monthly FCO_2 trend is heavily weighed by that of Barents and Greenland sector and looks similar to that of these sectors.

In the Chukchi sector, the temporal trend in FCO_2 is consistent with that reported by *Bates et al.* [2006] for the same region. In May-June, *Bates et al.* [2006] measured rates of FCO_2 ranging from <-0.1 to -1.0 mmol CO_2 m^{-2} d^{-1}; in this study we estimated FCO_2 to be -1.1±1.0 mmol CO_2 m^{-2} d^{-1} for this same sector. During July-August, the FCO_2 reported by *Bates et al.* [2006] ranged from 30-90 mmol CO_2 m^{-2} d^{-1} in the Central valley, Hanna Valley, and Barrow Canyon and <0.1-2.0 mmol CO_2 m^{-2} d^{-1} over the Chukchi Sea slope. Here we calculated a spatial mean FCO_2 of -13±10 mmol CO_2 m^{-2} d^{-1} for the Chukchi sector during July-Aug, with a maximum FCO_2 of -30 mmol CO_2 m^{-2} d^{-1} in mid-August. Our mean September FCO_2 of -14±10 mmol CO_2 m^{-2} d^{-1} agrees with the values observed by *Murata and Takizawa* [2003], who reported FCO_2 ranging from -17 mmol CO_2 m^{-2} d^{-1} over the shelves to -11 mmol CO_2 m^{-2} d^{-1} on the slopes. In the Greenland sector, the FCO_2 measured by *Takahashi et al.*

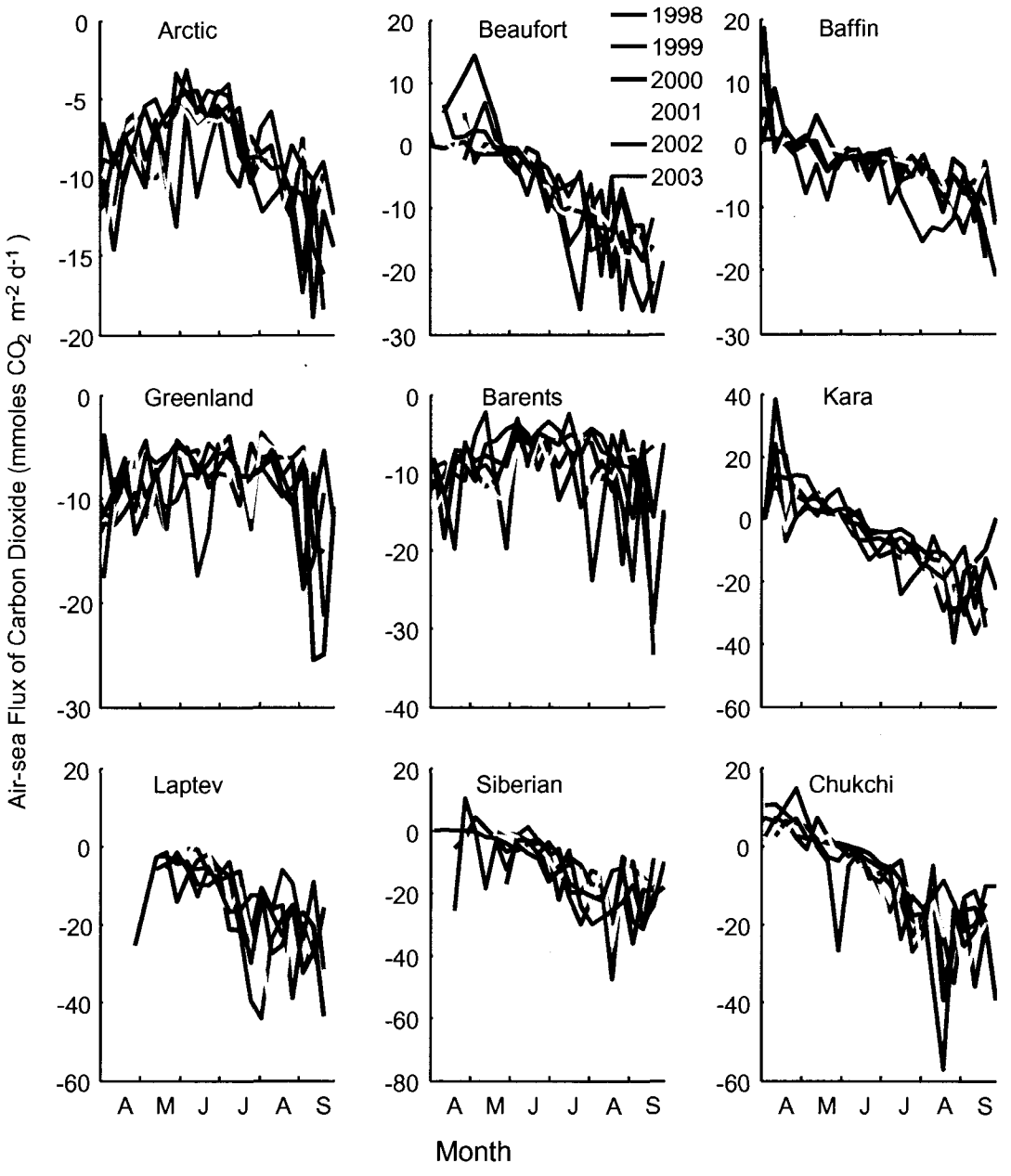

Figure 12. Time series of FCO_2 (mmoles CO_2 m^{-2} d^{-1}) in the Arctic Ocean and its geographical sectors.

[2002, *http://www.ldeo.columbia.edu/res/pi/CO2*] ranged from -16 to -48 mol m^{-2} $month^{-1}$ during the months of March-August, in agreement with the monthly FCO_2 of -28 mol m^{-2} $month^{-1}$ during the same period in this sector obtained in this study.

4.4. Annual FCO_2

The annual FCO_2 was negative in almost all regions of the Arctic Ocean, indicating that the Arctic Ocean is a net sink of atmospheric CO_2 [Fig 13]. Annual FCO_2 was most negative in the Greenland and the Barents sectors [Fig. 13] because of their relatively low pCO_2 throughout the year [Fig. 10] and their longer open water season (>320 days yr^{-1}) [Fig. 6]. In general, the annual FCO_2 into the ocean was lower (i.e. less negative) closer to the deep central basin. This was due to higher DIC concentrations in these regions resulting from deeper mixing as well as to increased pCO_2 as a result of lower alkalinity caused by melting of sea ice.

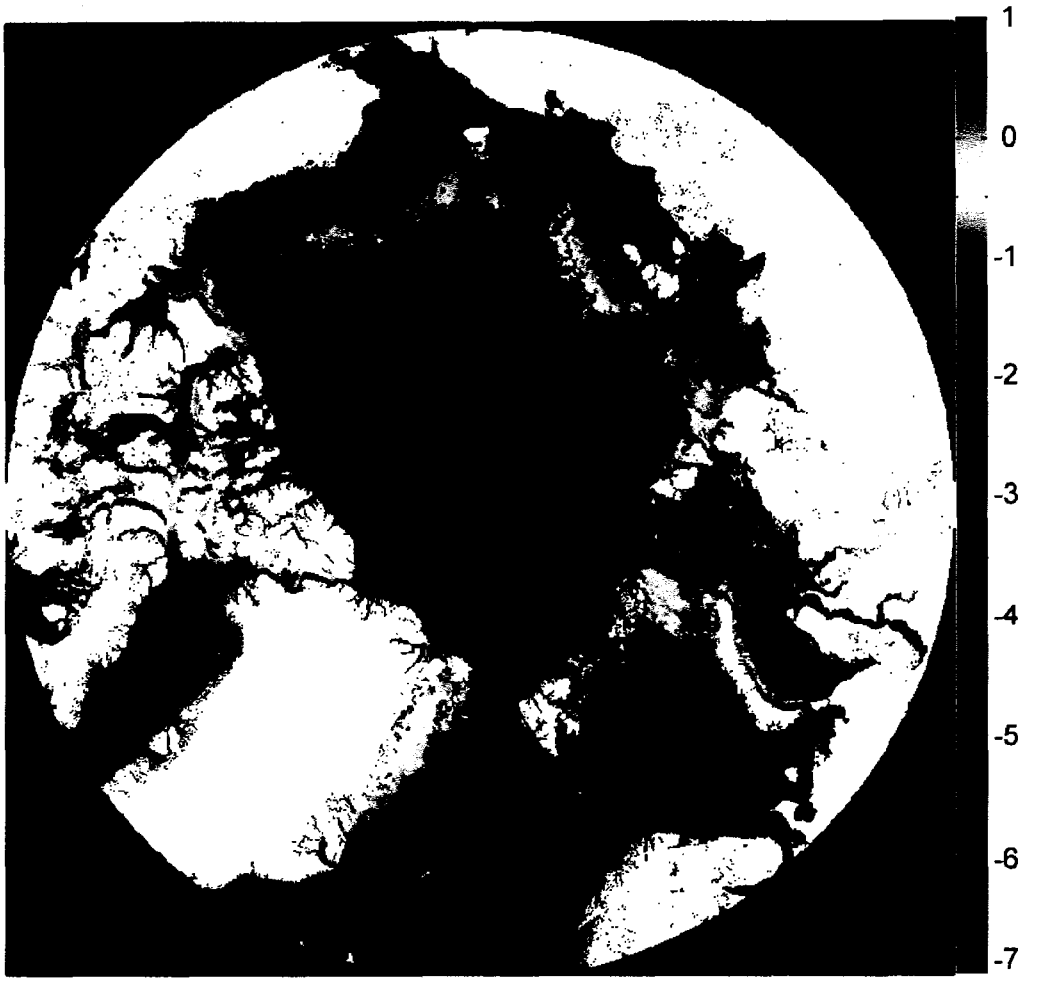

Figure 13. Map of mean annual FCO_2 (mmol m^{-2} yr^{-1}) in the Arctic Ocean.

Annual FCO_2 in the Barents sector averaged -37±14 g C m^{-2} yr^{-1} over the whole sector, in good agreement with previous estimates of -46±27 g C m^{-2} yr^{-1} by *Nakaoka et al.* [2006] and -44±10 g C m^{-2} yr^{-1} by *Fransson et al.* [2001], although these studies covered a much smaller spatial extent. In the Greenland sector, the annual FCO_2 was -38±15 g C m^{-2} yr^{-1}, which compares well with the estimate by *Takahashi et al.* [2002], who calculated an annual

FCO_2 of -25 to -50 g C m^{-2} yr^{-1} (after correction using 10 m winds from *http://www.ldeo.columbia.edu/res/pi/CO2*). After these sectors, the highest FCO_2 was in the Chukchi sector (-27 g C m^{-2} yr^{-1}). The lowest annual FCO_2 per unit area was in the Kara (-18 g C m^{-2} yr^{-1}) and Siberian sectors (-19 g C m^{-2} yr^{-1}).

The spatially-integrated annual FCO_2 in the Atlantic-dominated Barents and Greenland sectors was -88±5 Tg C (10^{12} g C) yr^{-1}, virtually identical to the value of -90 Tg C yr^{-1} reported by *Skjelvan et al.* [1999a, 1999b]. This comprised of -54±4 Tg C in the Greenland sector and -34±4 Tg C in the Barents sector. Thus, these two sectors comprised of the largest spatial integrated annual flux in the whole of the Arctic. The largest annual flux in the Greenland and Barents sectors was -59 Tg C in 1999 and -40 Tg C in 2000, respectively. The high flux in the Barents sector in 2000 also coincided with the year of maximum open water area (1,207,785 km^2) as well highest mean annual wind speed (5.4 m s^{-1}). However in the Greenland sector, the highest spatially integrated flux in 1999 was not the year of highest open water area (open water area was 1,665,777 km^2 in 1999, slightly less than the maximum of 1,677,023 km^2 attained in 2003). Rather, it was the highest wind speed in 1999 i (5.8 m s^{-1}) in conjunction with lowest pCO_2 (308 µatm) that led to the large spatially-integrated fluxes in this sector.

In the Chukchi sector, the annual FCO_2 was computed to be -13±1.6 Tg C yr^{-1}, about one third the total flux of -38±7 Tg C yr^{-1} reported by *Bates et al.*

[2006]. However, the Chukchi Sea boundaries used by *Bates et al.* [2006] encompassed an area 3-fold larger (595,000 km^2) than that used in the present study (192,887±39,639 km^2). Correcting for this difference in areas brings the two estimates much more in line. The highest flux in the Chukchi Sea was in 2003 (14.3 Tg C), which coincided with the year of maximum open water area during 1998-2003.

After the Greenland and Barents sectors, the highest spatially-integrated annual FCO_2 was in the Kara sector (-18±2 Tg C yr^{-1}), followed by the Baffin (-14±2 Tg C yr^{-1}) and Laptev (-14±2 Tg C yr^{-1}) sectors [Table 2]. Although the Baffin sector had more open water area than the Kara sector (Baffin: 415,973 km^2, Kara: 268,962 km^2) [Table 3], the higher FCO_2 in the Kara was due to lower pCO_2 values (Baffin: 310±9 µatm, Kara: 294±21 µatm) [Table 4] and higher wind speed (Baffin: 3.8 m s^{-1}, Kara: 4.2 m s^{-1}) [Table 5]. The spatially-integrated annual FCO_2 in the Laptev and Beaufort sectors was -14±2 Tg C yr^{-1} and -13±2 Tg C yr^{-1} [Table 2], respectively. Although both these sectors had open water areas comparable to the Kara (Kara: 268,962 km^2, Laptev: 222,143 km^2, Beaufort: 247,136 km^2) [Table 3], and comparable pCO_2 (Kara: 294±21 µatm, Laptev: 210±18 µatm, Beaufort: 254±16 µatm) [Table 4], these sectors also had lower annual wind speed than Kara (Kara: 4.2 m s^{-1}, Laptev: 3.4 m s^{-1}, Beaufort: 3.8 m s^{-1}) [Table 5]. The lowest spatially-integrated annual FCO_2 was

in the Siberian sector (-8±3 Tg C yr^{-1}) which had the lowest open water area among all Arctic sectors (159,593 km^2). However, the last two years (2002-2003) have shown a sharp increase in spatially-integrated annual FCO_2 in this sector due to a similar sharp increase in open water area [Fig 14].

Table 2: spatially-integrated annual FCO_2 (Tg C yr^{-1})

	Beaufort	Baffin	Greenland	Barents
1998	-17.32	-13.15	-50.54	-33.84
1999	-16.09	-12.22	-59.38	-28.46
2000	-11.58	-15.93	-55.73	-40.22
2001	-8.22	-10.03	-51.03	-35.99
2002	-11.38	-16.48	-49.99	-32.57
2003	-13.05	-15.59	-57.24	-35.84

	Kara	Laptev	Siberian	Chukchi
1998	-16.07	-10.77	-5.10	-13.88
1999	-14.29	-17.95	-6.19	-13.90
2000	-25.35	-17.29	-7.40	-10.08
2001	-22.58	-9.31	-6.15	-12.17
2002	-15.11	-15.12	-11.72	-12.80
2003	-13.15	-11.63	-11.62	-14.29

Table 3: Annual Average Open water area (km^2)

	Beaufort	Baffin	Greenland	Barents
1998	380758	423050	1575599	967402
1999	297668	372462	1665777	1070151
2000	203738	416672	1636341	1207785
2001	144982	396197	1611587	1191733
2002	224457	444381	1677023	1132343
2003	231216	443073	1669671	1008635

	Kara	Laptev	Siberian	Chukchi
1998	192915	200323	90138	236189
1999	235376	270142	139975	246303
2000	346908	251688	145737	184402
2001	360909	124219	117027	166381
2002	257410	231107	216279	251899
2003	220254	255381	248404	274871

Table 4: Annual Average Partial pressure of CO_2 (µatm)

	Beaufort	Baffin	Greenland	Barents
1998	278	308	318	292
1999	247	301	314	304
2000	245	309	308	301
2001	255	310	309	300
2002	233	308	317	289
2003	265	328	313	292

	Kara	Laptev	Siberian	Chukchi
1998	269	181	140	268
1999	317	226	234	307
2000	292	223	225	303
2001	271	194	195	286
2002	319	213	228	300
2003	294	224	206	300

Table 5: Annual Average wind speed (m s^{-1})

	Beaufort	Baffin	Greenland	Barents
1998	3.94	3.87	5.73	5.13
1999	3.82	3.81	5.76	5.03
2000	3.84	3.91	5.72	5.44
2001	3.91	3.81	5.38	5.16
2002	3.84	3.79	5.73	5.07
2003	4.00	4.07	5.48	5.14

	Kara	Laptev	Siberian	Chukchi
1998	4.18	3.39	3.92	4.56
1999	4.04	3.38	3.82	4.53
2000	4.39	3.43	4.02	4.67
2001	4.23	3.34	4.08	4.94
2002	4.12	3.42	4.08	4.74
2003	4.15	3.48	3.92	4.67

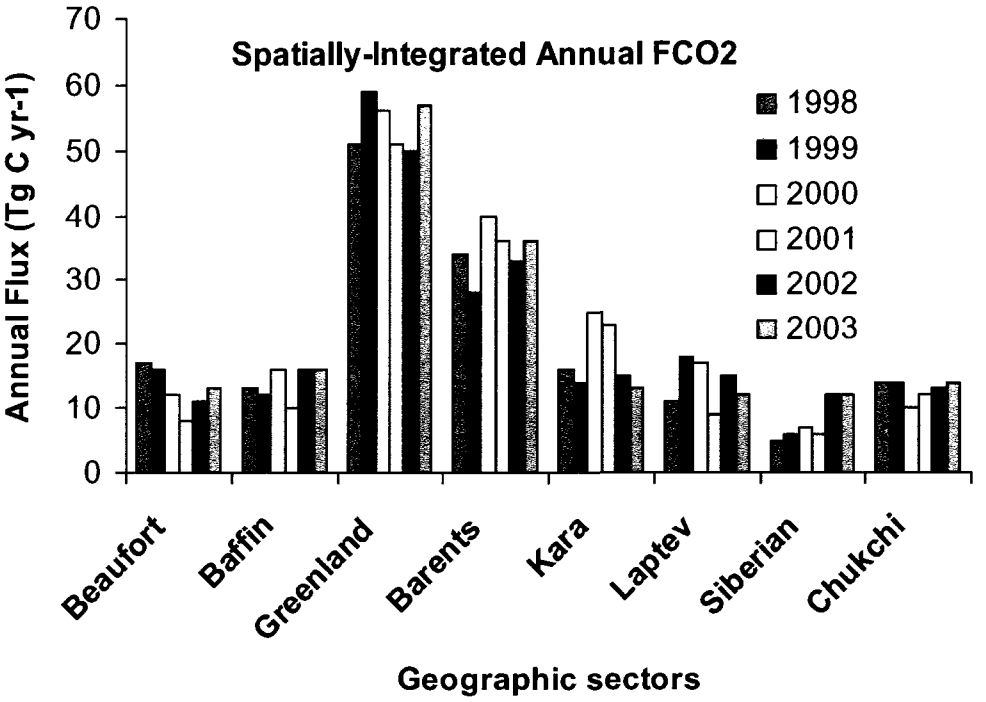

Figure 14. Spatially integrated annual FCO2 in the eight sectors of the Arctic Ocean.

The spatially-integrated annual FCO_2 for the pan-Arctic Ocean (north of 66°N) was calculated here to be -169±27 Tg C yr^{-1}. This is somewhat lower than the estimate of -310 Tg C yr^{-1} for waters north of 50°N by *Takahashi et al.* [2002]. However, the Arctic estimate by *Takahashi et al.* [2002] included the highly productive Bering Sea and North Atlantic, which were not part of our study. *Bates et al.* [2006] estimated pan-Arctic FCO_2 to be -66 Tg C yr^{-1}. However, given that annual FCO_2 for just the Barents and the Greenland Seas

has been estimated at -90 Tg C yr^{-1} [*Skjelvan et al.*, 1999a, 1999b], the pan-Arctic estimate by *Bates et al.* [2006] seems to be on the low side. Combining the annual FCO_2 estimate for the Chukchi Sea (-38 Tg C yr^{-1}) by *Bates et al.* [2006] with the estimates for the Barents and the Greenland Seas (-90 Tg C yr^{-1}) by *Skjelvan et al.* [1999a, 1999b] yields a pan-Arctic FCO_2 value of -128 Tg C yr^{-1}, indistinguishable from our estimate of -127 Tg C yr^{-1} for these same three sectors (after correcting for the 3-fold difference in Chukchi Sea area used by our study and that of *Bates et al.* [2006]).

4.6. Secular trends

There was no statistically significant secular trend in mean annual DIC during 1998-2003, averaged either over the whole Arctic or in any of the sectors. Similarly, no secular trend in pCO_2 or FCO_2 was also observed over this time period, with the exception of annual FCO_2 in the East Siberian sector, which exhibited a significant (R^2=0.77, p=0.02) increasing annual trend due to increasing open water area.

Although no significant secular trend was found for most of the Arctic, some significant trends appeared when we looked at sub-annual level. DIC in May-June increased significantly between 1998 and 2003 in the Baffin (R^2=0.66, p=0.05, slope=4.7 μmol kg^{-1} yr^{-1}) and Beaufort (R^2=0.88, p=0.006, slope=10.0 μmol kg^{-1} yr^{-1}) sectors. A concurrent increase in pCO_2 in May-June was observed in the Baffin sector (R^2=0.74, p=0.03, slope= increased 1.2 9 μatm yr^{-1})

but not the Beaufort. Interestingly, DIC decreased in these same sectors in August-September (Baffin: R^2=0.73, p=0.03, slope= -3.9 μmol kg^{-1} yr^{-1} and Beaufort R^2=0.69, p=0.04, slope=-18.3 μmol kg^{-1} yr^{-1}) as well as in the Chukchi sector (R^2=0.88, p=0.005, slope=-7.8 yr^{-1}).

As in the case of DIC, pCO_2 in August-September decreased significantly in the Chukchi sector during 1998-2003 (R^2=0.74, p=0.03, slope= -4.9 μatm yr^{-1}), making it a more intense sink through time during these months. This decrease in pCO_2 was most likely due to the combined effect of reduced DIC and reduced salinity. The Beaufort and Baffin sectors, which exhibited decreases in DIC, did not experience reduced pCO_2 in August-September, probably due to concurrent increases in temperature, although the secular SST trend was not statistically significant. On the other hand, sectors such as the Laptev and East Siberian, which experienced a significant decrease in salinity during August-September, did not exhibit a decrease in pCO_2 because DIC remained unchanged and because the impact of lower salinity was offset by a significant increase in SST in these sectors (Laptev: R^2=0.86, p=0.007, slope= 0.10 C yr^{-1} and East Siberian: R^2=0.87, p=0.007, slope=0.16 C yr^{-1}). Interestingly, no secular trend in FCO_2 was observed in August-September in these sectors, most likely due to the lack of a temporal trend in wind speed.

5. Discussion

Our basin wide estimate of FCO_2 for the Arctic Ocean of 169±9 Tg C yr^{-1} represents 8% of the global net air-sea CO_2 flux [*Takahashi et al.*, 2002]. Given that the Arctic Ocean (here north of ~66°N) occupies only 2.6% of the total area of world's ocean and <1% of the volume [*Jakobsson et al.*, 2004], this flux is significant. However, this total flux is much lower than the 570 Tg C yr^{-1} taken up by the Southern Ocean south of 50°S [*Takahashi et al.*, 2002]. With the Arctic Ocean expected to become ice free in the summer sometime this century [*Holland et. al.*, 2006], its role as a sink for atmospheric CO_2 could increase, particularly since recent declines in sea ice have been accompanied by an increase in primary production [*Pabi et al.*, 2008; *Arrigo et al.*, in press].

The results of this study are significant in that they assess the air-sea flux of the whole Arctic concurrently and lead the way for future monitoring with remote sensing data. The increasing availability of concurrently measured Chl, SST, SAL and DIC in all of the Arctic geographical sectors will lead to best possible estimates of Arctic wide FCO_2.

There are a number of pathways that control the exchange of CO_2 between the Arctic Ocean surface and its surroundings. CO_2 enters the ocean surface via direct air-sea flux as discussed in this study; it also enters the surface waters as a result of the entrainment of CO_2 from the deep ocean. CO_2 is

removed from the surface ocean by biological uptake and conversion to organic carbon. Part of this biogenic carbon exits the surface ocean and is exported to depth. A substantial amount of carbon also leaves the surface ocean via deep–water formation, as dense waters sink and carry dissolved organic and inorganic carbon with them. Surprisingly, the horizontal transport of this deep ocean carbon between basins often is larger than the flux of carbon by all the other mechanisms. For, example, *Skjelvan et al.* [2005] summarized carbon transport via these mechanisms for the Nordic Ocean (Greenland and Barents Sea). They estimated that 140 Tg C yr^{-1} entered the surface water, 90 Tg C yr^{-1} of which was via air-sea flux and 50 Tg C yr^{-1} from entrainment of deep, high DIC waters. In total, 170 Tg C yr^{-1} was calculated to exit these surface waters towards the deep ocean, including fluxes of 120 Tg C yr^{-1} from deep-water formation and 50 Tg C yr^{-1} via export production of particulate organic carbon (the difference between carbon entering and exiting surface waters is due to the large uncertainty in the export production estimate). The net lateral transport of carbon from the deep Nordic seas was calculated to be 100 Tg C y^{-1} [*Skjelvan et al.*, 2005].

The capacity of the polar ocean to take up CO_2 is reported to be decreasing [*Skejlvan et al.*, 2005] as the surface waters equilibrate with increasingly high atmospheric CO_2 concentrations, based on the long term assessment of annual surface fugacity of CO_2 [*Lefevre*, 2004] as well as from time series

measurements of DIC in the Norwegian sea [*Skjelvan et al.*, 2008]. On the other hand, *Bates et al.* [2006 b], report an increase in uptake capability based on the reduction in sea ice extent observed over the last three decades. In our five year study, no temporal trend in DIC or pCO_2 was found; but given that the increase in open water area in the East Siberian sector was associated with increasing annual FCO_2, we can speculate that an Arctic-wide increase in open water area may lead to an increase in FCO_2 into the ocean. However, this prediction will not hold if rapidly melting sea ice and large influxes of freshwater from rivers reduce the salinity enough to adversely affect the buffering capacity of the Arctic Ocean. Increased freshwater flux can also reduce deepwater formation, weakening the meridional circulation and reducing the deep transport of carbon between the Arctic and other ocean basins [*Aagaard and Carmack*, 1989].

Also, increased inflow of terrigenous DOC from these rivers can impede primary production by reducing the light availability, which will reduce CO_2 uptake. Remineralization and photooxidation of terrigenous DOC will increase the DIC pool within the Arctic basin, possibly reducing its capacity to act as a sink for atmospheric CO_2. However, most of the terrigenous DOC flowing into the Arctic Ocean is refractory and is remineralized to CO_2 on very long timescales [*Amon and Benner*, 2003].

Furthermore, if the wind speed increases in the Arctic, as is predicted for the Antarctic [*Russell et al.*, 2006], then changes in wind-driven mixing will also have pronounced effect on the air-sea flux of CO_2. Large mixing events caused by intense storms have been reported to reach not only the halocline but even the deeper thermocline [*Yang et al.*, 2004]. Thus, increases in wind speed or an increase in the frequency of storms, as has been witnessed in Alaska [*ACIA*, 2005], will result in entrainment of CO_2 from deep waters as well as deeper mixing of CO_2 into the subsurface.

While no temporal change in annual FCO_2 was observed in the Arctic over the time period of 1998-2003, it is important to continue to monitor changes in FCO_2 in light of the many dramatic changes happening in the Arctic environment. Moreover, as significant trends in annual primary production related to changes in open water area have been observed during the years 1998-2006 [*Pabi et al*, 2008], it is likely that similar temporal trend in FCO_2 will emerge. This study sets the path for future work in this direction by not only quantifying the interannual flux of CO_2 into the Arctic Ocean, but also providing a mechanism for future monitoring of this important biogeochemical region. Moreover, the application of this work will become even more relevant after the launch of two future salinity measuring satellites, Aquarius from National Aeronautics and Space Administration (NASA) that

is to be launched in 2010 and the Soil Moisture and Ocean Salinity (SMOS) from European space agency (ESA) to be launched in 2009.

References:

Aagaard, K., and E. C. Carmack (1989), The role of sea ice and other fresh water in the Arctic circulation. Journal of Geophysical Research, 94, 14,485-14,498.

ACIA (2005), Arctic Climate Impact Assessment – Scientific Report, , Cambridge University Press, UK.

Amon, R. M. W., and R. Benner (2003), Combined neutral sugars as indicators of the diagenetic state of dissolved organic matter in the Arctic Ocean, Deep-Sea Research, Part I (Oceanographic Research Papers), 50(1), 151.

Anderson, L. G., K. Olsson, and M. Chierici (1998), A carbon budget for the Arctic Ocean, Global Biogeochemical Cycles, 12(3), 455-465.

Bates, N. R. (2006), Air-sea CO2 fluxes and the continental shelf pump of carbon in the Chukchi Sea adjacent to the Arctic Ocean, Journal of Geophsical Research-Part C-Oceans, 111, 21.

Bates, N. R., S. B. Moran, D. A. Hansell, and J. T. Mathis (2006), An increasing CO2 sink in the Arctic Ocean due to sea-ice loss, Geophysical Research Letters, 33(23), L23609.

BROECKER, W. S., and T. H. PENG (1992), Interhemispheric transport of carbon dioxide by ocean circulation, Nature, 356(6370), 587-9.

Comiso, J. C., C. L. Parkinson, R. Gersten, and L. Stock (2008), Accelerated decline in the Arctic sea ice cover, Geophysical Research Letters, 35(1).

Dickson, A. G., And F. J. Millero (1987), A Comparison Of The Equilibrium-Constants For The Dissociation Of Carbonic-Acid In Seawater Media, Deep-Sea Research Part A-Oceanographic Research Papers, 34(10), 1733-1743.

Dmitrenko, I., J. A. Holemann, K. Tyshko, V. Churun, S. Kirillov, and H. Kassens (2001), The Laptev Sea flaw polynya, Russian Arctic: effects on the mesoscale hydrography, Annals of Glaciology, 33, 373-6.

Dyurgerov, M. B., and C. L. Carter (2004), Observational evidence of increases in freshwater inflow to the Arctic Ocean, Arctic Antarctic and Alpine Research, 36(1), 117-122.

Fransson, A., M. Chierici, L. C. Anderson, I. Bussmann, G. Kattner, E. P. Jones, and J. H. Swift (2001), The importance of shelf processes for the modification of chemical constituents in the waters of the Eurasian Arctic Ocean: implication for carbon fluxes, Continental Shelf Research, 21(3), 225-242.

influence pCO(2) in water transported over the Bering-Chukchi Sea shelf, Marine Chemistry, 94(1-4), 67-79.

Kaltin, S., L. G. Anderson, K. Olsson, A. Fransson, and M. Chierici (2002), Uptake of atmospheric carbon dioxide in the Barents Sea, Journal of Marine Systems, 38(1-2), 31-45.

Lee, K., L. T. Tong, F. J. Millero, C. L. Sabine, A. G. Dickson, C. Goyet, G. Park, R. Wanninkhof, R. A. Feely, and R. M. Key (2006), Global relationships of total alkalinity with salinity and temperature in surface waters of the world's oceans, Geophysical Research Letters, 33(19).

Levevre, N., A. J. Watson, A. Olsen, A. F. Rios, F. F. Perez, and T. Johannessen (2004), A decrease in the sink for atmospheric CO{sub 2} in the North Atlantic, Geophysical Research Letters, 31(7), L07306-4.

Markus, T., and B. A. Burns (1995), A method to estimate subpixel-scale coastal polynyas with satellite passive microwave data. Journal of Geophysical Research, 100, 4473-4487.

Mehrbach, C., C. H. Culberson, J. E. Hawley, And R. M. Pytkowicz (1973), Measurement Of The Apparent Dissociation Constants Of Carbonic-Acid In Sea Water At Atmospheric Pressure, Limnology and Oceanography, 18(6), 897-907.

Miller, L. A., M. Chierici, T. Johannessen, T. T. Noji, F. Rey, and I. Skjelvan (1999), Seasonal dissolved inorganic carbon variations in the Greenland

Hansell, D. A., D. Kadko, and N. R. Bates (2004), Degradation of terrigenous dissolved organic carbon in the western Arctic Ocean, Science, 304(5672), 858-61.

Harms, I. H., M. J. Karcher, and D. Dethleff (2000), Modelling Siberian river runoff - implications for contaminant transport in the Arctic Ocean, Journal of Marine Systems, 27(1-3), 95-115.

Hill, V., and G. Cota (2005), Spatial patterns of primary production on the shelf, slope and basin of the Western Arctic in 2002, Deep-Sea Research, Part II (Topical Studies in Oceanography), 52(24), 3344-54.

Holland, M. M., C. M. Bitz, and B. Tremblay (2006), Future abrupt reductions in the summer Arctic sea ice, Geophysical Research Letters, 33(23).

Intergovernmental Panel on Climate Change (IPCC) (2004), Special Report on Emissions Scenarios, Cambridge Univ. Press, New York.

Jakobsson M., A. Grantz, Y. Kristoffersen, R. Macnab (2004), , in The organic carbon cycle in the Arctic Ocean.edited by Stein R, Macdonald RW, pp. 1-32, Springer-Verlag, Berlin.

Kalnay, E., et al (1996), The NCEP/NCAR 40-year reanalysis project, Bulletin of the American Meteorological Society, 77(3), 437.

Kaltin, S., and L. G. Anderson (2005), Uptake of atmospheric carbon dioxide in Arctic shelf seas: evaluation of the relative importance of processes that

Sea and implications for atmospheric CO{sub 2} exchange, Deep-Sea Research, Part II (Topical Studies in Oceanography), 46(6), 1473-96.

Murata, A., and T. Takizawa (2003), Summertime CO2 sinks in shelf and slope waters of the western Arctic Ocean, Continental Shelf Research, 23(8), 753-776.

Najjar, R. G., and J. C. Orr (1999), Biotic-HOWTO, internal OCMIP report, 15 pp., Lab. des Sci. du Clim. et de l'Environ./CEA Saclay, Gif-sur-Yvette, France. (Available at http://www.ipsl.jussieu.fr/OCMIP

Nakaoka, S., S. Aiki, T. Nakazawa, G. Hashida, S. Morimoto, T. Yamanouchi, and H. Yoshikawa-Inoue (2006), Temporal and spatial variations of oceanic pCO(2) and air-sea CO2 flux in the Greenland Sea and the Barents Sea, Tellus Series B Chemical and Physical Meteorology, 58(2), 148-161.

Omar, A., T. Johannessen, S. Kaltin, and A. Olsen (2003), Anthropogenic increase of oceanic pCO(2) in the Barents Sea surface water, Journal of Geophysical Research-Oceans, 108, 3388.

O'Reilly, J., S. Maritorena, B. Mitchell, D. iegel, K. Carder, S. Garver, M. Kahru, and C. McClain (1998), Ocean color chlorophyll algorithms for SeaWiFS. Journal of Geophysical Research, 103(C11), 24937-53.

Pabi, S., G. L. van Dijken, and K. R. Arrigo. 2008. Primary production in the Arctic Ocean, 1998-2006. Journal of Geophysical Research 113. doi:10.1029/2007JC004578.).

Pavelsky, T. M., and L. C. Smith (2004), Spatial and temporal patterns in Arctic river ice breakup observed with MODIS and AVHRR time series, Remote Sensing of Environment, 93(3), 328-338.

Peterson, B. J., R. M. Holmes, J. W. McClelland, C. J. Vorosmarty, R. B. Lammers, A. I. Shiklomanov, I. A. Shiklomanov, and S. Rahmstorf (2002), Increasing river discharge to the Arctic Ocean, Science, 298(5601), 2171-3.

Peterson, B. J., J. McClelland, R. Curry, R. M. Holmes, J. E. Walsh, and K. Aagaard (2006), Trajectory shifts in the Arctic and subarctic freshwater cycle, Science, 313(5790), 1061-6.

Pipko, I. I., I. P. Semiletov, P. Y. Tishchenko, S. P. Pugach, and J. P. Christensen (2002), Carbonate chemistry dynamics in Bering Strait and the Chukchi Sea, Progress in Oceanography, 55(1-2), 77-94.

Richter-Menge, J., J. Overland, A. Proshutinsky, V. Romanovsky, L. Bengtsson, L. Brigham, M. Dyurgerov, J.C. Gascard, S. Gerland, R. Graversen, C. Haas, M. Karcher, P. Kuhry, J. Maslanik, H. Melling, W. Maslowski, J. Morison, D. Perovich, R. Przybylak, V. Rachold, I. Rigor, A. Shiklomanov, J. Stroeve, D. Walker, and J. Walsh (2006). State of the Arctic Report, NOAA OAR Special Report, NOAA/OAR/PMEL, Seattle, WA, 36 pp.

Russell, J. L., K. W. Dixon, A. Gnanadesikan, R. J. Stouffer, and J. R. Toggweiler (2006), The Southern Hemisphere westerlies in a warming

world: propping open the door to the deep ocean, Journal of Climate, 19(24), 6382-90.

Sabine, C., et al (2004), The oceanic sink for anthropogenic CO2, Science, 305(5682), 367-71.

Sarma, V. V. S. S., T. Saino, K. Sasaoka, Y. Nojiri, T. Ono, M. Ishii, H. Y. Inoue, and K. Matsumoto (2006), Basin-scale pCO(2) distribution using satellite sea surface temperature, Chla, and climatological salinity in the North Pacific in spring and summer, Global Biogeochemical Cycles, 20(3), GB3005.

Siegenthaler, U., And J. L. Sarmiento (1993), Atmospheric carbon dioxide and the ocean, Nature, 365(6442), 119-25.

Skjelvan, I., T. Johannessen and L.A. Miller, Interannual variability of $fCO2$ in the Greenland and Norwegian Seas, Tellus, 51B, pp. 477-489, 1999a.

Skjelvan, I., M. Chierici and J. Ólafsson, Horizontal distributions of NCT, NAT and fCO2 in the Nordic Seas, in Carbon and oxygen fluxes in the Nordic Seas, edited by I. Skjelvan, Ph-D thesis, University of Bergen, Norway, 1999b

Skjelvan, I., Olsen A., Anderson, L. G., Bellerby, R. G. J., Falck, E., Kasajima, Y., Kivimäe, C., Omar, A., Rey, F., Olsson, K. A., Johannessen, T., and Heinze, C., A Review of the Inorganic Carbon Cycle of the Nordic Seas and

Barents Sea, in The Nordic Seas: An Integrated Perspective, AGU Monograph 158, American Geophysical Union, Wash. DC

Skjelvan, I., E. Falck, F. Rey, and S. B. Kringstad (2008), Inorganic carbon time series at Ocean Weather Station M in the Norwegian Sea, Biogeosciences, 5(2), 549-560.

Swift, J. H., and K. Aagaard (1981), Seasonal transitions and water mass formation in the Iceland and Greenland seas, Deep-Sea Research, Part A (Oceanographic Research Papers), 28(10), 1107-29.

Takahashi, T., et al (2002), Global sea-air CO2 flux based on climatological surface ocean pCO(2), and seasonal biological and temperature effects, Deep-Sea Research Part Ii-Topical Studies in Oceanography, 49(9-10), 1601.

Wallace, D. W. R., P. J. Minnett, And T. S. Hopkins (1995), Nutrients, oxygen, and inferred new production in the Northeast Water Polynya, 1992, Journal of Geophysical Research, 100, 4323-40.

Wanninkhof, R. (1992), Relationship between wind-speed and gas-exchange over the ocean, Journal of Geophysical Research, 97, 7373-7382.

Weiss, R. F., and B. A. Price (1980), Nitrous Oxide solubility in water and seawater, Marine Chemistry, 8(4), 347.

Yang, J. Y., J. Comiso, D. Walsh, R. Krishfield, and S. Honjo (2004), Storm-driven mixing and potential impact on the Arctic Ocean, Journal of Geophysical Research-Oceans, 109, C04008.

Chapter 5

Conclusion

1. Concluding Remarks

This work attains three significant milestones towards quantifying the biogeochemistry of the polar oceans. First, a novel method was developed to determine particulate organic carbon (POC) in surface waters of the Southern Ocean. Second, annual variability in primary production was determined in the Arctic Ocean with unprecedented spatial coverage. Third, the air-sea flux of carbon dioxide (CO_2) was quantified at high spatial and temporal resolution in the Arctic Ocean.

In Chapter 2, a novel method was developed to determine particulate organic carbon from space. This was a departure from the conventional method of converting satellite estimates of chlorophyll (Chl) to carbon (C) using a C to Chl ratio. The direct estimate of POC bypassed most of the variability associated with the C to Chl ratio. Moreover, this is one of the few studies that included *in-situ* measured data to develop an empirical algorithm for estimating POC. This study also includes an example application of satellite estimation of POC in the Ross Sea, Antarctica.

In Chapter 3, interannual changes in primary production, by ecological zone and by geographic sector, of the Arctic Ocean were quantified for the period 1998-2006. For this purpose, sea ice dynamics were analyzed using a method that yields presence or absence of sea ice at a much higher resolution (6.25 km) compared with the sea ice concentration data (25 km) typically used in Arctic investigations. The results show that since 1998, open water area in the Arctic has increased at a rate of 0.07×10^6 km^2 yr^{-1}, with the greatest increases in the Barents, Kara and Siberian sectors, particularly over the continental shelf. Between 1998 and 2006, mean annual open water area in the Arctic Ocean increased by 19%. This increase was primarily driven by longer periods of open water in recent years (2005-2006). Pan-Arctic primary production averaged 419±33 Tg C yr^{-1} during 1998-2006, reaching a nine-year peak in 2006. Annual production was approximately equally distributed between pelagic (less productive but greater area) and continental shelf (more productive but smaller area) waters. Interannual differences were most tightly linked to changes in open water area.

In Chapter 4, the air-sea flux of CO_2 was quantified in the pan-Arctic Ocean and its geographic sectors during 1998-2003. This allowed assessment of the role of the Arctic Ocean as a net sink or source of atmospheric CO_2. For this purpose, satellite and model-derived distributions of salinity, temperature, chlorophyll, and wind were used to estimate dissolved inorganic

carbon, pCO_2 and air-sea CO_2 flux in Arctic waters. This was the first time that such a high-resolution assessment of air-sea flux of Arctic Ocean has been performed. Although no interannual trends were found in the area-normalized DIC, pCO_2, and FCO_2, the analysis was limited to years 1998-2003 because model-derived data were available only for that time period. Increasing annual FCO_2 with time was observed only in Siberian sector and was due to a significant increase in open water area. The Arctic was found to be a net sink of atmospheric CO_2, with a total annual flux of 169±9 Tg CO_2 yr^{-1}. This is about 8% of the world ocean's uptake of CO_2. This is significant because the Arctic Ocean comprises of only 2.6% of the ocean area and only 1% of its volume.

Annual primary production in the Arctic Ocean (as assessed in Chapter 3) must certainly affect the air-sea flux of CO_2 (Chapter 4). The other factors that affect this flux are export to the deep ocean, entrainment from the deep ocean, and horizontal advection. It is difficult to quantify the exact contribution of each of these mechanisms towards annual air-sea flux due to large uncertainties. However, the assessment in Chapter 4 indicates that the dominant factor that affects the annual flux in the changing environment of Arctic Ocean is the freshwater influx.

2. Future prospects and challenges

2. 1. Satellite estimation of POC

It is hoped that in the future, satellite remote sensing of POC can be extended to other parts of the world to obtain direct measurements of POC. Although we employed a two-phytoplankton taxa algorithm here, with simple modification, this algorithm should be applicable to waters with more than two taxa. This method will become especially relevant once different taxa and their concentration can be identified using remote sensing data. The foremost challenge is that there is not enough relevant *in-situ* data to be able to apply algorithms like this in other parts of the world. For example, concurrent measurements of POC and optical properties are scarce. It is also difficult to get phytoplankton composition data for many parts of the world's oceans. Once these obstacles are overcome, POC algorithms should prove to be much more feasible.

2.2. Primary-production in the Arctic Ocean

The future scope of this work lies in the assessment of interannual changes in primary production in future years. It is possible that that future changes in the Arctic environment will affect the area-normalized rates of primary

production in addition to open water area. For example, increased ice melt and river influx may increase water column stratification to the extent that nutrient flux from deeper waters ceases and phytoplankton become nutrient limited. Under those circumstances, a reduction in the area-normalized production will decrease primary production, rather than allow it to increase at the current rate. On the other hand, an increase in water temperature may favorably affect the growth rate of phytoplankton, resulting in an increase in the area-normalized production. Continuing to monitor production in the coming years will be required to improve estimates of changes in the primary production in this ocean.

In addition, primary production estimates could be greatly improved by the development of Arctic region-specific algorithms to derive surface chlorophyll concentration. The algorithm currently in use exhibits the same range of chlorophyll variability as the global algorithm (OC4v4). Moreover, Arctic waters require the development of an algorithm to quantify chlorophyll in Case 2 waters with high sediment and colored dissolved organic matter (CDOM) content. The extent of these Case 2 waters is expected to increase in the Arctic Ocean along with the expected increases in riverine freshwater influx. Unfortunately, to date there is a paucity of data required for the validation of both chlorophyll as well as primary production algorithms.

2.3 Air-sea flux of CO_2 in the Arctic Ocean

Similar to Chapter 3, it will be of interest to continue the assessment of air-sea FCO_2 in the Arctic Ocean. While the current study points to the fact that the Arctic Ocean is a sink of CO_2, future changes in primary production will affect the size of this sink. Expected increases in freshwater influx will act to intensify the CO_2 sink, but future changes in alkalinity will also affect the influx of CO_2. It will be of interest to observe whether natural variations such as the Arctic Oscillation and Pacific Decadal Oscillation have any effect on the air-sea CO_2 flux through their impacts on the speed and direction of wind.

One serious challenge is that there is not enough concurrently measured Chl, SST, and salinity data to improve the algorithm developed here. Ideally, data would be available in every sector to quantify regional variability in greater detail. In addition, an ocean circulation model that provides estimates of the entrainment of waters below the mixed layer would also improve of the FCO_2 assessment. Although Chl and SST are available from satellite remote sensing data, to date salinity is not. However, this may change in the near future with the anticipated launch of the Aquarius salinity sensor. Furthermore, while measurements of air-sea flux of CO_2 have been made in various regions of the Arctic, a pan-Arctic database would go a long way towards assessing the changes in the Arctic Ocean.

In spite of the many challenges, there is still great potential to obtain a better understanding of the biogeochemistry in these polar oceans.